

Karlsruher Forschungsberichte aus dem
Institut für Hochfrequenztechnik und Elektronik

Band
59

Juan Pontes

Analysis and Design of Multiple Element Antennas for Urban Communication



Scientific
Publishing

Juan Pontes

Analysis and Design of Multiple Element Antennas for Urban Communication

Karlsruher Forschungsberichte
aus dem Institut für Hochfrequenztechnik und Elektronik

Herausgeber: Prof. Dr.-Ing. Thomas Zwick

Band 59

Analysis and Design of Multiple Element Antennas for Urban Communication

by

Juan Pontes

Dissertation, Karlsruher Institut für Technologie
Fakultät für Elektrotechnik und Informationstechnik, 2010

Impressum

Karlsruher Institut für Technologie (KIT)
KIT Scientific Publishing
Straße am Forum 2
D-76131 Karlsruhe
www.uvka.de

KIT – Universität des Landes Baden-Württemberg und nationales
Forschungszentrum in der Helmholtz-Gemeinschaft



Diese Veröffentlichung ist im Internet unter folgender Creative Commons-Lizenz
publiziert: <http://creativecommons.org/licenses/by-nc-nd/3.0/de/>

KIT Scientific Publishing 2010
Print on Demand

ISSN: 1868-4696
ISBN: 978-3-86644-513-0

Vorwort des Herausgebers

Die permanent steigende Nachfrage nach höheren Datenraten im Bereich der mobilen Kommunikation führt zu einer andauernden Suche nach neuen Methoden, die beschränkte Ressource des existierenden Frequenzspektrums besser zu nutzen und damit die Kanalkapazität zu steigern. Seit einigen Jahren werden hierzu auch Mehrantennensysteme eingesetzt. Diese sogenannten MIMO (Multiple-Input-Multiple-Output) Verfahren nutzen gezielt die Eigenschaften von Mehrwegefunkkanälen. Im Gegensatz zu dem schon seit vielen Jahrzehnten im Einsatz befindlichen Diversity, bei dem das Signal-zu-Rausch-Verhältnis durch möglichst optimales Kombinieren der Signale mehrerer Empfangsantennen maximiert wird, werden bei MIMO mehrere unabhängige Datenströme auf sogenannten Subkanälen übertragen, wodurch die Kanalkapazität gesteigert werden kann. Ausschlaggebend für maximale Kanalkapazität eines MIMO-Systems sind optimale Antennenkonfigurationen an Sender und Empfänger. Da MIMO allerdings die Mehrwegeeigenschaften des Funkkanals nutzt, wird für eine simulationsbasierte Optimierung der Antennenkonfigurationen ein hochgenaues Modell des Mehrwegefunkkanals benötigt. An dieser Stelle setzt die Arbeit von Herrn Juan Pontes an. Basierend auf dem intensiv verifizierten Wellenausbreitungsmodell des Instituts für Hochfrequenztechnik und Elektronik entwickelte Herr Pontes eine Methodik zur Analyse und Optimierung von Mehrantennensystemen für die urbane Funkkommunikation. Damit stellt die Arbeit von Herrn Pontes eine wesentliche Grundlage für weitere Forschungen dar und wird weltweit sicher einige darauf aufbauende Arbeiten nach sich ziehen. Ich wünsche ihm, dass er seine exzellenten Fähigkeiten auch weiterhin erfolgreich einsetzen kann.

Prof. Dr.-Ing. Thomas Zwick
- Institutsleiter -

**Forschungsberichte aus dem
Institut für Höchstfrequenztechnik und Elektronik (IHE)
der Universität Karlsruhe (TH) (ISSN 0942-2935)**

Herausgeber: Prof. Dr.-Ing. Dr. h.c. Dr.-Ing. E.h. Werner Wiesbeck

- Band 1 Daniel Kähny
**Modellierung und meßtechnische Verifikation polarimetrischer,
mono- und bistatischer Radarsignaturen und deren Klassifi-
zierung (1992)**
- Band 2 Eberhardt Heidrich
**Theoretische und experimentelle Charakterisierung der polari-
metrischen Strahlungs- und Streueigenschaften von Antennen
(1992)**
- Band 3 Thomas Kürner
**Charakterisierung digitaler Funksysteme mit einem breit-
bandigen Wellenausbreitungsmodell (1993)**
- Band 4 Jürgen Kehrbeck
**Mikrowellen-Doppler-Sensor zur Geschwindigkeits- und Weg-
messung - System-Modellierung und Verifikation (1993)**
- Band 5 Christian Bornkessel
**Analyse und Optimierung der elektrodynamischen Eigenschaften
von EMV-Absorberkammern durch numerische Feldberechnung
(1994)**
- Band 6 Rainer Speck
**Hochempfindliche Impedanzmessungen an Supraleiter / Fest-
elektrolyt-Kontakten (1994)**
- Band 7 Edward Pillai
**Derivation of Equivalent Circuits for Multilayer PCB and Chip
Package Discontinuities Using Full Wave Models (1995)**
- Band 8 Dieter J. Cichon
**Strahlenoptische Modellierung der Wellenausbreitung in urbanen
Mikro- und Pikofunkzellen (1994)**
- Band 9 Gerd Gottwald
**Numerische Analyse konformer Streifenleitungsantennen in
mehrlagigen Zylindern mittels der Spektralbereichsmethode
(1995)**

**Forschungsberichte aus dem
Institut für Höchstfrequenztechnik und Elektronik (IHE)
der Universität Karlsruhe (TH) (ISSN 0942-2935)**

- Band 10 Norbert Geng
**Modellierung der Ausbreitung elektromagnetischer Wellen in
Funksystemen durch Lösung der parabolischen Approximation
der Helmholtz-Gleichung (1996)**
- Band 11 Torsten C. Becker
**Verfahren und Kriterien zur Planung von Gleichwellennetzen für
den Digitalen Hörrundfunk DAB (Digital Audio Broadcasting)
(1996)**
- Band 12 Friedhelm Rostan
**Dual polarisierte Microstrip-Patch-Arrays für zukünftige satelli-
tengestützte SAR-Systeme (1996)**
- Band 13 Markus Demmler
**Vektorkorrigiertes Großsignal-Meßsystem zur nichtlinearen Cha-
rakterisierung von Mikrowellentransistoren (1996)**
- Band 14 Andreas Froese
**Elektrochemisches Phasengrenzverhalten von Supraleitern
(1996)**
- Band 15 Jürgen v. Hagen
**Wide Band Electromagnetic Aperture Coupling to a Cavity: An In-
tegral Representation Based Model (1997)**
- Band 16 Ralf Pötzschke
**Nanostrukturierung von Festkörperflächen durch elektro-
chemische Metallphasenbildung (1998)**
- Band 17 Jean Parlebas
**Numerische Berechnung mehrlagiger dualer planarer Antennen
mit koplanarer Speisung (1998)**
- Band 18 Frank Demmerle
**Bikonische Antenne mit mehrmodiger Anregung für den räumli-
chen Mehrfachzugriff (SDMA) (1998)**
- Band 19 Eckard Steiger
**Modellierung der Ausbreitung in extrakorporalen Therapien ein-
gesetzter Ultraschallimpulse hoher Intensität (1998)**

**Forschungsberichte aus dem
Institut für Höchstfrequenztechnik und Elektronik (IHE)
der Universität Karlsruhe (TH) (ISSN 0942-2935)**

- Band 20 Frederik Küchen
Auf Wellenausbreitungsmodellen basierende Planung terrestrischer COFDM-Gleichwellennetze für den mobilen Empfang (1998)
- Band 21 Klaus Schmitt
Dreidimensionale, interferometrische Radarverfahren im Nahbereich und ihre meßtechnische Verifikation (1998)
- Band 22 Frederik Küchen, Torsten C. Becker, Werner Wiesbeck
Grundlagen und Anwendungen von Planungswerkzeugen für den digitalen terrestrischen Rundfunk (1999)
- Band 23 Thomas Zwick
Die Modellierung von richtungsaufgelösten Mehrwegegebäudefunkkanälen durch markierte Poisson-Prozesse (2000)
- Band 24 Dirk Didascalou
Ray-Optical Wave Propagation Modelling in Arbitrarily Shaped Tunnels (2000)
- Band 25 Hans Rudolf
Increase of Information by Polarimetric Radar Systems (2000)
- Band 26 Martin Döttling
Strahlenoptisches Wellenausbreitungsmodell und Systemstudien für den Satellitenmobilfunk (2000)
- Band 27 Jens Haala
Analyse von Mikrowellenheizprozessen mittels selbstkonsistenter finiter Integrationsverfahren (2000)
- Band 28 Eberhard Gschwendtner
Breitbandige Multifunktionsantennen für den konformen Einbau in Kraftfahrzeuge (2001)
- Band 29 Dietmar Löffler
Breitbandige, zylinderkonforme Streifenleitungsantennen für den Einsatz in Kommunikation und Sensorik (2001)
- Band 30 Xuemin Huang
Automatic Cell Planning for Mobile Network Design: Optimization Models and Algorithms (2001)

**Forschungsberichte aus dem
Institut für Höchstfrequenztechnik und Elektronik (IHE)
der Universität Karlsruhe (TH) (ISSN 0942-2935)**

- Band 31 Martin Fritzsche
**Anwendung von Verfahren der Mustererkennung zur Detektion
von Landminen mit Georadaren (2001)**
- Band 32 Siegfried Ginter
**Selbstkonsistente Modellierung der Erhitzung von biologischem
Gewebe durch hochintensiven Ultraschall (2002)**
- Band 33 Young Jin Park
**Applications of Photonic Bandgap Structures with Arbitrary Sur-
face Impedance to Luneburg Lenses for Automotive Radar (2002)**
- Band 34 Alexander Herschlein
**Entwicklung numerischer Verfahren zur Feldberechnung kon-
former Antennen auf Oberflächen höherer Ordnung (2002)**
- Band 35 Ralph Schertlen
**Mikrowellenprozessierung nanotechnologischer Strukturen am
Beispiel von Zeolithen (2002)**
- Band 36 Jürgen von Hagen
**Numerical Algorithms for the Solution of Linear Systems of Equa-
tions Arising in Computational Electromagnetics (2002)**
- Band 37 Ying Zhang
**Artificial Perfect Magnetic Conductor and its Application to An-
tennas (2003)**
- Band 38 Thomas M. Schäfer
**Experimentelle und simulative Analyse der Funkwellenausbrei-
tung in Kliniken (2003)**
- Band 39 Christian Fischer
**Multistatisches Radar zur Lokalisierung von Objekten im Boden
(2003)**
- Band 40 Yan C. Venot
**Entwicklung und Integration eines Nahbereichsradsensor-
systems bei 76,5 GHz (2004)**
- Band 41 Christian Waldschmidt
**Systemtheoretische und experimentelle Charakterisierung integ-
rierbarer Antennenarrays (2004)**

**Forschungsberichte aus dem
Institut für Höchstfrequenztechnik und Elektronik (IHE)
der Universität Karlsruhe (TH) (ISSN 0942-2935)**

- Band 42 Marwan Younis
Digital Beam-Forming for high Resolution Wide Swath Real and Synthetic Aperture Radar (2004)
- Band 43 Jürgen Maurer
Strahlenoptisches Kanalmodell für die Fahrzeug-Fahrzeug-Funkkommunikation (2005)
- Band 44 Florian Pivit
Multiband-Aperturantennen für Basisstationsanwendungen in rekonfigurierbaren Mobilfunksystemen (2005)
- Band 45 Sergey Sevskiy
Multidirektionale logarithmisch-periodische Indoor-Basisstationsantennen (2006)
- Band 46 Martin Fritz
Entwurf einer breitbandigen Leistungsendstufe für den Mobilfunk in Low Temperature Cofired Ceramic (2006)
- Band 47 Christiane Kuhnert
Systemanalyse von Mehrantennen-Frontends (MIMO) (2006)
- Band 48 Marco Liebler
Modellierung der dynamischen Wechselwirkungen von hochintensiven Ultraschallfeldern mit Kavitationsblasen (2006)
- Band 49 Thomas Dreyer
Systemmodellierung piezoelektrischer Sender zur Erzeugung hochintensiver Ultraschallimpulse für die medizinische Therapie (2006)
- Band 50 Stephan Schulteis
Integration von Mehrantennensystemen in kleine mobile Geräte für multimediale Anwendungen (2007)
- Band 51 Werner Sörgel
Charakterisierung von Antennen für die Ultra-Wideband-Technik (2007)
- Band 52 Reiner Lenz
Hochpräzise, kalibrierte Transponder und Bodenempfänger für satellitengestützte SAR-Missionen (2007)

**Forschungsberichte aus dem
Institut für Höchstfrequenztechnik und Elektronik (IHE)
der Universität Karlsruhe (TH) (ISSN 0942-2935)**

- Band 53 Christoph Schwörer
Monolithisch integrierte HEMT-basierende Frequenzvervielfacher und Mischer oberhalb 100 GHz (2008)
- Band 54 Karin Schuler
Intelligente Antennensysteme für Kraftfahrzeug-Nahbereichs-Radar-Sensorik (2007)
- Band 55 Christian Römer
Slotted waveguide structures in phased array antennas (2008)

Fortführung als
"Karlsruher Forschungsberichte aus dem Institut für Hochfrequenztechnik und Elektronik" bei KIT Scientific Publishing
(ISSN 1868-4696)

**Karlsruher Forschungsberichte aus dem
Institut für Hochfrequenztechnik und Elektronik
(ISSN 1868-4696)**

Herausgeber: Prof. Dr.-Ing. Thomas Zwick

**Die Bände sind unter www.ksp.kit.edu als PDF frei verfügbar oder als
Druckausgabe bestellbar.**

Band 55 Sandra Knörzer

**Funkkanalmodellierung für OFDM-Kommunikationssysteme bei
Hochgeschwindigkeitszügen (2009)**

ISBN 978-3-86644-361-7

Band 56 Fügen, Thomas

**Richtungsaufgelöste Kanalmodellierung und Systemstudien für
Mehrantennensysteme in urbanen Gebieten (2009)**

ISBN 978-3-86644-420-1

Band 57 Pancera, Elena

**Strategies for Time Domain Characterization of UWB Components
and Systems (2009)**

ISBN 978-3-86644-417-1

Band 58 Timmermann, Jens

**Systemanalyse und Optimierung der Ultrabreitband-Übertragung
(2010)**

ISBN 978-3-86644-460-7

Band 59 Pontes, Juan

**Analysis and Design of Multiple Element Antennas for Urban
Communication (2010)**

ISBN 978-3-86644-513-0

Karlsruher Institut für Technologie (KIT)
Institut für Hochfrequenztechnik und Elektronik

Analysis and Design of Multiple Element Antennas for Urban Communication

Zur Erlangung des akademischen Grades eines

DOKTOR-INGENIEURS

der Fakultät für
Elektrotechnik und Informationstechnik
am Karlsruher Institut für Technologie

vorgelegte

DISSERTATION

von

Dipl.-Ing. Juan Pontes
aus Caracas

Hauptreferent:
Korreferent:

Prof. Dr.-Ing. Thomas Zwick
Prof. Dr.-Ing. Christoph Mecklenbräuker

Vorwort

Die vorliegende Dissertation entstand während meiner Tätigkeit als wissenschaftlicher Mitarbeiter am Institut für Hochfrequenztechnik und Elektronik (IHE) des Karlsruher Instituts für Technologie (KIT).

Mein Dank geht zunächst an Herrn Prof. Wiesbeck, Leiter des Instituts zum Zeitpunkt meiner Einstellung, dessen Unterstützung mir half mich professionell zu entwickeln. Weiter geht mein Dank an Herrn Prof. Zwick, der in den letzten zwei Jahren nicht nur für eine sehr gute Betreuung gesorgt hat, sondern darüber hinaus durch seine konstruktive Kritik als Hauptreferent zum Gelingen dieser Arbeit beigetragen hat. Ebenso danke ich Herrn Prof. Christoph Mecklenbräuker, Leiter des Instituts für Nachrichtentechnik und Hochfrequenztechnik der Technischen Universität Wien, für die Übernahme des Korreferats. Außerdem möchte ich mich ausdrücklich bei der Firma KATHREIN Werke KG, ihren Mitarbeitern und besonders bei Herrn Prof. Roland Gabriel für die gute Zusammenarbeit bedanken, denn sie haben den Anstoß zu meiner Dissertation gegeben.

Bedanken möchte ich mich auch bei Dr. Thomas Fügen für seine Hilfe bei der Einarbeitung in die Themen Mehrantennensysteme und MIMO, den vielen wertvollen Diskussionen und insbesondere für das Korrekturlesen der Dissertation. Diese Arbeit hätte ohne seine ausführliche Kritik und Unterstützung nicht den jetzigen Stand erlangt. Des Weiteren möchte ich mich bei allen Kollegen bedanken, die sich oft Zeit für Diskussionen genommen haben und die für mich durch unsere Zusammenarbeit und gemeinsame Freizeitaktivitäten zu Freunden geworden sind. Ebenso geht mein Dank an alle Studenten, die sich mit mir fachlich weiterentwickelt und so aus mir einen anderen Menschen gemacht haben.

Mein herzlicher Dank geht an meine Mutter, die mir durch ihre stetige Unterstützung jeden Tag leichter fallen lässt.

Und mein letzter Dank geht an Kimberly, die aus meinem Leben eine Begegnung mit der Freude gemacht hat.

Karlsruhe, im Februar 2010

Juan Pontes

Abstract

With the increasing interest in sophisticated algorithms and network configurations in order to increase the data rates demands of current and future communication systems, less attention is paid to the antenna in-system optimization. Yet, network providers and antenna engineers are still faced with the problem of addressing upcoming infrastructure needs, such as more cost efficient antenna solutions. To aid in this decision making process, the attention of this work is focused on the analysis and design of multiple element antennas (MEA) and their interaction with the propagation channel. Moreover, focus is given to the "Karlsruhe" propagation channel and how its information throughput, i.e. capacity, can be improved. With this in mind, an existing network model of the communication system is extended to include a modal description of both mobile and base station antennas in order to reduce computation time. Reduction of simulation time is proven to increase linearly with the number of antennas, when it exceeds the number of modes considered. On the basis of this model, an extensive capacity study of different antenna setups based on measured radiation patterns of commercial antennas is performed, with varying inter element spacing at both the base and mobile station. As result, a set of guidelines for optimum antenna placement and setup selection is given based on the capacity of equivalent isotropic normalized channels. This type of normalization, however, is not unique. Depending on the evaluation needs other norms might be used and comparison among different works results in a difficult task. To address this issue the adoption of an eigenvalue dispersion metric as a compact and information rich evaluation measure is proposed, with which the capacity for any normalization and SNR regime can be estimated. Finally, the communicational limits of linear arrays in different propagation scenarios are explored and a synthesis method for achieving maximum information throughput is derived. In this way it is proven that even better capacities to those achieved by the studied commercial antenna setups could be attained, not by increasing the number of antennas, but by adding subchannels to the existing ones. Hence, antenna driving networks capable of producing several array excitations are suggested as the next step toward better capacities in urban mobile communication systems.

Table of Contents

1	Introduction	1
1.1	The urban communication channel	2
1.2	Previous works & motivation	3
1.3	Goal & Thesis outline	5
2	The wireless communication channel	7
2.1	Input/Output model of the wireless communication channel	7
2.1.1	Single antenna channels	8
2.1.2	Multiple antenna channels	9
2.2	The antennas	9
2.2.1	Antennas on transmit mode	10
2.2.2	Antennas on receive mode	12
2.2.3	Circuit model of communicating antennas	13
2.2.3.1	Antenna losses	13
2.2.3.2	Feeding circuit losses	15
2.2.3.3	Polarization losses	16
2.3	The propagation channel	17
2.3.1	The free space propagation channel	17
2.3.2	Multipath propagation channels	19
3	Modeling of multiple element antenna systems	23
3.1	Exact system model	23
3.2	Modal network model of communication channel	26
3.2.1	Inclusion of the modal expansion	27
3.2.2	Computational gain	28
3.2.3	Modal description of mobile station	29
3.2.4	Modal description of base station	31
3.3	Modeling of the "Karlsruhe" urban propagation channel	32
3.3.1	Urban Environment Model	33
3.3.2	Wave propagation Model	34
3.3.3	SISO to MIMO Extrapolation	35
3.4	Final remarks	36
4	Information content of multiple element antenna systems	37
4.1	Spatial gain of MEA systems	37
4.1.1	Diversity gain	38
4.1.2	Multiplexing gain	39

4.1.3	Diversity and multiplexing effects on the channel matrix	39
4.1.4	Spatial gain comparison issues	41
4.2	Capacity of multiple element antenna systems	43
4.2.1	Uniform Power Distribution	45
4.2.2	Waterfilling	46
4.2.3	Beamforming on transmit	48
4.3	Channel capacity of temporal and spatial bandlimited systems	49
4.4	Final remarks	52
5	Capacity study of the “Karlsruhe” communication channel	55
5.1	Antennas and antenna arrays under study	55
5.2	Antenna placement effects on system capacity	57
5.2.1	Vertically polarized antennas	58
5.2.2	Dual polarized antennas in single polarization mode	60
5.2.3	Dual polarized antennas in dual polarization mode	62
5.2.4	Influence of mobile unit rotation on antenna placement	65
5.3	Setup comparison	67
5.4	Final remarks	69
6	Improved evaluation metric for multiple element antenna systems	71
6.1	Eigenmode-based metric for Frobenius-normalized channels	72
6.1.1	Rank-2 systems	73
6.1.2	Rank-K systems	75
6.2	Eigenmode-based metric for arbitrarily normalized systems	78
6.3	Capacity analysis with eigenmode-based metric	79
6.3.1	Rank-2 systems	79
6.3.2	Rank-K systems	86
6.4	Final remarks	91
7	Communicational limits of linear multiple element antennas	93
7.1	Spatial degrees of freedom in free space	93
7.2	Spatial degrees of freedom in multipath channels	100
7.3	Spatial degrees of freedom of the “Karlsruhe” communication channel	103
7.3.1	Degrees of freedom definitions for non-ideal channels	103
7.3.2	Degrees of freedom of single channel realizations	104
7.3.3	Degrees of freedom of all channel realizations	110
7.4	Final remarks	112
8	Antenna design for wireless communication channels	115
8.1	Multiple element antenna synthesis method	115
8.2	Antenna array synthesis for the urban communication channel	119
8.3	Antenna design concepts for the future	123
8.4	Final remarks	127

9 Conclusions	129
Bibliography	133

Acronyms and symbols

Acronyms

BTS	Base Transceiver Station
DMC	Discrete Memoryless Channel
DOA	Direction Of Arrival
DOD	Direction Of Departure
FF	Far Field
FPGA	Field Programmable Gate Array
IEE	The Institution of Electrical Engineers
IEEE	Institute of Electrical and Electronics Engineers
LOS	Line Of Sight
MEA	Multiple Element Antenna
MIMO	Multiple Input Multiple Output
NDF	Number of Degrees of Freedom
NLOS	No Line Of Sight
OSI	Open System Interconnection reference model
PPC	Perfect Power Control
RF	Radio Frequency
SISO	Single Input Single Output
SNR	Signal to Noise Ratio
SVD	Singular Value Decomposition
TDD	Time Division Duplex
TMA	Tower Mounted Amplifier
TMPU	Tower Mounted Pre-processing unit
UMTS	Universal Mobile Telecommunications System
TSP	Transferred Signal Power

Lower case letters

<i>d</i>	distance
<i>f</i>	frequency

j	imaginary unit (see Mathematical notations and symbols)
n	channel
n	noise
s	antenna inter element spacing
\hat{t}	time (variance of the channel)
t	time (relative to the communication signal)
x, y	input, output signal
x, y, z	cartesian coordinates

Capital letters

A_{eff}	Antenna effective area
C	Radiation pattern
C	Capacity
D	Directivity
\mathbf{I}	Identity matrix
E	Electric field
G	Gain
\mathbf{H}	Channel matrix
\mathbf{W}	Normalized channel matrix
H	Channel matrix coefficient
L	Array length
M	Number of transmitting antennas
N	Number of receiving antennas
\mathcal{M}	Total number of transmitting antennas studied
\mathcal{N}	Total number of receiving antennas studied
P	Transmit power
R	Resistance
R	Number of spherical modes at the receiver
Q	Number of spherical modes at the transmitter
\mathbf{T}	Transmission matrix
T	Transmission matrix coefficient
Z	Impedance
\mathbf{S}	Scattering matrix
\mathbf{S}	Diagonalmatrix der SVD
S	Scattering matrix coefficient

S	Power density
V	Voltage

Greeks symbols

β	Propagation constant
δ	Difference in differential cosines
Γ	Reflection coefficient
$\Delta\varphi$	Phase difference
Ω	Space angle $\Omega = (\vartheta, \psi)$
ϑ	Elevation in spherical coordinates
λ	Wavelength
μ	Mean value
ρ	SNR
$\hat{\rho}$	Unitary polarization vector
σ	standard value
τ	Propagation time
ψ	Azimuth in spherical coordinates
η	Antenna efficiency
ζ	ρN
ξ	Eigenvalue dispersion as defined in [SSV ⁺ 08]
ϕ	Eigenvalue dispersion as defined in this work
Φ	Normalized ϕ

Mathematical notations and symbols

j	Imaginary unit $j = \sqrt{-1}$
a	Variable
\hat{a}	Modified variable (used to distinguish variables of the same type)
\check{a}	Variable in terms of spherical waves
\vec{a}	Vector
$\hat{\vec{a}}$	Unitary vector
\mathbf{A}	Matrix
\mathbf{a}	Matrix (vector)
$(\cdot)^\dagger$	Complex conjugate transpose

$(\cdot)^*$	Complex conjugate
$(\cdot)^T$	Transpose
*	Convolution
$\Re\{\dots\}$	Real part
$E\{\dots\}$	Expectation
Tr	Trace
log	Logarithm
det	Determinant
cos	Cosinus
sin	Sinus
prob	Probability
$ \cdot $	Absolute value (length of vector)
$\ \cdot\ _F$	Frobenius-Norm

Subscripts and superscripts

0	Freiraum (Wellenzahl oder Impedanz)
REF	Reference
n	Noise
norm	Normalized matrix
Tx	Transmit mode
Rx	Receive mode
TxA	Transmit antenna
RxA	Receive antenna
TxU	Transmit unit
RxU	Receive unit
max	Maximum
min	Minimum
eff	Effective
sim	Simulated
vir	virtual
A	Antenna
p	p-th path
k	k-th channel realization
m	m-th transmitting antenna
n	n-th receiving antenna

<i>r</i>	r-th spherical mode
<i>q</i>	q-th spherical mode
<i>i</i>	Index
<i>j</i>	Index
Az	Azimuth
El	Elevation
L	Load
+,-	Positive and negative propagation direction

List of constants

Z_{F0}	Characteristic wave impedance in free space $Z_{F0} = \sqrt{\frac{\mu_0}{\epsilon_0}} \approx 377\Omega$
c_0	Velocity of light in free space: $2,997925 \cdot 10^8$ m/s
e	Euler constant 2,718...
ϵ_0	Free space permittivity: $8,854 \cdot 10^{-12}$ As/(Vm)
μ_0	Free space permeability: $4\pi \cdot 10^{-7}$ Vs/(Am)
π	Pi 3,1415...

1 Introduction

Traditional communication systems are based on the transmission of modulated signals (in time) through a communication channel, consisting of the matching networks, the antennas and the propagation channel. With the advent of the digital communications and the whole spectrum of applications and improvements that it has to offer, more and more digital communication systems are being used in a wide range of applications. In this process, focus has shifted from the analogous part of the system, i.e. the transmission chain (or radio frequency (RF) transmission chain if signal transmission is wireless), to the processing part, i.e. the encoders and modulators responsible of digitally processing the input signals (either digital or analog) into analog signals suited for transmission with analog components. This has lead to a layered view of communications, as described in the Open System Interconnection (OSI) reference model [ITU94]. In this way, several advances have taken place, but in exchange less efforts are being made in improving the description and understanding of the analog part of the system (lowest layer), responsible for the actual transmission of electromagnetic waves. Because of this, relevance of high frequency and antenna engineers is even more valuable now where a more intuitive description of the communication channel can facilitate simulation and experimenting of complex algorithms at higher communication layers.

To better understand the role played by the RF transmission channel within the digital communication system, a block diagram of such a system is depicted in Figure 1.1. As it can be seen, the whole system consists on a series of blocks responsible for the signal processing in order to convey information between two points. Even though, details of each system component will not be discussed in this work (a thorough description can be found in [Pro01]), it can be seen that the whole system is divided into three segments: the transmitter processing chain, the communication channel, and the receiving processing chain. Both transmitter and receiver processing chains deal with the conversion between the digital and the analog domain, whereas the communication channel, also known as the RF transmission chain for wireless applications, is responsible for the physical information transmission. It follows that the communication channel represents a waveform channel, in which the signals are transmitted at a certain time and frequency, whereas the whole communication system is equivalent to a Discrete Memoryless Channel (DMC), where digital words or symbols are transmitted. In consequence, inaccurate modeling of the communication channel can lead to false results for the DMC in the same manner that too complex depictions can result too restrictive to experiment and understand the functioning of the system as a whole. To overcome these difficulties, several assumptions are

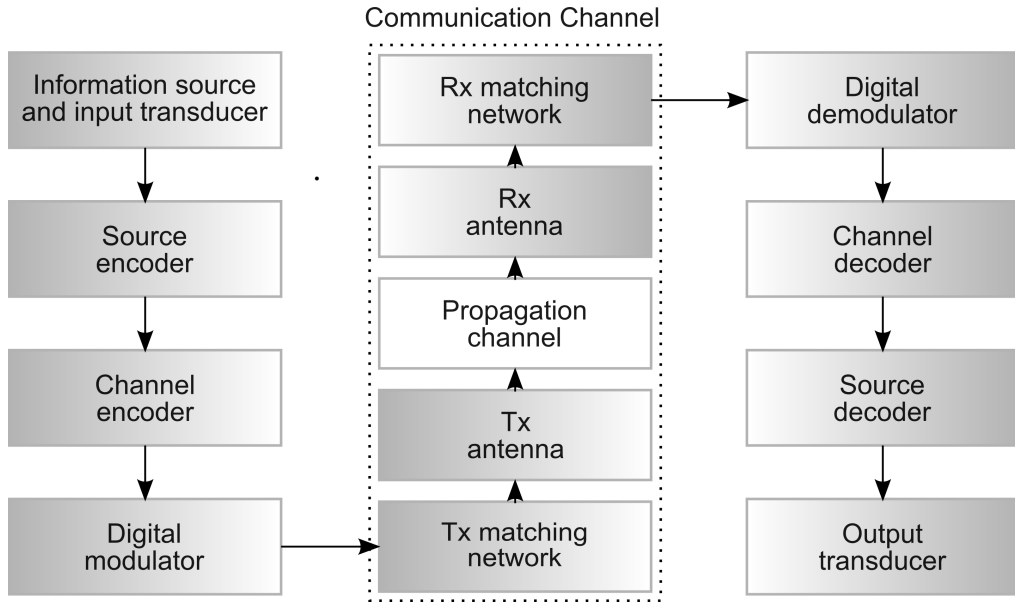


Figure 1.1: Block diagram of a digital communication system.

made regarding the communication channel and focus is given mostly to the coding schemes that optimize the system. Yet, optimization at the lowest communication layer can still result in remarkable improvements in the system as a whole. Furthermore, in order to guarantee the advances of upcoming standards and technologies, a choice of optimal hardware (antennas infrastructure) is still required.

1.1 The urban communication channel

As previously mentioned, the communication channel results from the interaction between feeding circuits, antennas, and propagation channel, where different types of sceneries or antennas lead to different communication channels. Throughout this thesis, focus will be given solely to the urban communication channel.

In this work, two classifications are used for distinguishing between different communication channels. The first communication channel classification and perhaps most important one, is the number of antennas involved in the communication process. If more than one radiating element is used, so that an antenna can be viewed as the result of multiple radiating elements, the term multiple element antenna (MEA) is used. The resulting channel is thus considered to be a MEA channel as opposed to the more common single-input single-output (SISO) channel.

The main difference between these two channels, other than the number of antennas, is that MEA channels are capable of making better use of the spatial resources of the communication

channel. Because of this, antenna arrangements capable of performing spatial signal processing through multiple antenna links have come to be known as smart antennas. However, since communication systems do inherently exploit the spatial properties of the channel regardless of the number of antennas used, the term smart antenna system will be dropped in this work.

In general, one could also refer to MEA systems with multiple antennas at both transmitter and receiver as Multiple-Input Multiple-Output (MIMO) systems. However, this is not entirely accurate given the fact that MIMO systems are mostly associated with the multiplexing capabilities of systems with multiple antennas in highly scattered propagation channels. As result, the use of multiple antennas in a scenario with dominant Line of Sight (LoS) component would not make sense from a multiplexing perspective. Even though this statement is only partially true, since LoS at small distances does not exclude benefits from multiplexing approaches [CPGZ09], the fact remains that not in every multiple antenna communication system multiplexing is used. Therefore, in order to provide a broader framework the terms MEA system and MEA channel are used, when more than one antenna on transmit, receive or both is considered.

The second classification that can be made depends on the type of propagation scenario considered. In this manner, one can differentiate between indoor or outdoor channels and the different types of channel in each case. For mobile communications, however, even though communication can take place at a wide range of propagation channels, the most relevant one is the outdoor channel for urban settings. Therefore, in this work, investigation of the communication channel resulting from the use of multiple element antennas within a urban propagation scenario is what will be referred to as the urban communication channel.

Urban propagation channels are specially relevant, since the larger number of users are located within urban settings. One could argue, though, that not all people are on the street, but within the buildings and vehicles. While true, it is first within the urban environment that propagation takes place until it finally reaches those users located inside the buildings, either by means of repeating stations or through direct wave transmission. As result, investigation of urban settings in general is of great importance and has been the driving force behind a significant number of works during the last decades [TFS99, OT02, CP07, LST⁺07, DC08].

1.2 Previous works & motivation

Antenna and system integration for the urban propagation scenario has been widely studied. However there seems to be no general agreement for the optimal antenna spacing, configuration and polarization of a MEA system for a specific scenario. This is mainly because all previous works are done under different frameworks which, in most cases, are not comparable

or flexible enough. In addition, the complexity of such systems has also been an impediment, where consideration of real multipath environments is either oversimplified or not considered at all. To overcome these limitations several measurement campaigns have been undertaken. However, the significant amount of data to be processed, as well as the considerable difficulties it poses, have also limited a more precise and extended study. As result, from the point of view of mobile or base station antenna designers, there doesn't seem to be a clear guideline as to which setup delivers the best results.

Furthermore, due to the important number of variables involved and the slow standardization process of scientific concepts, no universal evaluation framework or metric exists which is able to accurately capture in an insightful way the channel (or system) performance. Depending on whether antennas, channels or MIMO setups are being studied, different evaluation criteria are chosen, whereas, in some cases, even works of related topics present their results with non-comparable metrics. This leads to additional difficulties in the assessment of previously published MIMO antennas and configurations for the urban channel.

In addition, there is no general body of work available dealing with the communicational limits of typical urban communication channels. Some works are found in the area of free space and other analytical propagation channel models. For physical channel models, though, very little work has been done. Therefore, most of the knowledge in improving the capacities of current communication systems has been gained from experience and through cumbersome simulations, as the ones previously mentioned. Yet, no thorough study has been done on the attainable capacities and how they can be realized. This lack of understanding of the achievable information throughputs in real scenarios has lead to the current suboptimal antenna solutions. Moreover, it has also fueled current research trends toward the use of more elaborate antenna schemes, such as cooperative MIMO, which in most cases results in the addition of antennas and therefore cost to existing networks.

From the previous discussion follows that being able to make an informed choice in current urban communication channels has become increasingly difficult for both antenna designers and network providers. Due to the wide range of results obtained under different assumptions, a concise and systematic framework is needed for determining which antennas work best. Furthermore, the lack of understanding of the communicational limits of antenna systems has turned the process of network design into a rather empirical one. This work intends to provide such a simulation and evaluation framework, while leaving room for increased system complexity.

1.3 Goal & Thesis outline

In light of the discussed difficulties surrounding the study of the urban communication channel the goal of this thesis is to facilitate the study of current and future antenna systems. In this way the results to be presented in this work are intended as guidelines for both network designers and antenna engineers toward an efficient analysis, use and design of upcoming antenna setups. In addition this work expects to aid in the decision making process of network providers and antenna engineers with respect to upcoming infrastructure needs.

In order to achieve this goal, the main needs in the study of urban communication channels need to be addressed. This means providing a faster but accurate simulation framework, a general and flexible evaluation framework, and improved antenna solutions based on the better use of the channel spatial resources. With this in mind, aside from chapter 1 and 8, where an introduction and outlook to this work are given, this thesis is outlined as follows.

In chapter 2 a mathematical description of communication channels and more specifically of the urban communication channel will be given. First, the channel matrix concept will be discussed for SISO and MEA channels along with its normalization. Then some antenna fundamentals relevant for its computation will be discussed. Based on this, evaluation of the channel matrix will be explained for free space and multi path propagation channels.

On this ground, a flexible modeling approach will be introduced in chapter 3 for use with both communication channels and systems. Here, an existing network model is introduced for the whole communication system and later extended for increased computation speed based on the modal description of the antennas. Finally, the "Karlsruhe" urban communication channel to be used throughout this work will be defined.

Having provided a flexible simulation framework for communication systems, in chapter 4 the foundations for evaluating the performance of the communication channel from an information perspective will be discussed. First, the concept of capacity in the context of MEA channels, i.e. spatially limited channels, will be discussed. Then its meaning for simultaneously temporally and spatially limited channels will be analyzed on the basis of Shannon's capacity definition. On this basis a thorough study of the capacity limits from a spatial perspective will be investigated for free space.

In chapter 5, the simulation framework of chapter 4 will be used to study the capacity of various antenna configurations in the urban communication channel. Different antenna setups at different antenna inter-element spacings will be compared. Based on the results obtained, some

comparison and evaluation issues will be discussed. As result, the need for a better evaluation metric will be verified. This need will be then addressed in chapter 6, where a new evaluation metric will be proposed. In doing so, the cases of Frobenius and arbitrary normalized channels will be handled.

Having investigated the achievable capacities of typical antenna setups for the “Karlsruhe” urban communication channel, in chapter 6 focus is shifted to the theoretical limits behind such implementations. More specifically, the limits of the wireless channel in free space are investigated. Later on, the same approach is applied to the “Karlsruhe” urban communication channel and, from the experience gained in the study of typical antenna setups, the communicational limits of such systems will be investigated in chapter 7.

Finally, the issue of antenna design will be considered in chapters 7 and 8. First, the spatial degrees of linear systems will be investigated with respect to transmit power and antenna length in chapter 7. Then in chapter 8 a synthesis procedure will be given for computing the optimal array excitations capable of diagonalizing the channel matrix with any given polarization and antenna element. The capacity of optimally synthesized arrays will be studied and compared with that of commercial antennas. As final step, optimum antenna implementations will be suggested.

2 The wireless communication channel

The communication channel as already mentioned is considered in this work to be the part of the communication system involving the transmission and reception of electromagnetic energy. Therefore, it includes the antennas and the physical propagation channel. It follows that its analysis and design should consider the antenna properties and the channel characteristics. Most importantly, though, the way how channel and antennas interact to convey information from point A to point B must be known as well. As result, a communication channel description depicts the way in which a signal x is transmitted through a certain propagation channel and received as signal y . In other words, the relationship between x and y for a certain communication setup, i.e. the channel transfer function, should be known.

In the following the underlying concepts used as basis for the research done throughout this work will be presented. First, the channel transfer function in single and multiple antenna channels will be defined and discussed. Then the theoretical framework for its computation will be given. When not otherwise stated the word channel will refer to the communication channel, whereas the physical channel will be referred as such or as propagation channel.

2.1 Input/Output model of the wireless communication channel

The relationship between the input and output signal of a communication channel is given by the channel transfer function, where the input and output signals are waveforms (i.e. continuous signals in contrast to the discrete ones found at the input and output of the system modulator and demodulator). It involves the accurate representation of the antennas, their matching networks and the propagation channel used and it describes the way these interact in order to convey information within a communication system. In general this means finding the relationship between a certain input and output signal, which in practical terms results in obtaining the ratio between the transmitted and received voltages. As it will be shown, for single input single output (SISO) communication channels this results in a single transmission coefficient H , whereas for systems with multiple antennas it yields a channel matrix \mathbf{H} .

2.1.1 Single antenna channels

Assuming only one antenna on transmit and receive, i.e. a single input single output (SISO) system, and a linear and time-variant channel, such as multipath propagation channels explained below, the resulting channel transfer function between both communicating ends can be expressed as a function of frequency f and time \hat{t}

$$H_{nm}(f, \hat{t}) = \frac{y(f, \hat{t})}{x(f)} = \frac{V_{Rx,n}(f, \hat{t})}{V_{Tx,m}(f)}, \quad (2.1)$$

given by the ratio of the received voltage $V_{Rx,n}$ and the transmitted voltage $V_{Tx,m}$, where the subscripts n and m denote the receiving and transmitting antennas. In consequence, the output signal y results from the sum of the transmitted continuous waveform signal x and the additive white gaussian noise n corrupting the output

$$y(f, \hat{t}) = x(f)H_{nm}(f, \hat{t}) + n(f). \quad (2.2)$$

Furthermore, since the time variable \hat{t} expresses the time variance of the channel, and not the time domain t of the output and input waveform signals, (2.2) can be written as

$$y(t, \hat{t}) = x(t) * H_{nm}(t, \hat{t}) + n(t). \quad (2.3)$$

For a time invariant propagation channel or when considering only one snapshot of a propagation channel the dependence of H_{nm} on \hat{t} can be dropped. Moreover, if a channel with given bandwidth B and ideal frequency response within this bandwidth (flat frequency response) is considered H_{nm} loses its frequency dependence as well and becomes a fixed link coefficient. In consequence, when considering a time-invariant channel with ideal frequency response within the bandwidth B , as is considered in the entirety of this work, only the input and output voltage relationship, computed at a single frequency and at a single instant, is of interest.

Even though this is not the general case, investigation of the effects due to the time-variant and broadband characteristics of many communication channels has been subject of investigation in many works such as [Zwi99, Kat02]. Furthermore, results of this nature for the urban communication channel to be introduced in chapter 5 can be found in [Füg09]. In this work, though, interest lies in the study of the multiple element antennas within the communication channel, rather than the channel as such. Therefore, throughout this work, without loss of generality and for simulation ease, a time-invariant channel with ideal frequency response will be considered.

2.1.2 Multiple antenna channels

Up to this point the communication link H_{nm} between the nm antenna pair has been considered. If the number of antennas is increased, then a link coefficient set for each antenna pair results, which can be expressed in form of a channel matrix

$$\mathbf{H} = \begin{pmatrix} H_{11} & \dots & H_{1M} \\ \vdots & \ddots & \vdots \\ H_{N1} & \dots & H_{NM} \end{pmatrix}, \quad (2.4)$$

where H_{nm} stands for complex transfer function between the n -th receive antenna and the m -th transmit antenna and is computed with aid of (2.1). The difference between both is that instead of one communication link in (2.4) $N \times M$ links result, where N and M are the maximum number of antennas at the receiver and transmitter, respectively. This means that contrary to the implementation of antenna arrays, where multiple radiating elements are driven with a feeding network and a single antenna port, in MEA systems each antenna is driven individually. As result independent communication links can be built and parallel data streams can be used.

With (2.4) it is now possible to describe the received signal vector \mathbf{y} of such a communication system analog to (2.3) as

$$\mathbf{y}(t) = \mathbf{H}(t, \hat{t}) * \mathbf{x}(t) + \mathbf{n}(t), \quad (2.5)$$

or in frequency domain and dropping notation of the frequency dependence

$$\mathbf{y} = \mathbf{H}\mathbf{x} + \mathbf{n}, \quad (2.6)$$

with \mathbf{x} being the transmitted signal vector and \mathbf{n} representing the system's noise vector. As result (2.6) describes now the vector waveform signals involved in the multiple transmission links. From this it is seen that the two components to be accurately reproduced are the channel matrix and the system's noise. For the latter, both interference effects and Gaussian noise have to be considered. In this work focus will be given solely to the channel matrix in order to optimize the analysis and design of multiple antenna systems.

2.2 The antennas

Communication between two points is based on the transformation of bounded energy in the form of circuit voltages into electromagnetic fields capable of propagating in space and its receiving counterpart. Once the electromagnetic fields are generated the way they propagate

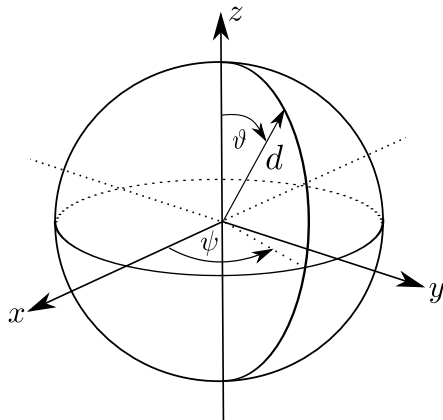


Figure 2.1: Coordinate system and geometrical description seen by an antenna.

depends on the channel properties, such as morphology, topography, etc. Depending on these factors different propagation phenomena take place. In free space, however the most significant role is played by the antennas, which act as electromagnetic transducers. Here antennas are classified into two groups: antennas on transmit and antennas on receive.

2.2.1 Antennas on transmit mode

In a communication channel, each antenna is responsible of using an input voltage V_{Tx} to radiate an electromagnetic field E and later transform this radiated field into a received voltage V_{Rx} . It thus follows that a relationship between the used voltage and the electric field exists. This relationship, called antenna gain, is also the paramount measure when evaluating antennas since it is a compact comparison measure. This can be seen from the fact that the antenna gain results from the quotient between the maximum power density (magnitude) of the antenna, $S_{Tx,max}$, resulting from

$$S_{Tx}(d, \vartheta, \psi) = \frac{|\vec{E}(d, \vartheta, \psi)|^2}{2Z_{F0}}, \quad (2.7)$$

and the power density of an isotropic source $S_{Tx,iso}$ with equal transmitting power, i.e. equal input power P_{Tx} at the antenna terminals ($V_{Rx} = 0$),

$$S_{Tx,iso} = \frac{P_{Tx}}{4\pi d^2}, \quad (2.8)$$

which serves as reference for all antennas. Here and in the rest of this thesis d , ϑ and ψ will be the distance, the elevation and the azimuth angle as depicted in 2.1. In this way the known expression for antenna gain results

$$G = \frac{|S_{Tx}(d, \vartheta, \psi)|_{max}}{S_{Tx,iso}} = 4\pi d^2 \frac{|\vec{E}(d, \vartheta, \psi)|_{max}^2}{2Z_{F0} P_{Tx}} \Bigg|_{d=const \geq FF}, \quad (2.9)$$

where d is a constant distance sufficiently far away from the antenna at which the electric field is observed. In this way the far field condition (FF) [Bal97] is guaranteed. Z_{F0} is the free-space impedance and $|\vec{E}(\vartheta, \psi)|_{\max}^2$ results from the maximum of

$$|\vec{E}(d, \vartheta, \psi)|^2 = \left(\sqrt{|E_\vartheta(d, \vartheta, \psi)|^2 + |E_\psi(d, \vartheta, \psi)|^2} \right)^2, \quad (2.10)$$

being E_ϑ and E_ψ the respective polar components of the electric field $\vec{E}(d, \vartheta, \psi)$ written as

$$\vec{E}(d, \vartheta, \psi) = E_\vartheta(d, \vartheta, \psi) \hat{\vec{\vartheta}} + E_\psi(d, \vartheta, \psi) \hat{\vec{\psi}}, \quad (2.11)$$

with $\hat{\vec{\vartheta}}$ and $\hat{\vec{\psi}}$ being the unitary vectors in the ϑ and ψ directions. In addition, since real antennas are angle dependent a directive gain also exists and is defined as

$$G(\vartheta, \psi) = 4\pi d^2 \frac{|\vec{E}(d, \vartheta, \psi)|^2}{2Z_{F0}P_{Tx}} \Bigg|_{d=\text{const} \geq \text{FF}}. \quad (2.12)$$

Finally, from the relationship between (2.9) and (2.12) a new measure widely used in the context of antennas, called the antenna radiation pattern, results

$$|\vec{C}(\vartheta, \psi)| = \sqrt{\frac{G(\vartheta, \psi)}{G}} = \frac{|\vec{E}(d, \vartheta, \psi)|}{|\vec{E}(d, \vartheta, \psi)|_{\max}} \Bigg|_{d=\text{const} \geq \text{FF}}, \quad (2.13)$$

where $\vec{C}(\vartheta, \psi)$ is given by

$$\vec{C}(\vartheta, \psi) = \frac{\vec{E}(d, \vartheta, \psi) e^{j\beta d}}{|\vec{E}(d, \vartheta, \psi)|_{\max}} \Bigg|_{d=\text{const} \geq \text{FF}}, \quad (2.14)$$

with β being the wavenumber defined as

$$\beta = \frac{2\pi}{\lambda}. \quad (2.15)$$

As result $G(\vartheta, \psi)$ can now be rewritten as

$$G(\vartheta, \psi) = |\vec{C}(\vartheta, \psi)|^2 G. \quad (2.16)$$

It should be noted, though, that none of the previous gain definitions are dependent on the distance d . The reason for this is that the radiated field itself is also distance dependent. Therefore, in (2.9) and (2.12) influence of d is cancelled and the previous gain definitions result.

If, however, either one of these gain definitions is solved for the electric field then an inverse dependence to d can be proven, as seen in (2.9) when solved for $|\vec{E}(d, \vartheta, \psi)|_{\max}$

$$|\vec{E}(d, \vartheta, \psi)|_{\max} = \sqrt{\frac{GZ_{F0}P_{Tx}}{2\pi d^2}}, \quad (2.17)$$

which, after substitution in (2.13), yields a general expression for the electric field $\vec{E}(d, \vartheta, \psi)$

$$\vec{E}(d, \vartheta, \psi) = \vec{C}(\vartheta, \psi) \sqrt{\frac{GZ_{F0}P_{Tx}}{2\pi}} \frac{e^{-j\beta d}}{d}. \quad (2.18)$$

In this way a compact expression describing the antenna behavior as electromagnetic transducer on transmit mode is found, that expresses the generated electromagnetic field in terms of input power P_{Tx} .

2.2.2 Antennas on receive mode

The expression in (2.18) is valid when an antenna is used to send information or electromagnetic signals. When used on receive mode a similar expression to the antenna gain exists. This expression is known as the antenna effective area A_{eff} and represents the, with power density S_{Tx} , radiated area seen by an antenna so that a power P_{Rx} can be delivered to the load. Therefore A_{eff} is given by the ratio between P_{Rx} and S_{Tx}

$$A_{\text{eff}} S_{Tx} = P_{Rx} \implies A_{\text{eff}} = \frac{P_{Rx}}{S_{Tx}}. \quad (2.19)$$

However, contrary to antenna gain, substitution of (2.7) in (2.19) shows no distance d term in the computation of A_{eff}

$$A_{\text{eff}} = \frac{2Z_{F0}P_{Rx}}{|\vec{E}(d, \vartheta, \psi)|_{\max}^2}. \quad (2.20)$$

This expresses mathematically the intuitively expected result that, in order to have a distance independent measure A_{eff} for the antenna on receive, P_{Rx} must depend on d . This means that the further the distance the smaller the received power becomes. Because of this, in order to derive the effective aperture of a single antenna both the received power and the incoming field should be known. In general, this requires a numerical computation. However, for certain antennas, P_{Rx} and $\vec{E}(d, \vartheta, \psi)$ can be computed analytically and out of it the following expression for A_{eff} results

$$A_{\text{eff}} = G \left(\frac{\lambda^2}{4\pi} \right), \quad (2.21)$$

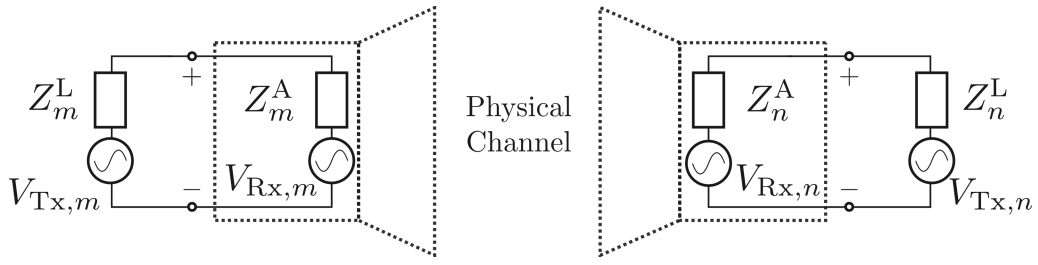


Figure 2.2: Equivalent circuit of transmit and receive antennas.

where λ is the wavelength of a certain frequency f . In general, it is not necessary to derive this expression for every antenna, since it can be proven valid for all reciprocal antennas [Bal97]. Here, as was the case with the gain, a non-directive measure is obtained. However, if $G(\vartheta, \psi)$ is used instead of G a directive $A_{\text{eff}}(\vartheta, \psi)$ is found.

2.2.3 Circuit model of communicating antennas

From a circuit perspective the previous discussion shows that antennas can act as loads when used together with a generator (source) or as electric sources when electromagnetic energy is received. The latter can be depicted for two communicating antennas by means of their Thevenin equivalent circuits [Bal97] as shown for antennas m and n in Figure 2.2. An equivalent Norton circuit can also be used [Kil00], but is less common and will therefore be omitted throughout this work.

2.2.3.1 Antenna losses

When energy is transmitted V_{Rx} becomes zero (in general¹) for the respective antenna and only the antenna impedance Z^A at the antenna terminals is seen. If, on the contrary, energy is received then V_{Tx} disappears, and the antenna only sees the load impedance Z^L (when transmitting, Z^L acts as the generator impedance as it is commonly known). In this way P_{Tx} in the previous equations becomes

$$P_{\text{Tx}} = \frac{|V_{\text{Tx}}|^2}{2} \left[\frac{R^A}{|Z^L + Z^A|^2} \right], \quad (2.22)$$

which in the case of a conjugate matched antenna (no resulting reactance, i.e. $X^A = -X^L$, and equal load and antenna resistance, i.e. $R^A = R^L$) is found to be

¹In scenarios where the antennas are located in the proximity of scattering objects, some energy will be reflected back to the antennas and V_{Rx} will not be zero. Here, this fact is ignored and it is assumed that the antennas are placed far enough from all possible scatterers so that $V_{\text{Rx}} = 0$ can be assumed

$$P_{\text{Tx}} = \frac{|V_{\text{Tx}}|^2}{8R^{\text{A}}} \quad (2.23)$$

and for a non-lossy antenna represents the total radiated power. If losses are considered, though, the antenna resistance R^{A} can be expressed as

$$R^{\text{A}} = R_{\text{rad}}^{\text{A}} + R_{\text{L}}^{\text{A}} \quad (2.24)$$

and the radiated power results only from the power seen at the radiating component $R_{\text{rad}}^{\text{A}}$, whereas the remaining power is delivered to the loss resistance R_{L}^{A} . In consequence an expression for the radiated power of the form

$$P_{\text{rad}} = \frac{|V_{\text{Tx}}|^2}{8R^{\text{A}}} \left[\frac{R_{\text{rad}}^{\text{A}}}{(R_{\text{L}}^{\text{A}} + R_{\text{rad}}^{\text{A}})} \right] = P_{\text{Tx}}\eta \quad (2.25)$$

results, where the quotient between the radiating and total antenna resistance

$$\eta = \frac{R_{\text{rad}}^{\text{A}}}{(R_{\text{L}}^{\text{A}} + R_{\text{rad}}^{\text{A}})} = \frac{R_{\text{rad}}^{\text{A}}}{R^{\text{A}}} \quad (2.26)$$

is known as the antenna radiation efficiency. In this way η accounts for both conductive and dielectric losses present in the antenna. Finally, with (2.25) an analogous expression to the antenna gain can be defined, based solely on the radiated power, known as directivity and equal to

$$D = 4\pi d^2 \frac{|\vec{E}(d, \vartheta, \psi)|_{\max}^2}{2Z_{\text{F0}}P_{\text{rad}}} \Bigg|_{d=\text{const} \geq \text{FF}} = \frac{G}{\eta}, \quad (2.27)$$

which leads to

$$G = \eta D. \quad (2.28)$$

In this case, as with antenna gain, consideration of a directive electric field, instead of its maximum value, results in an angle dependent measure for directivity $D(\vartheta, \psi)$ as well.

For a receiving antenna no equivalent definition to directivity exists, instead different types of antenna apertures are defined [Bal97]. These result from considering the power delivered to each part of the receiving circuit. Therefore, defining P_{Rx} as the induced (received) power at the load and assuming conjugate matching at the receiver the following expression for P_{Rx} can be found

$$P_{\text{Rx}} = \frac{|V_{\text{Rx}}|^2}{2} \left[\frac{R^{\text{L}}}{|Z^{\text{L}} + Z^{\text{A}}|^2} \right] = \frac{|V_{\text{Rx}}|^2}{8R^{\text{L}}} = \frac{|V_{\text{Rx}}|^2}{8R^{\text{A}}}, \quad (2.29)$$

which leads to the effective aperture A_{eff}

$$A_{\text{eff}} = \frac{|V_{\text{Rx}}|^2}{8R^{\text{L}}S_{\text{Tx}}}. \quad (2.30)$$

When $R^{\text{A}} = R_{\text{rad}}^{\text{A}}$, i.e. non-lossy antenna, (2.30) is equal to

$$A_{\text{s}} = \frac{|V_{\text{Rx}}|^2}{8R_{\text{rad}}^{\text{A}}S_{\text{Tx}}}, \quad (2.31)$$

as seen from (2.29). Yet, in the case of a conjugate matched lossy antenna, where $R^{\text{L}} = R^{\text{A}} = R_{\text{rad}}^{\text{A}} + R_{\text{L}}^{\text{A}}$, the relationship between (2.30) and (2.31) is given by η . It thus follows that A_{eff} results from multiplying (2.31), defined as the scattering area A_{s} in [Bal97], with the radiation efficiency η

$$A_{\text{eff}} = \eta \frac{|V_{\text{Rx}}|^2}{8R_{\text{rad}}^{\text{A}}S_{\text{Tx}}} = \eta A_{\text{s}}. \quad (2.32)$$

In a similar way substituting G in (2.21) with ηD from (2.27) yields

$$A_{\text{eff}} = \eta D \left(\frac{\lambda^2}{4\pi} \right). \quad (2.33)$$

With (2.28) and (2.33) antenna losses can now be considered in both transmit and receive mode. However, other forms of power loss also occur in antenna systems, such as non perfectly matched feeding circuits and polarization mismatch between receiving and transmitting antennas. In the following these two loss types will be introduced.

2.2.3.2 Feeding circuit losses

Up to this point, when computing the transmitted or received power, conjugate antenna matching has been assumed. However, real antenna driving circuits need not to be matched to the antenna. Furthermore, in some cases due to high bandwidths they can't be perfectly matched in the whole frequency range. This mismatch between driving circuit and antenna causes power to be inefficiently delivered to the antenna, when transmitting, or to the load, when receiving. To account for impedance (load) mismatches a measure called the reflection efficiency exists and it is defined based on the ratio between the power effectively delivered to a loading circuit (for example antenna) and the available power as

$$\eta_{\ell} = \frac{P_{\text{delivered}}}{P_{\text{available}}} = \frac{P^{+} - P^{-}}{P^{+}} = 1 - |\Gamma|^2, \quad (2.34)$$

where the superscripts + and - refer, respectively, to the incident and reflected wave at the interface between two circuit parts and Γ is the reflection coefficient given by the ratio between the incident and reflected voltages, V^{+} and V^{-} , found to be

$$\Gamma = \frac{V^-}{V^+} = \frac{Z_1 - Z_2}{Z_1 + Z_2}, \quad (2.35)$$

with Z_1 and Z_2 being the impedances seen at the interface between two circuits. In the case here discussed, Z_1 and Z_2 are equal to either Z^A and Z^L (antenna on transmit) or Z^L and Z^A (antenna on receive) and η_ℓ is a measure of the amount of power used at the antenna or the load, depending on the operation mode considered. In this way, the maximum antenna gain achievable in a mismatched circuit, also called realized gain \hat{G} , is

$$\hat{G} = \eta(1 - |\Gamma|^2)D, \quad (2.36)$$

where (2.16) in this case yields

$$\hat{G}(\vartheta, \psi) = |\vec{C}(\vartheta, \psi)|^2 \hat{G}. \quad (2.37)$$

Therefore, the effective antenna aperture is

$$A_{\text{eff}} = \eta(1 - |\Gamma|^2)D \left(\frac{\lambda^2}{4\pi} \right). \quad (2.38)$$

As result P_{Tx} and P_{Rx} are given, in a mismatched circuit, as

$$P_{\text{Tx}} = \frac{|V_{\text{Tx}}|^2}{8R^A} \frac{1}{(1 - |\Gamma|^2)} \quad \text{and} \quad P_{\text{Rx}} = \frac{|V_{\text{Rx}}|^2}{8R^A} (1 - |\Gamma|^2). \quad (2.39)$$

This result is very important since it shows a clear difference between P_{Tx} and P_{Rx} . P_{Tx} represents the available power needed in order to achieve (2.28), i.e. the maximum gain under matched conditions, whereas P_{Rx} represents the power delivered to the load in receiving mode.

2.2.3.3 Polarization losses

Polarization losses refer to the loss of power due to polarization mismatch between transmitting and receiving antennas. It assumes the existence of a communication link, i.e. signal transmission from point A to point B. And can therefore only occur when a signal is received, since it results from the interaction between the receiving antenna radiation pattern and the impinging electric field. In general, it is the result of the scalar product between the electric field vectors of the incoming signal and the receiving antenna. Therefore, if the electric field \vec{E} is expressed in terms of a polarization vector $\hat{\rho}$, instead of $\hat{\vartheta}$ and $\hat{\psi}$ as in (2.11), the Polarization Loss Factor (PLF) [Bal97] can be expressed as

$$\text{PLF} = |\hat{\rho}_{\text{Tx}} \cdot \hat{\rho}_{\text{Rx}}|^2, \quad (2.40)$$

where $\hat{\vec{\rho}}_{\text{Tx}}$ and $\hat{\vec{\rho}}_{\text{Rx}}$ are the polarization vectors of impinging electric field (same as that of the transmitting antenna) and the receiving antenna. In this way only the performance of the antenna on receive mode is affected by polarization mismatches and yields an A_{eff} equal to

$$A_{\text{eff}} = \eta(1 - |\Gamma|^2)D \left(\frac{\lambda^2}{4\pi} \right) |\hat{\vec{\rho}}_{\text{Tx}} \cdot \hat{\vec{\rho}}_{\text{Rx}}|^2 = \hat{G} \left(\frac{\lambda^2}{4\pi} \right) |\hat{\vec{\rho}}_{\text{Tx}} \cdot \hat{\vec{\rho}}_{\text{Rx}}|^2. \quad (2.41)$$

In the following it will be shown how, out of the definitions previously given and under consideration of the previously discussed types of losses, a relationship between the input and output signal can be found for different types of propagation channels.

2.3 The propagation channel

In this section the mathematical background for the computation of the transmission coefficient H_{mn} in different propagation channels is presented. As reference the communication channel of Figure 2.2 is used. However, a single operation mode at each side of the communication link [Bal97] will be assumed, given the fact that in real systems at any given moment antennas work either on transmit or receive, which is equivalent to having either $V_{\text{Tx}} = 0$ or $V_{\text{Rx}} = 0$, depending on the case. Because of this, in the following, the assumption will be made that in Figure 2.2 antenna m is transmitting and antenna n is receiving. In this way it will be described how a transmission coefficient H_{nm} can be found that summarizes the antenna and wave propagation effects in different channel types.

2.3.1 The free space propagation channel

Free space propagation channels are defined as those in which the propagation channel does not interfere with the electromagnetic waves since no objects are present to modify the behavior of the electromagnetic field. Therefore, in free space finding the transmission coefficient H_{nm} reduces to finding an expression for the received voltage in terms of transmitted voltage. This can be done by using (2.19) to express the received power $P_{\text{Rx},n}$ in terms of the impinging power density $S_{\text{Tx},m}$ and $A_{\text{eff},n}$

$$P_{\text{Rx},n} = A_{\text{eff},n}(\vartheta_n, \psi_n) S_{\text{Tx},m}(d_{nm}, \vartheta_m, \psi_m). \quad (2.42)$$

Here, two changes have been made with respect to previous expression (2.19) the subscripts m and n have been introduced to refer to the transmitting and receiving antennas and the directive expressions for A_{eff} and S_{Tx} have been used. In addition the distance d_{nm} refers now to the distance between the nm antenna pair. Substituting (2.7) and (2.41) in (2.42) and equating this expression with (2.39)

$$P_{\text{Rx},n} = A_{\text{eff},n} \frac{|\vec{E}_m(d_{nm}, \vartheta_m, \psi_m)|^2}{2Z_{F0}} = \frac{|V_{\text{Rx},n}|^2}{8R_n^A} (1 - |\Gamma_n|^2)$$

allows solving for $|V_{\text{Rx},n}|$, thus yielding

$$|V_{\text{Rx},n}| = \sqrt{\left(\hat{G}_n(\vartheta_n, \psi_n) |\hat{\rho}_{\text{Tx}} \cdot \hat{\rho}_{\text{Rx}}|^2 \frac{\lambda^2}{4\pi} \right) \left(\frac{|\vec{E}_m(d_{nm}, \vartheta_m, \psi_m)|^2}{2Z_{F0}} \right) \frac{8R_n^A}{1 - |\Gamma_n|^2}}. \quad (2.43)$$

(2.43) can now be rewritten, using (2.36) and (2.37), into

$$|V_{\text{Rx},n}| = \sqrt{\eta_n D_n \frac{\lambda^2}{\pi} \frac{R_n^A}{Z_{F0}} |\vec{C}_n(\vartheta_n, \psi_n)| |\vec{E}_m(d_{nm}, \vartheta_m, \psi_m)| |\hat{\rho}_{\text{Tx}} \cdot \hat{\rho}_{\text{Rx}}|}, \quad (2.44)$$

which is equivalent to

$$V_{\text{Rx},n} = \sqrt{\eta_n D_n \frac{\lambda^2}{\pi} \frac{R_n^A}{Z_{F0}}} \vec{C}_n(\vartheta_n, \psi_n) \cdot \vec{E}_m(d_{nm}, \vartheta_m, \psi_m). \quad (2.45)$$

If now (2.18) is used in place of \vec{E}_m a compact expression for $V_{\text{Rx},n}$ based only on known system parameters results

$$V_{\text{Rx},n} = \sqrt{8R_n^A \eta_n D_n \hat{G}_m P_{\text{Tx},m}} \left(\frac{\lambda}{4\pi} \right) \vec{C}_n(\vartheta_n, \psi_n) \cdot \vec{C}_m(\vartheta_m, \psi_m) \frac{e^{-j\beta d_{nm}}}{d_{nm}}. \quad (2.46)$$

Finally, replacing $P_{\text{Tx},m}$ with (2.39) gives

$$V_{\text{Rx},n} = |V_{\text{Tx},m}| \sqrt{\frac{R_n^A}{R_m^A} \eta_n \eta_m D_n D_m} \left(\frac{\lambda}{4\pi} \right) \vec{C}_n(\vartheta_n, \psi_n) \cdot \vec{C}_m(\vartheta_m, \psi_m) \frac{e^{-j\beta d_{nm}}}{d_{nm}}, \quad (2.47)$$

which, after noting that $V_{\text{Tx},m}$ is equal to $|V_{\text{Tx},m}|$ (phase term $e^{j\varphi_m(d)}$ vanishes at $d = 0$), yields the desired transmission coefficient H_{nm}

$$H_{nm} = \frac{V_{\text{Rx},n}}{V_{\text{Tx},m}} = \sqrt{\frac{R_n^A}{R_m^A} \eta_n \eta_m D_n D_m} \left(\frac{\lambda}{4\pi} \right) \vec{C}_n(\vartheta_n, \psi_n) \cdot \vec{C}_m(\vartheta_m, \psi_m) \frac{e^{-j\beta d_{nm}}}{d_{nm}}. \quad (2.48)$$

This expression for the SISO case resembles the one found in terms of P_{Tx} and P_{Rx} in [GW98, Eq. (2.45)]. Yet, it extends its significance by explicitly addressing all type of losses present in the antennas when operated in both transmit and receive modes. In this way it is shown from an electromagnetic perspective that the transmission coefficient H_{nm} does not depend on the driving or loading circuits at either end of the communication link. The amount of power

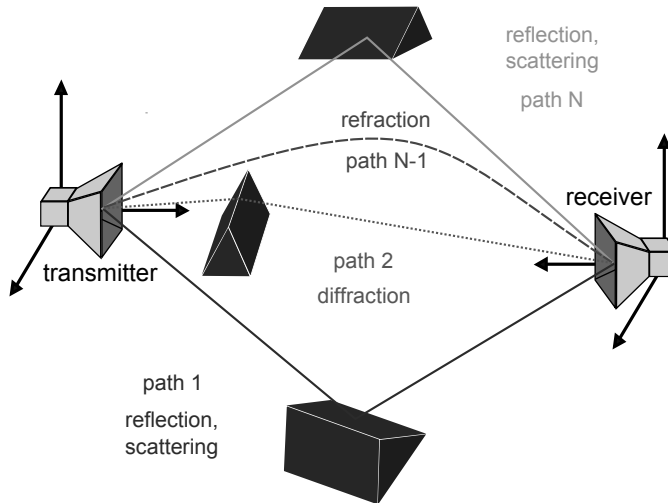


Figure 2.3: Equivalent circuit of transmit and receive antennas.

delivered to both the transmitting antenna and the load, on the other hand, does indeed depend on the matching circuits.

2.3.2 Multipath propagation channels

In free space, there are no objects capable of interacting with the propagating electromagnetic wave containing the communication signal. Real scenarios, however, do not resemble the free space behavior. On the contrary, in most cases several interactions with the environment occur before the electromagnetic signal is received at the other end of the communication channel. Furthermore, the interaction type needs not to be of a certain kind, but several propagation phenomena can occur. These are scattering, reflection, diffraction and refraction, as depicted in Figure 2.3. Discussion of each of these interactions goes beyond the scope of this introductory chapter and it is not the focus of this work. Therefore, at this point it suffices to mention that due to these different interactions, in general, more than one propagation path exists, as shown in Figure 2.3. Furthermore, because of these multiple interactions (2.48) needs to be revised for the case of multiple propagating paths.

In (2.48), the transmission coefficient H_{nm} is given in terms of the scalar multiplication from the vectorial radiation patterns for both the receiving and transmitting antennas. This means that each polar component of the transmitting antenna is multiplied with its equal on the receiving side. Furthermore, since in (2.48) free space is considered then no interaction between the different polarization types exists. In consequence (2.48) can be rewritten as

$$H_{nm} = \sqrt{\frac{R_n^A}{R_m^A} \eta_n \eta_m D_n D_m} \left(\frac{\lambda}{4\pi} \right) \begin{pmatrix} C_{\vartheta,n} \\ C_{\psi,n} \end{pmatrix}^T \frac{e^{-j\beta d_{nm}}}{d} \begin{bmatrix} 1 & 0 \\ 0 & 1 \end{bmatrix} \begin{pmatrix} C_{\vartheta,m} \\ C_{\psi,m} \end{pmatrix}, \quad (2.49)$$

where the angle dependences have been dropped for brevity. In addition, the subscript nm for the distance factor has also been omitted. This is justified since when dealing with arrays small variations in the distance have little impact on the amplitude of the incoming signal, but not so in the phase. With (2.49) it is thus seen that transmission in free space can be expressed also in terms of a transmission matrix \mathbf{T}

$$\mathbf{T}_{nm} = \frac{e^{-j\beta d_{nm}}}{d} \begin{bmatrix} 1 & 0 \\ 0 & 1 \end{bmatrix}, \quad (2.50)$$

which describes the way in which a certain communicating path is modified by the propagation channel. Here, as done in the context of MIMO systems, \mathbf{T} is referred to as a matrix, however in terms of tensors \mathbf{T} can be seen as a second order tensor or in terms of dyads as a dyadic function, in which case it is written as $\overset{\leftrightarrow}{T}$. All of these definitions are equivalent and need to be kept in mind for later when the concept of dyadic Green's function appears. Resuming with H_{nm} , (2.49) is now given by

$$H_{nm} = \sqrt{\frac{R_n^A}{R_m^A} \eta_n \eta_m D_n D_m} \left(\frac{\lambda}{4\pi} \right) \begin{pmatrix} C_{\vartheta,n} \\ C_{\psi,n} \end{pmatrix}^T \mathbf{T}_{nm} \begin{pmatrix} C_{\vartheta,m} \\ C_{\psi,m} \end{pmatrix}. \quad (2.51)$$

In free space the expression for \mathbf{T} is straightforward and results only in an attenuation and phase change of the electromagnetic wave. Multi path channels, however, result not only in more complex interactions between the transmitted and received polar components, but also in an additional number of paths that needs to be considered. In consequence, both effects need to be considered.

Assuming that there is only one path between antennas n and m , but that it is subject to one or more propagation phenomena, no conclusion can be drawn regarding the elements of \mathbf{T} . Most likely, however, no term will vanish and \mathbf{T} will be a full matrix. If now, in addition multiple paths are considered, as result of scattering objects, then for each path p a transmission matrix \mathbf{T}_p results. The received signal is therefore obtained from the sum of all incoming paths which renders the following equation

$$H_{nm} = \sqrt{\frac{R_n^A}{R_m^A} \eta_n \eta_m D_n D_m} \left(\frac{\lambda}{4\pi} \right) \sum_{p=1}^P \begin{pmatrix} C_{\vartheta,n}(\Omega_{n,p}) \\ C_{\psi,n}(\Omega_{n,p}) \end{pmatrix}^T \mathbf{T}_{nm,p} \begin{pmatrix} C_{\vartheta,m}(\Omega_{m,p}) \\ C_{\psi,m}(\Omega_{m,p}) \end{pmatrix}, \quad (2.52)$$

where Ω represents the pair of angles (ϑ, ψ) . P is the number of paths propagating from antenna m to antenna n , where each path is subject to a different propagation (fading) process. And \mathbf{T}_p contains the channel polarization response in amplitude and phase of path p and accounts also

for any coordinate changes that might be desired. As example T_{22} in [GW98] is -1 for a free space transmission due to the coordinate system definition used at the receiver (see Figure 2.3).

Throughout the following chapters it will be seen that the existence of multiple paths is of great importance for maximizing the transmitted information since it can enrich the diversity of the signal. This means that having a significant number of scattering objects can result in a better angular spread of the outgoing and incoming signals at the transmitter and receiver. This richness (or lack of) thus defines the scenario and favors the existence of independent signal paths when multiple antennas are used. This is the fundamental principle behind multiple element antenna systems and the following chapters will build on its understanding for the evaluation and design of multiple element antenna systems in regard to information throughput maximization.

3 Modeling of multiple element antenna systems

Given the fact that most systems are subject to multipath propagation a research trend toward physical channel models exists [ABB⁺07]. Furthermore, these models have shown to be valuable from a simulative perspective, and more recently also for the channel estimation of measured scenarios [THL⁺03], since they make possible the analysis of different antenna types and configurations. However, so far, the complexity of such systems has been an impediment leading to consideration of real multi-path environments in an oversimplified or not sufficiently detailed manner [ABB⁺07]. In the case of channel estimation from measurements the significant amount of data to be processed as well as the considerable difficulties it poses have also limited more generalized studies. Therefore, a need for easy integration of double-directional multipath propagation models with flexible and realistic system evaluation seems at hand. In this chapter, a faster, general and flexible simulation framework for multiple element antenna systems is presented along with its integration with path-based propagation channels. Even though the model is general and extensible for system analysis, focus will lie on the communication channel, i.e. the interaction between the antennas and the propagation channel. For this, network theory will be used, which is a convenient way to describe the interaction of fields and waves through power waves and scattering parameters.

This chapter is divided in two main parts. The first one dealing with the generalized network model [WSW04] of the whole communication chain, comprising the antennas, matching network and propagation channel. And the second section where a modal extension of this model is introduced along with the simulation assumptions and criteria used in this work.

3.1 Exact system model

At least two rigorous network models for path-based channels have been independently published in the past [WJ04, WSW04]. In this section the generalized network model of [WSW04], further explained in [Wal04], will be presented. It consists of a network theory model of the whole transmission chain, i.e. transmitter unit (signal source), transmit antennas, physical channel, receive antennas, and receiver unit (signal drain) modeled as networks described by scattering matrices as seen in Fig. 3.1 for the antenna pair nm , where the S-Parameter matrix of the propagation channel $\mathbf{S}^{\hat{C}}$ is of the form

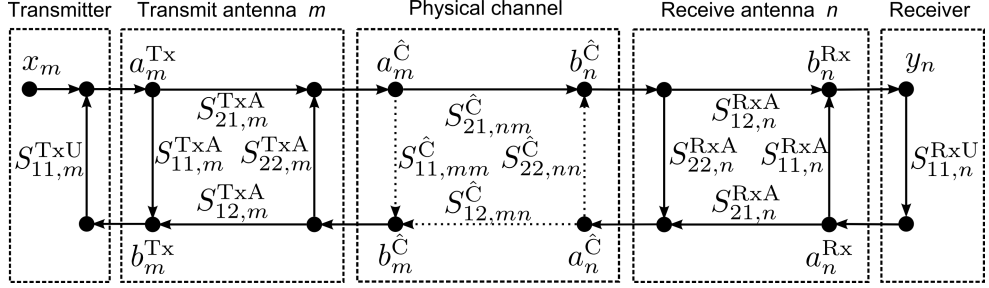


Figure 3.1: Signal flow graph of generalized network model.

$$\mathbf{S}^{\hat{C}} = \begin{pmatrix} \mathbf{S}_{11}^{\hat{C}} & (M \times M) & | & \mathbf{S}_{12}^{\hat{C}} & (M \times N) \\ - & \hline & | & - & \hline & \mathbf{S}_{21}^{\hat{C}} & (N \times M) & | & \mathbf{S}_{22}^{\hat{C}} & (N \times N) \end{pmatrix}, \quad (3.1)$$

with N and M being the number of receiving and transmitting antennas for the system under test.

With this model it is possible to take into account effects like signal correlation or antenna coupling and additional components such as matching networks [WJ04]. However, in order to use the previous model an accurate description of all S-Parameters needs to be given. In the case of the antennas and the physical channel, this can only be done through measurements or use of numerical methods that deterministically model the interaction between the antennas and the scenario. This results in a path-based description of the propagation, which comes at a high computational cost and complexity. Therefore, in order to simplify the understanding of the whole transmission chain, it makes sense to use a joint network for the antennas and channel, as done in [WSW04], resulting in the extended channel of Figure 3.2.

This compact form of the generalized network model results from two assumptions: (1) there is no back transmission ($\mathbf{S}_{12}^{\hat{C}} = 0$), i.e. unilateral propagation channel, and (2) there are no scatterers in the proximity of both the transmit and receive antennas ($\mathbf{S}_{11}^{\hat{C}} = 0$ and $\mathbf{S}_{22}^{\hat{C}} = 0$). It

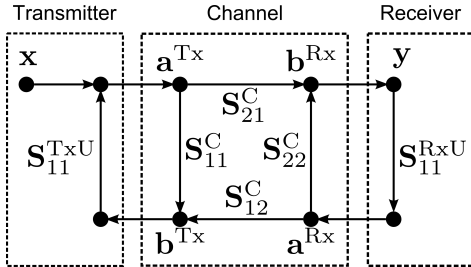


Figure 3.2: Signal flow graph of generalized network model in its compact form, i.e. transmit antennas, physical channel and receive antennas merged into one network.

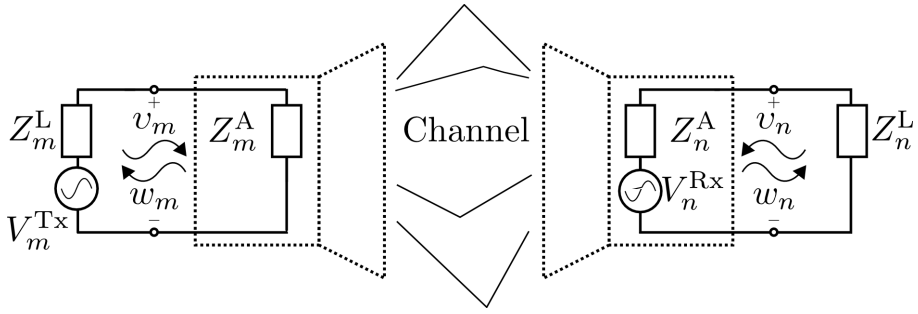


Figure 3.3: Equivalent circuit of transmit and receive antennas.

thus follows that, after some algebraic transformations of the original model (Figure 3.1), the merged inner network can be expressed as

$$\mathbf{S}^C = \begin{pmatrix} \mathbf{S}_{11}^{TxA} & | & \mathbf{0} \\ \mathbf{S}_{21}^{TxA} \hat{\mathbf{S}}_{21}^C \mathbf{S}_{12}^{RxA} & | & \mathbf{S}_{11}^{RxA} \end{pmatrix}. \quad (3.2)$$

Here, the term \mathbf{S}_{21}^C given by $\mathbf{S}_{21}^{TxA} \hat{\mathbf{S}}_{21}^C \mathbf{S}_{12}^{RxA}$ results from the transmission coefficients between all transmitting and receiving ports and constitutes the transmission submatrix of the extended channel scattering matrix \mathbf{S}^C .

For the case of a signal transmitted from port m to port n under matched conditions, $S_{21,nm}^C$ yields the channel matrix \mathbf{H} , i.e. the ratio between the received voltage V_n induced by the incoming field \vec{E}_m and the excitation voltage V_m as seen in section 2.3. Here, we rewrite (2.52) as

$$H_{nm} = S_{21,nm}^C = \sqrt{\frac{R_n^{RxA}}{R_m^{TxA}} G_n^{Rx} G_m^{Tx}} \left(\frac{\lambda}{4\pi} \right) \gamma_{nm},$$

with the link γ_{nm} given by

$$\gamma_{nm} = \sum_{p=1}^P \left(\vec{C}_n^{Rx}(\Omega_{p,n}^{Rx}) \cdot \mathbf{T}_{p,nm} \cdot \vec{C}_m^{Tx}(\Omega_{p,m}^{Tx}) \right). \quad (3.3)$$

What this equation shows is that once a certain physical channel $S_{21,nm}^C$, expressed here through the full polarimetric transmission matrix \mathbf{T} , is known for a certain nm communication link, the gains G_n^{Rx} and G_m^{Tx} and the normalized radiation patterns \vec{C}_n^{Rx} and \vec{C}_m^{Tx} of both receive antenna n and transmit antenna m at the $\Omega_{p,n}^{Rx}$ direction of arrival and the $\Omega_{p,m}^{Tx}$ direction of departure have to be included for all P paths. Therefore, for each combination of antenna types, orientations or polarizations of interest, a new \mathbf{S}^C has to be calculated. The latter greatly limits the amount

of possible configurations that can be studied and thus represents a great bottleneck common to both simulations and measurements when dealing with multi-path propagation channels. To overcome this difficulty, the inclusion of a modal antenna representation is suggested.

3.2 Modal network model of communication channel

A limitation of the previous modeling approach, used throughout the literature, is that computation of the transmission matrix S_{12}^C for a certain configuration requires the processing of every single path p for every communication link nm . In addition, if it is considered that for statistic purposes in each studied scenario there are L channel realizations, in the case of this work L possible positions for the mobile station, with several thousand paths each, the computational cost becomes restrictive.

A modal description of antennas for investigation of communication systems has been already proposed in the literature [AGW⁺02, KHE05, KAE06, GN06, CPGZ09]. In [AGW⁺02] it is proven that a modal description of the base station antenna results in very similar radiation patterns to those of measured antennas. Yet, no integration into the modeling of the MIMO system is discussed. In [KHE05], on the other hand, a complete MIMO system based on the modal description of dipoles is shown, whereas in [KAE06] spiral antennas are used. In these works it is proven that the use of a spherical mode expansion can reproduce accurately the channel behavior with respect to capacity (see 4) and correlation. However, this is done on the basis of a current based spherical expansion, similar to that of [CS91], which poses a considerable limitation when dealing with typical antennas for which no current distribution is known. Moreover, in [KHE05, KAE06] no typical base station antennas were handled or discussed. In a similar manner in [GN06] also a very simplified channel with non realistic antenna configurations is used. Nonetheless, a simpler expression for the antenna electric field in terms of spherical waves (without currents) is found for dipole antennas. Finally, in [CPGZ09] a MIMO system based on the spherical description of dipoles under consideration of mutual coupling is introduced for short range MIMO applications. Even though [CPGZ09] provides an accurate representation of the communication problem it does not consider complex propagation scenarios such as the urban one and does not provide a system simulation framework. In fact, this is a common issue among all the previously discussed works [AGW⁺02, KHE05, KAE06, GN06, CPGZ09]. Therefore, in this work the use of a modal description of typical base station and mobile station antennas is done in conjunction with a complex propagation scenario, without knowledge of the antenna currents. In this manner multipath processing becomes significantly reduced and the study of multiple antennas and/or orientations becomes feasible.

3.2.1 Inclusion of the modal expansion

A way in which the computational effort of exact network models can be reduced is if the transmission coefficient S_{21}^C of the extended channel is expressed as a sum of basis functions (basis channels). In this way, once the basis functions have been determined, computing the channel response for another antenna reduces to finding an adequate set of coefficients for the basis functions. However, this does not seem practical in general since both the antennas and the physical channel change depending on the configuration and the channel realization. An alternative approach is found by expressing the antenna radiation patterns as a sum of the normalized outgoing spherical wave functions \vec{E} [Han88]

$$\vec{C}(\vartheta, \psi) \approx \sum_{w=1}^W b_w \vec{E}_{w,norm}, \quad (3.4)$$

where b_w are the wave coefficients of the radiated pattern approximated by the first W spherical wave functions, thus, not an identity. And where the normalized spherical wave function $\vec{E}_{w,norm}$ can be expressed as

$$\vec{E}_{w,norm} = \frac{\vec{E}_i(\vartheta, \psi)}{|\vec{E}_w(\vartheta, \psi)|_{\max}} = \check{e}_{\vartheta,w}(\vartheta, \psi) \hat{\vartheta} + \check{e}_{\psi,w}(\vartheta, \psi) \hat{\psi}, \quad (3.5)$$

where $\check{e}_{\vartheta,w}$ and $\check{e}_{\psi,w}$ are the ϑ and ψ polar components of the i -th normalized spherical wave function. In this way the radiation patterns of both transmit and receive antennas in (3.1) can be rewritten according to (3.4) thus resulting in the following expression for $S_{21,nm}^C$ and the link transmission coefficient γ_{nm} of the extended channel

$$S_{21,nm}^C = \kappa_{nm} \gamma_{nm}, \quad (3.6)$$

$$\gamma_{nm} = \sum_{r=1}^R \sum_{q=1}^Q b_{r,n}^{\text{Rx}} b_{q,m}^{\text{Tx}} \check{\gamma}_{rq,nm}, \quad (3.7)$$

where $\check{\gamma}_{rq,nm}$ constitutes the rq subfunction of the link γ_{nm} defined as

$$\check{\gamma}_{rq,nm} = \sum_{p=1}^{P_l} \begin{pmatrix} \check{e}_{\vartheta,r}(\Omega_{p,n}^{\text{Rx}}) \\ \check{e}_{\psi,r}(\Omega_{p,n}^{\text{Rx}}) \end{pmatrix}^T \mathbf{T}_{p,nm} \begin{pmatrix} \check{e}_{\vartheta,q}(\Omega_{p,m}^{\text{Tx}}) \\ \check{e}_{\psi,q}(\Omega_{p,m}^{\text{Tx}}) \end{pmatrix} \quad (3.8)$$

and κ_{nm} is a multiplicative factor resulting from (3.1)

$$\kappa_{nm} = \sqrt{\frac{Z_{0,m}}{Z_{0,n}}} \sqrt{\frac{R_n^{\text{Rx}}}{R_m^{\text{Tx}}} G_n^{\text{Rx}} G_m^{\text{Tx}}} \left(\frac{\lambda}{4\pi} \right). \quad (3.9)$$

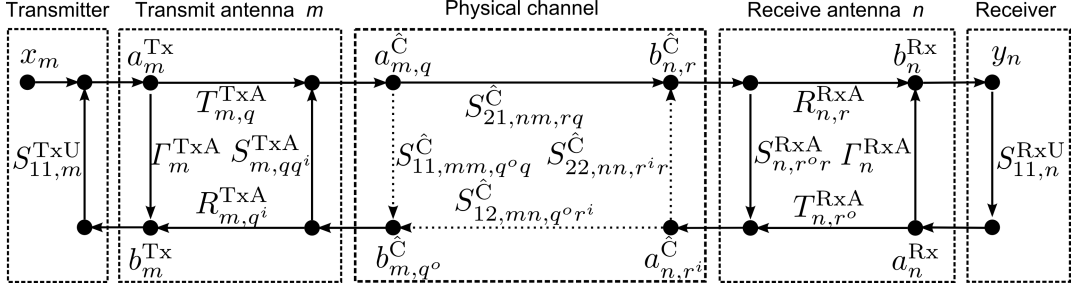


Figure 3.4: Signal flow graph of modal network model.

It follows from (3.6) that through the use of antenna propagation modes, in this case spherical wave functions, a pseudo modal expression for the transmission coefficient of the extended channel has been found, where the $\check{\gamma}_{rq,nm}$ functions build the scenario-dependent basis set. As result the extended channel transmission coefficient of any desired antenna pair can now be expressed as a weighted sum of basis functions for the specific scenario considered, assuming that the number of modes R and Q accurately describe the antennas to be studied (see sections 3.2.3 and 3.2.4). It should be noted that for wideband applications it suffices to consider a finite set of modes. This is due to the high Q-factors (strong reactive near field) in higher order modes, which leads to high losses and low bandwidth [Han81, Han88]. The resulting modal network model is shown in Figure 3.4 for the nm antennas pair and the rq modes pair.

In Figure 3.4 the notation of the antennas S-Parameter matrix used in Figure 3.1 and [WSW04] has been replaced, for conformity, with the notation used by Hansen [Han88] for spherical wave propagation, where the antenna scattering matrix is of the form

$$\mathbf{S} = \begin{pmatrix} \check{\Gamma} & \check{\mathbf{R}} \\ \check{\mathbf{T}} & \check{\mathbf{S}} \end{pmatrix}. \quad (3.10)$$

In addition, since the assumption of no channel backscattering and no back transmission matrices is taken over from the generalized network model, the submatrices $\check{\mathbf{S}}^{\text{TxA}}$, $\check{\mathbf{R}}^{\text{TxA}}$, $\check{\mathbf{S}}^{\text{RxA}}$ and $\check{\mathbf{T}}^{\text{RxA}}$ vanish. Therefore, it can be seen in Figure 3.4 that the inclusion of the signal source and signal drain remains unchanged in spite of the newly defined model. In consequence, this approach allows the computation of the \mathbf{H} extended channel matrix in a modal manner without adding complexity to the evaluation of port mismatches. Because of this, the study of feeding network effects will be omitted in the following.

3.2.2 Computational gain

From Figure 3.4 it is seen that the complexity of the system is increased since the interactions of every received (incoming) and transmitted (outgoing) mode r and q related to all scattered

(outgoing) and reflected (incoming) mode r^o and q^i need to be known at both the channel and the antennas. This suggests that if too many modes are used for the antennas description, the modal approach presented may become unfavorable. To explore this issue, the computational cost of the modal implementation vs. the traditional one is considered. In the generalized network model of section 3.1, regardless of M and N , evaluation of \mathcal{N} and \mathcal{M} different receiving and transmitting antennas requires \mathcal{NM} computations of γ_{nm} . This yields $P\mathcal{NM}$ operations for each antenna (position) pair nm at each channel realization (3.3). For the modal case computation of all necessary basis functions requires PRQ operations (3.8) and computation of the \mathcal{NM} antennas of interest additional $RQ\mathcal{NM}$ (3.6). This leads to the inequality

$$RQ(P + \mathcal{NM}) < P(\mathcal{NM}), \quad (3.11)$$

which can be rewritten as

$$\frac{aP}{P - a} < b, \quad (3.12)$$

where $a = RQ$ and $b = \mathcal{NM}$. Considering now that in scattering scenarios the number of paths P is significantly greater than the number of modes to be considered, (3.12) reduces to $a < b$, which means that for the modal network model to be efficient more antennas than modes have to be considered. It follows that the quotient b/a gives a measure of the simulation gain. For the case of dipoles, it will be shown that this means studying more than three different antenna orientations, since dipoles can be exactly described at all desired orientations with only three spherical modes. When considering different antenna types, the number of antennas to be studied have to exceed the number of modes required for adequate description, which depend on the antenna size as discussed in [RGZ05].

With this modal network model it is now possible to save valuable time in otherwise very lengthy simulations and, more importantly, significantly increase the number of configurations that can be studied. For example, if a modal description of the base station is available for outdoor channels, in addition to being able to consider different antenna types, different cell sectorizations can be considered with only a one time computation of the link γ_{nm} . In the case of the mobile station, on the other hand, different orientations can be analyzed. Based on this in the following section a thorough study of the mobile station antenna effects on an urban MIMO scenario will be presented.

3.2.3 Modal description of mobile station

In the previous section it was shown how the whole transmission chain of a certain communication link could be more easily computed through the modal description of the transmit and

receive antennas. Furthermore, it was shown that by doing so it is possible to obtain the channel matrix \mathbf{H} of any desired configuration by a weighted sum of the transmission coefficients of the basis modes. In the general case, these modes correspond to both the transmit and receive antennas, but this is not always the case. For example, it might be of interest to evaluate several mobile station antennas referenced to only one base station. In this case (3.6) becomes

$$S_{21,nm}^C = \kappa_{nm} \sum_{r=1}^R b_{r,m}^{\text{Rx}} \sum_{p=1}^{P_l} \check{\gamma}_{r,nm} \quad (3.13)$$

with

$$\check{\gamma}_{r,nm} = \begin{pmatrix} \check{e}_{\vartheta,r}(\Omega_{p,n}^{\text{Rx}}) \\ \check{e}_{\psi,r}(\Omega_{p,n}^{\text{Rx}}) \end{pmatrix}^T \mathbf{T}_{p,nm} \begin{pmatrix} C_{\vartheta}(\Omega_{p,m}^{\text{Tx}}) \\ C_{\psi}(\Omega_{p,m}^{\text{Tx}}) \end{pmatrix}, \quad (3.14)$$

where C_{ϑ} and C_{ψ} are the ϑ and ψ components of the radiation pattern \vec{C} .

In chapter 5, (3.13) will be used to investigate the effect of antenna inter-element spacing and polarization in an urban scenario for modal described ideal dipoles at the mobile station. For this purpose the modal description of an arbitrarily oriented dipole will be used.

Arbitrarily oriented dipoles

In [Han88] the modal description of dipoles oriented along the x , y and z axis is given. Out of it, the coefficients needed to express an arbitrary oriented dipole can be deduced to be:

$$b_2(\alpha_{Az}, \alpha_{El}) = \frac{\sqrt{2}}{2} \sin(\alpha_{Az}) (\sin(\alpha_{El}) + j \cos(\alpha_{El})), \quad (3.15a)$$

$$b_6(\alpha_{Az}, \alpha_{El}) = -j \frac{\sqrt{2}}{2} \sin(\alpha_{Az}) (\sin(\alpha_{El}) - j \cos(\alpha_{El})), \quad (3.15b)$$

$$b_4(\alpha_{Az}) = \cos(\alpha_{Az}), \quad (3.15c)$$

$$b_i = 0, i \neq 2, 4, 6, \quad (3.15d)$$

where α_{Az} is the rotation angle with respect to the z axis, i.e. rotation angle in elevation, and α_{El} is the rotation angle with respect to the x axis, i.e. rotation angle in azimuth. Thus, for the ideal dipole, the nm link in (3.6) can be written as a function of α_{Az} and α_{El} as well, i.e. $\gamma_{nm}(\alpha_{Az}, \alpha_{El})$, for which only three modes are needed in order to consider all possible orientations, i.e. polarizations. Moreover, for the specific case of a vertically oriented dipole, $\alpha_{Az} = 0$, only one mode is needed, as seen from (3.15). The potential of this will be now used to evaluate the effects of antenna placement and rotation.

3.2.4 Modal description of base station

A modal base station model poses one major problem: base stations are usually big antennas, so the number of spherical modes needed to have their radiated field rigorously characterized may be prohibitive [Han88, RGZ05] to be inserted into the proposed network model. In order to overcome this problem, instead of modeling the antenna as a whole the single elements can be modelled and out of it the antenna array can be generated. In this way it is possible to expand the base station field into a number of pseudomodes. Here, the main objective is to obtain a main beam width as close as possible to the measured pattern. In this case, the major variation of the field from the base station will be in the elevation plane, as it is mainly given by the array factor.

Modal array description

At this point the modal array description of a base station antenna will be demonstrated for the 742445 vertically polarized base station antenna only [KG06]. This is a typical antenna for outdoor applications and will therefore be used for the analysis of different antenna configurations in chapter 5 as well.

Given the fact that the 742445 Kathrein antenna consists of 10 dipole pairs arranged vertically and separated approximately by 0.8λ , in front of a metallic plane, the expansion of the radiated field can be carried out by focusing on the radiation pattern of one dipole pair. Therefore, our task consists in finding a modal representation for the single antenna element (dipole pair) for later multiplication with the antenna array factor. For this, the elevation radiation pattern of one $\lambda/2$ dipole in front of an infinite ground plane is used [Kra88]

$$C_\vartheta(\vartheta) = \frac{\cos\left(\frac{\pi}{2}\cos(\vartheta)\right)}{\sin\vartheta}, \quad (3.16)$$

whereas in the azimuthal plane, the direct measured plane from the base station (for example, in the broadside direction) is used to synthesize the necessary b coefficients. By applying a projection synthesis method it follows that the b coefficients that reproduce the radiated pattern of one antenna element of the base station can be synthesized from their projection on the set of normalized outgoing spherical wave functions:

$$b_w = \frac{\iint \vec{C}(\vartheta, \psi) \vec{\tilde{E}}_{w,norm}^*(\vartheta, \psi)}{\iint \vec{\tilde{E}}_{w,norm}(\vartheta, \psi) \vec{\tilde{E}}_{w,norm}^*(\vartheta, \psi)}. \quad (3.17)$$

In the case of the 742445 Kathrein antenna, 35 spherical modes are needed to satisfactorily represent the single antenna configuration. At this point, to get the base station radiation pattern

from these coefficients, each spherical mode must be multiplied by the array factor in order to obtain a “pseudomodal” representation of the base station. This means that for the suggested modal approach the b coefficients of the base station antenna are coefficients of a different modal basis, i.e. the pseudomodes resulting from multiplying the original spherical modes with the array factor.

Figure 3.5 shows the elevation and azimuth plane patterns achieved with this procedure, compared to the measured patterns from the 742445 vertically polarized Kathrein base station antenna. As can be seen, a good degree of compliance is reached. In this way, with this pseudomodal description of the base station antenna, different antenna elements could be investigated, as is the case for the modal mobile station. Yet, in addition, optimum antenna sectorization schemes could be tried out with ease and at a very low computational cost, since spherical mode rotations in azimuth can be easily realized by means of multiplicative factors as was the case for dipoles.

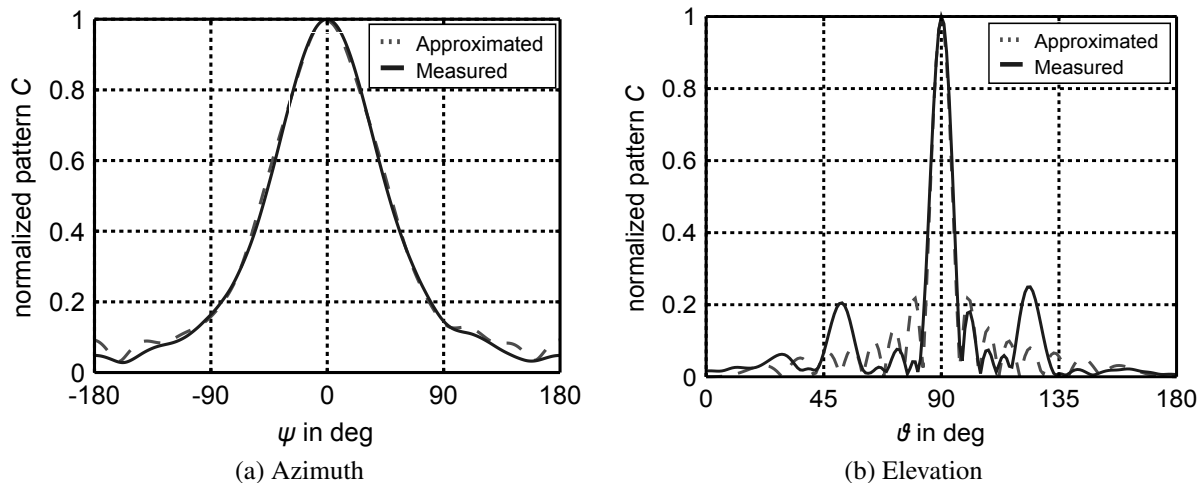


Figure 3.5: Comparison of synthesized radiation pattern and Kathrein 742445 vertically polarized Kathrein antennas.

3.3 Modeling of the “Karlsruhe” urban propagation channel

It has been shown up to this point that the modeling of a MEA system focuses mainly on finding an adequate description of the channel matrix, since the noise can be assumed Gaussian as is the case in this work. At first, this may be seen as a simple task, however, a proper propagation channel description and thus an accurate modeling of the whole communication system,

requires taking into account effects such as polarization and multipath propagation characteristics. Therefore, a poor system representation can end in misleading conclusions. Furthermore, results obtained through different assumptions can result in contradicting assessments. In consequence, in this section all relevant simulation parameters and models used will be introduced.

Modeling of physical channels and more specifically multipath environments can be approached in two different ways: direct computation of the channel matrix H based upon a statistical description or direct description of the physical multipath propagation channel properties. In macrocells, since the base station is usually located on a high tower, simple empirical and statistical models can be used with satisfactory accuracy. However, only a multipath model can describe the true behavior of the MIMO physical channel. The drawback is, though, increased computational resources. Furthermore, models capturing multipath behavior range in complexity from deterministic site-specific ray tracing to simpler statistical descriptions. A brief review of these approaches can be found in [IY02].

In this work a 3D ray tracing model developed at the “Karlsruhe Institute of Technology” is presented [FMKW06]. The model has been validated with wideband channel measurements at 2 and 5.2 GHz showing high accuracy for fixed to mobile and mobile to mobile communications in macrocell scenarios. It consists of two major parts: a realistic model of an urban propagation environment and a model to calculate the multipath wave propagation between the transmitter and the receiver.

3.3.1 Urban Environment Model

The urban environment model consists of a digital description of the city of Karlsruhe by means of a vector database containing the exact position and size of buildings, trees and other objects. It is generated based on two-dimensional plan information of the buildings along with a digital height profile of the environment. The complete digital model of the city of Karlsruhe is shown in Figure 3.6. The shaded area is the area which will be used for simulation. It was picked accordingly to the base station location selected, which corresponds to a current location of the German Vodafone provider. The use of only one base station was decided with the purpose of reducing the computational resources needed to compare the proposed antenna configurations. The simulated area spans about 1 km^2 . The base station antenna is positioned 30 m above street level and at (567, 309) m with respect to the lower left corner. Possible mobile station locations were given by a $17.7 \times 17.7 \text{ m}$ grid over the simulation area.

In order to obtain a more realistic description of the actual site, influenced to a lesser extent by the base station looking direction, a three-sectorized cell is used. This means that effectively three possible scenarios for the base station are considered, namely the ones resulting from

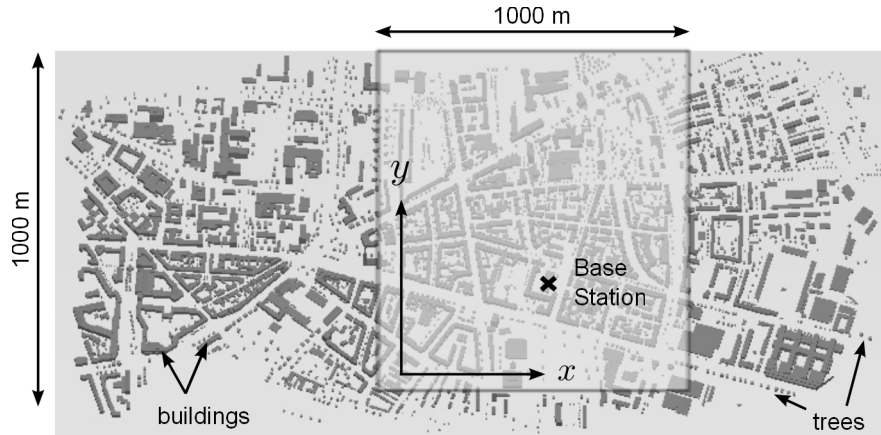


Figure 3.6: Digital model of the city of Karlsruhe (Simulation area is shaded).

each sector landscape. If the cell orientation was rotated or the antenna position shifted then many more scenarios would be considered. However, this is very lengthy and time consuming. Because of this, the decision was made to keep the antennas location and orientation fixed. And even though this does not result by any means in a complete statistical description depicting the behavior of all urban base station sites, it suggests the way urban scenarios in general might behave. In addition it is assumed that the scenario is perfectly sectorized, meaning that only rays coming from mobile station locations from within the current sector under study are considered and all others are omitted. In consequence, no neighboring cell interference and no handover are considered.

3.3.2 Wave propagation Model

The model to calculate the multipath wave propagation between the transmitter and the receiver is a double-directional 3D ray tracing model developed at the "Karlsruhe Institute of Technology" based on a ray-optical approach, where each path is represented by a ray defined in terms of its complex polarimetric transfer matrix, direction of departure (DoD), direction of arrival (DoA) and time delay.

As result, impulse responses containing the complete channel information between two points are obtained. This means that the model can be directly used to analyze the narrowband and wideband as well as the spatial channel characteristics, the details of which are exhaustively explained in [FMKW06]. Furthermore, the model is able to capture the polarization effects on the wave propagation and can resolve each polarization component, so that a full polarimetric transmission matrix \mathbf{T} for each path p can be found

$$\mathbf{T}_p = \begin{pmatrix} T_{\vartheta\vartheta,p} & T_{\vartheta\psi,p} \\ T_{\psi\vartheta,p} & T_{\psi\psi,p} \end{pmatrix}, \quad (3.18)$$

where the single matrix elements contain the gain and phase information of the path between a transmit and a receive antenna and ϑ and ψ denote the two orthogonal and linear polarization components, defined respectively as perpendicular to the wave propagation and to each other.

Since computational resources are scaled by the number of objects and wave interactions (reflection, diffraction, scattering) taken into account, the following parameters partly suggested in [FMKW06] were used:

- Diffuse scattering from buildings and trees.
- Coherent addition of diffuse scattering to reduce number of paths and avoid memory allocation problems.
- UTD second order coefficients, i.e. slope diffraction coefficients
- 5000-th Fresnel zone
- 50 dB dynamic range
- Maximum 5 reflections per path

Additionally, since only one channel snapshot is considered the system initial time $t_0 = 0$, whereas f_0 is set to 2 GHz.

3.3.3 SISO to MIMO Extrapolation

As previously described the wave propagation model considers the existence of a punctual transmitter and receiver for each of the M transmit and N receive MIMO antennas. Strictly speaking, this would imply the need for the ray-tracing model to compute all rays resulting of all the possible n and m antenna combinations. Yet, if it is assumed that the distance between the array and its nearest obstacle is big enough that only plane waves arrive at the array and second, that the array dimensions are small enough that the same plane waves impinge at all antenna elements, then the MIMO channel matrix can be obtained with the use of virtual antennas [WFW02, FSM⁺02]. As result, the urban model with a simulation grid of 17.7 m for the receiver with only one transmit antenna can still be used to obtain the whole MIMO channel description at each point (i.e. channel realization). This is done by computing the phase difference $\Delta\varphi$ (see Figure 3.7) in both transmitting and receiving ends of the simulation link for each n and m antenna as follows:

$$\begin{aligned} \Delta\varphi = \beta((x_{\text{sim}} - x_{\text{vir}}) \cos \psi \sin \theta + (y_{\text{sim}} - y_{\text{vir}}) \sin \psi \sin \theta + \\ (z_{\text{sim}} - z_{\text{vir}}) \cos \theta). \end{aligned} \quad (3.19)$$

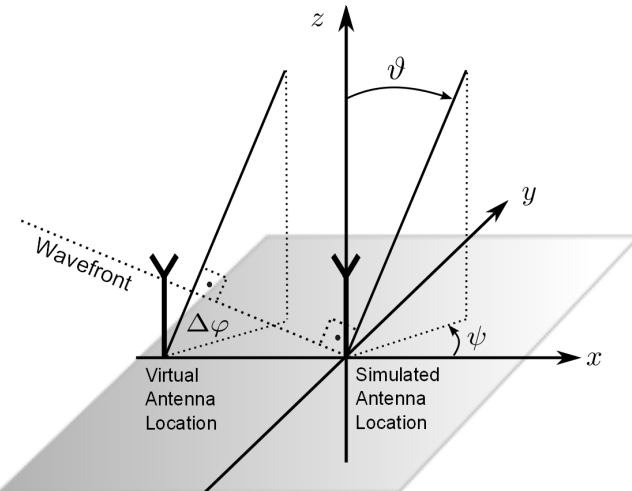


Figure 3.7: Plane wave impinging at the array. The phase difference of the plane waves at the different antenna positions is $\Delta\varphi$ [WFW02].

Here, the subscripts “sim” and “vir” are the abbreviated forms of simulated and virtual antenna positions $(x_{\text{sim}}, y_{\text{sim}}, z_{\text{sim}})$ and $(x_{\text{vir}}, y_{\text{vir}}, z_{\text{vir}})$. With (3.19), the channel coefficient for the m -th transmit antenna and n -th receive antenna for the p -th path of the l -th channel realization becomes

$$H_{l,p(l),nm} = H_{k,p(l)} \cdot e^{-j\Delta\varphi_n^p} e^{-j\Delta\varphi_m^p}. \quad (3.20)$$

3.4 Final remarks

Network models for MIMO systems have already been proposed in the literature for path-based channels [WSW04, Wal04, WJ04]. In both cases a general framework for the use of scattering parameters was presented for the evaluation of the system focusing on mutual coupling effects. As result, processing of all paths for each antenna type under study was required. When considering a small number of antennas or for propagation channels with few propagation paths, doing so poses no problem. However, in the case of multiple channel realizations (i.e. multiple links per channel), of several thousands paths each, the computational cost of extensive antenna evaluations becomes steep. To address this need, in this chapter, these previous efforts are extended, without loss of generality, through the inclusion of a modal description of the antennas [Han88]. In this manner multipath processing becomes significantly reduced and study of multiple antennas and/or orientations becomes feasible. Moreover, for base station antennas, consideration of different sectorization arrangements with a small computational footprint is also possible. In chapter 5 the proposed approach will be validated for the very complex case of a 3D path-based urban channel simulated with a non-commercial ray-tracing tool [FMKW06]. But first, in chapter 4 the evaluation framework to be used for this analysis will be explained.

4 Information content of multiple element antenna systems

Given that the goal in communication systems is the transmission of information, the paramount measure is the amount of information conveyed. Because of this, an essential part in understanding a communication system is knowing the information content of the received signals and the communicational limits of the system. In achieving this goal, up to this point, the wireless communication channel and its computation by means of a modal network model have been shown. On the basis of this extended model the implementation of the "Karlsruhe" communication channel, to be used throughout this work, was explained. However, up to this point no metric to measure the performance of the communication system or channel was given. This chapter will deal with the former problem by introducing a suitable metric to study the amount of information transmitted by multiple element antennas (MEA) systems, in general.

In this chapter the amount of information contained in communication systems, in general, is investigated in both time and spatial domains. As result, the concepts of capacity and spatial capacity are derived as basis for the analysis and design of MEA systems. But first, a discussion on the mechanisms of MEA systems in conveying information will be given. In the following, the concept of signal vectors will be used, where signal vectors represent signal ensembles either in time or space and do not necessarily refer to a linear sum of orthogonal components as in the vector concept handled so far.

4.1 Spatial gain of MEA systems

The process of conveying information between two points is what characterizes communication systems in general. Yet depending on the quality of the communication link and the resources available, the quality and/or quantity of the conveyed information can be improved depending mostly on the coding and transceiver approach used.

In SISO systems without any coding the quality of the information transmitted is solely determined by the quality of the communication link¹, which in wireless systems is given by the

¹In practice this is not true, given the fact that redundant coding can significantly improve the quality of the received signal by using more efficiently the time and frequency resources

channel coefficient as in (2.52). The amount of possible transmitted information, on the other hand, depends on the available resources, i.e. time and frequency. As result, these resources determine the dimensions, i.e. degrees of freedom, of the received signal space, i.e. all possible states of the received vector. In MEA systems, space becomes an additional resource for transmitting additional information. In consequence a spatial degree of freedom gain results, also known as multiplexing gain, since it allows to multiplex the signals. Yet, not only can space increase the amount of information conveyed but it can also improve the quality of the transmitted signals by providing antenna diversity gain. This two fold increase in system performance constitutes what is referred here as the spatial gain of MEA systems and can be used to increase the quality and/or quantity of the transmitted signals.

Assuming that a system with no losses and perfect matching is implemented in a multipath propagation channel, the power distribution, and thus information content, between each antenna pair will vary depending on the propagation channel properties and the antenna interactions with it. In the following it will be briefly described how these interactions provide spatial gain, in the form of diversity and multiplexing gains, as well as their effects on the channel matrix. A more detailed discussion can be found in [TV05]. Finally, some comparison issues regarding the evaluation of spatial gain in different systems will be discussed.

4.1.1 Diversity gain

In a single input multiple output (SIMO) system where the receiving antennas are considerably apart from each other, attenuation and propagation disturbances will most likely occur independently across the antennas. Therefore, even though each received signal contains the same information the probability of not receiving any information due to deep fades in the propagation channel is averaged over all receiving antennas [Bre59, Jak74]. If in addition the received signals are coherently added, then an array gain is obtained, similar to the implementation of an antenna array instead of many single element antennas. These two effects constitute therefore the so-called antenna receive diversity. If on the other hand a multiple input single output (MISO) system is considered, a similar antenna transmit diversity, i.e. parallel communication links, will also result. In this case, if all antennas transmit the same information then diversity is achieved through repetition. Yet if intelligent coding (receiving) schemes, like so-called space-time codes [Ala98], are used then significant coding, i.e. diversity gain, can be attained. An overview of approaches that benefit from diversity can be seen in [LS03].

From the study of SIMO and MISO systems follows that independent propagation paths at one communicating end allow for more reliable communication since they increase the probability of having at least one strong signal in addition to the inherent array gain of coherently

combining the signals. Remarkably though this does not occur only when the antennas are sufficiently spaced apart [VA87], but also when the scenario is sufficiently rich for the given antenna spacing. As it will be thoroughly discussed in chapter 7, finding this measure of richness is fundamental in the dimensioning of antenna systems.

4.1.2 Multiplexing gain

Until now it has been considered that either transmitting or receiving antennas are subject to changes in antenna spacing or scenario richness. In this way, the nature of the diversity gain in SIMO and MISO systems was explained. In order to see how a degree of freedom gain takes place in MEA systems, in general, simultaneous changes at both transmitter and receiver are now assumed. In the most simple case that the transmitting and receiving antennas are sufficiently apart from each other the channel transfer coefficients between antenna pair will most likely become independent regardless of the scenario richness. As result, not only independent but also parallel signals can be transmitted. The transmission of parallel signals is called spatial multiplexing and it is key to exploiting space as a resource. Some communication schemes that benefit from multiplexing effects can be found in [IN02, KJUN02, Fos96]. If small antenna spacings are considered at both communicating ends then a scattered scenario is necessary to ensure that the transfer functions between each antenna pair are independent. If, on the contrary, the scenario exhibits insufficient richness and small antenna spacings are used then the signal among all antennas will be very similar and the received signals will not be independently faded, i.e. little diversity and degree of freedom gain.

4.1.3 Diversity and multiplexing effects on the channel matrix

The way diversity and degree of freedom gain contribute to the total spatial gain is key in determining the amount of information that can be transmitted in MEA systems, since they define what kind of structure the channel matrix \mathbf{H} will have. In Figure 4.1 some possible distributions are shown. Here, the shaded squares will represent the non-zero elements of the channel matrix \mathbf{H} , i.e. the antenna pairs between which a significant amount of information is transmitted. This depiction was originally used in [WHÖB06] to better model propagation channels. However, it wasn't used to depict the channel matrix as such but a decomposed form of it. The type of matrix decompositions leading to the interpretation of [WHÖB06] will be discussed in chapter 7. Assuming that all active links propagate independently the effects of spatial diversity and spatial multiplexing can be seen in the different examples.

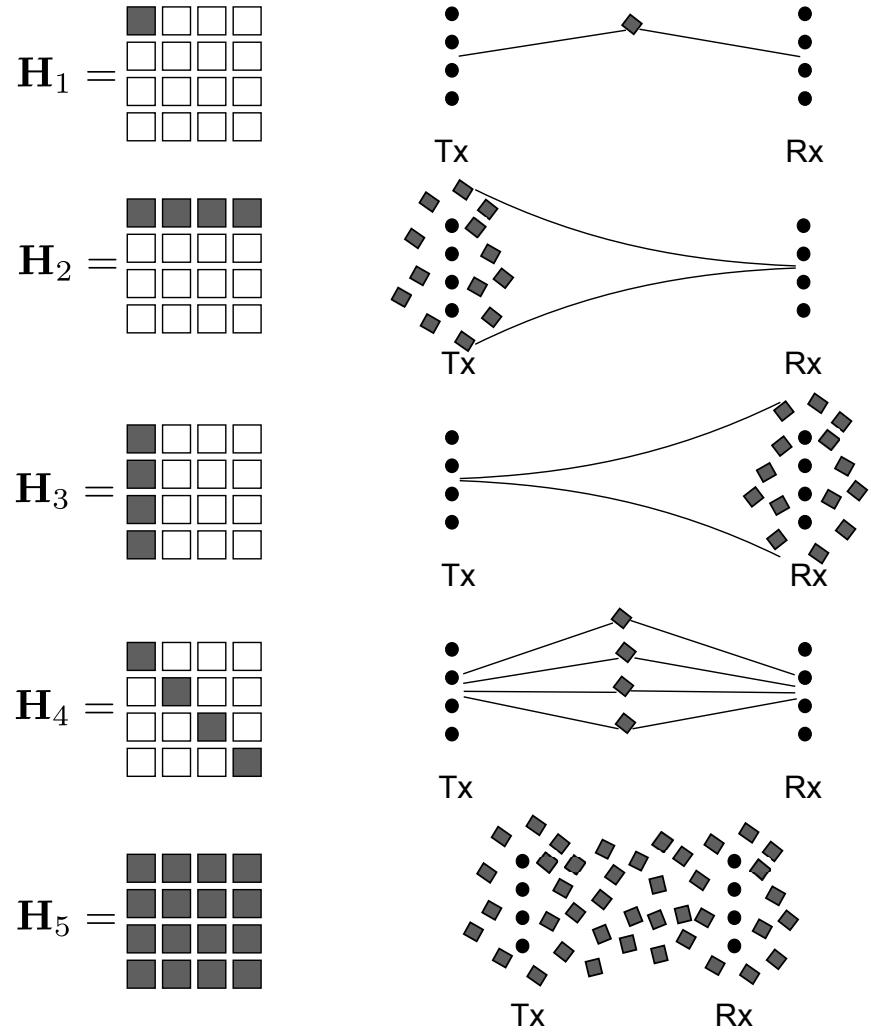


Figure 4.1: Different structures of the channel matrix \mathbf{H} and corresponding propagation environments (cf. [WHÖB06]). Gray squares denote significant magnitude relative to blank squares, which are almost zero valued.

The most simple example is given by \mathbf{H}_1 . This represents the case in which there is only one non-zero channel coefficient. This means that the antenna-channel interaction results in such a way that only one link is established. In this case no diversity or multiplexing gain is obtained, and the system is equivalent to a SISO one, due to both the nature of the channel (few scatterers) and small antenna spacings. In \mathbf{H}_2 , on the other hand, a scenario with scatterers located at the transmitting end of the system yield a matrix with a non-zero row. This means that all available antennas are used for transmitting but only one antenna is effectively receiving, i.e. a MISO case. In a similar manner, \mathbf{H}_3 is reciprocal to \mathbf{H}_2 . In this case, though, only one antenna is transmitting and the scenario richness suffices to have independently faded receive signals, i.e. SIMO case. In this way an additional gain in the received signal is obtained. Both \mathbf{H}_2 and \mathbf{H}_3 benefit from the use of multiple antennas at either one of the communicating ends and

therefore exhibit diversity gain, since independently faded signals are used. This means that from the perspective of antenna arrays by coherently adding the signals a beamforming pattern is realized. However no parallel data streams can be used since information is limited at either the transmitting or receiving end. \mathbf{H}_4 overcomes this problem and is capable of establishing several communication links between each antenna pair. Yet, only one antenna per link is used. This means that in this case a multiplexing gain is achieved but no diversity gain, i.e. no array. Finally \mathbf{H}_5 shows the most ideal case in which each single coefficient fades independently. As result in \mathbf{H}_5 the maximum number of communication links is established while benefiting at the same time from having several transmitting and receiving antennas for each link. From an antenna perspective, this means that multiple beamforming patterns on the transmitting and receiving end can be simultaneously used when processing the signals.

In general the antennas used in communication systems do not sample the propagation channel so that the sparse channel matrices of Figure 4.1 result ($\mathbf{H}_1\text{-}\mathbf{H}_4$). In consequence, real antenna systems exhibit less sparse channel matrices. As example, a MEA system with very high signal correlation due to the channel would yield a full matrix where all coefficients are almost equal. In terms of information throughput this would mean that only one signal, i.e. no multiplexing, could be independently transmitted since all links are subject to essentially the same fading. However, due to the parallel transmission of the same signal a certain diversity gain would be possible. In this way it is seen that a full-matrix is not equivalent to maximum information throughput if it doesn't have uncorrelated coefficients. It follows thus that the \mathbf{H} matrix implicitly describes the channel nature and the amount of transmitted information can be determined at hand from it. In chapter 7 this will be further clarified from an antenna perspective in terms of the available spatial signatures.

4.1.4 Spatial gain comparison issues

As previously seen, the \mathbf{H} matrix contains all information related to the communication system. Depending on the channel and system characteristics the elements of \mathbf{H} , i.e. the H_{nm} transmission coefficients, take on different values and are distributed in a different manner. The way these values are distributed then yields better information throughput in form of the two aforementioned diversity and multiplexing gains. Yet, the individual contribution of each system component, such as antennas, matching networks or propagation channel might not be known. Therefore, when comparing different system configurations, normalization of the \mathbf{H} matrix with a common reference can ease the analysis of the system. In the following a brief discussion on the different norms used in the context of MEA systems will be given.

In the case that no power control schemes are used received signals can have significant differences due to varying received power at two points distant from one another. For example, if

one were to evaluate the diversity and multiplexing effects of the exact same system one could conclude that the diversity and multiplexing gain for the nearest receiver is larger, even though this might be only due to larger signal attenuation at the other receiver. These differences make it difficult to compare two distant channel realizations and, thus, normalization is required. A common approach is the use of the Frobenius norm, which normalizes the channel with respect to the expectation of the square root of the total power gain of each channel realization, i.e. each transmitter and receiver link

$$\mathbf{H}_{\text{norm}} = \frac{\sqrt{MN}}{\mathbb{E}\left\{\left(\sum_{i=1}^N \sum_{j=1}^M |H_{ij}|^2\right)^{\frac{1}{2}}\right\}} \mathbf{H}, = \frac{\sqrt{MN}}{\mathbb{E}\{\|\mathbf{H}\|_F\}} \mathbf{H}, \quad (4.1)$$

where $\|\mathbf{H}\|_F$ is the Frobenius norm of \mathbf{H} resulting from

$$\|\mathbf{H}\|_F = \left(\sum_{i=1}^N \sum_{j=1}^M |H_{ij}|^2 \right)^{\frac{1}{2}}. \quad (4.2)$$

Once a channel has been Frobenius normalized the total power of the normalized channel is equal to one, which depicts to some extent the power control behavior of real mobile network systems. This method has, however, the disadvantage of masking small changes (with respect to slow fading) in signal strength. This is the case, for example, of antenna effects [WSW04], where capacity improvements due to increased received power at the receiver are masked. The antenna multiplexing effects remain, but no conclusions regarding the antennas benefit to the system diversity can be made. On the other hand, this type of normalization permits investigation of correlation between the channel matrix entries and thus of the richness of the multipath environment [WJ04, LOKM05, Jan02]. In consequence, whether this metric is suited or not for a certain comparison depends mostly on the type of benchmarking needed.

In this manner, alternative norming procedure consists in normalizing \mathbf{H} with respect to the Frobenius norm of a reference MIMO realization. The idea is to norm out known system effects in order to concentrate on those parts of the system that are of interest. For antenna comparison it is common to consider ideal isotropic antennas as reference. The normalized channel matrix for each link is then computed as

$$\mathbf{H}_{\text{norm}} = \frac{\sqrt{MN}}{\|\mathbf{H}_{\text{REF}}\|_F} \mathbf{H}, \quad (4.3)$$

where \mathbf{H}_{REF} is the channel matrix equivalent to the average isotropic MIMO channel. The channel normalized in this way contains the effects of the antennas, while excluding multiplexing and diversity effects of the channel. This will be the norm used throughout this work. However, other norms also exist, some of which can be found in [OEP03, SSV07].

4.2 Capacity of multiple element antenna systems

Since each communication channel results from a specific choice of antennas, antenna setups and their interaction with the propagation channels, benchmarking of the different scenarios becomes essential. In order to do so one or many benchmarking parameters are needed, depending on the application at hand. Regarding communication systems either the quality or quantity of the information transmitted can be evaluated. The former is usually given by the bit error rate (BER) and is closely related to the coding scheme used and the quantity of information conveyed. Therefore, it results in a too complex measure when benchmarking propagation channels or antenna configurations, as is the case in this work. Instead, it is more common to focus mainly on the amount of information transmitted, given by the capacity. In the following, the term channel capacity will refer to the use of the channel matrix \mathbf{H} , rather than consideration of only the propagation or communication channel. In general though, it is possible to determine the capacity of both the channel alone and the whole communication system. Therefore, the results presented here apply to both.

The capacity of a system or channel results from the maximization of the average mutual information (or transinformation) $I(\mathbf{x}; \mathbf{y})$ between the transmitted signal vector \mathbf{x} (in space) and the received signal vector \mathbf{y} (in space) [FG98, Tel99]

$$C = \max_{f(\mathbf{x})} I(\mathbf{x}; \mathbf{y}), \quad (4.4)$$

where $f(\mathbf{x})$ is the probability distribution of vector \mathbf{x} and C is measured in bits per second per Hertz. Therefore, using the procedure shown in [Tel99] and [PNG03] and considering the input-output relation of the MEA channel at snapshot time t_0 to be the one shown in (2.6), the average mutual information between vectors \mathbf{x} and \mathbf{y} can be expressed as

$$I(\mathbf{x}; \mathbf{y}) = H(\mathbf{y}) - H(\mathbf{y}|\mathbf{x}). \quad (4.5)$$

In this way the problem of determining the system capacity is reduced to maximizing the differential entropy of vector \mathbf{y} , i.e. $H(\mathbf{y})$. This results from the fact that for statistically independent vectors, as is the case of \mathbf{x} and \mathbf{n} , the conditional differential entropy of the vector \mathbf{y} , i.e. $H(\mathbf{y}|\mathbf{x})$, given knowledge of the vector \mathbf{x} , simplifies to the differential entropy of vector \mathbf{n} , i.e. $H(\mathbf{n})$. In this way (4.5) is rewritten to

$$I(\mathbf{x}; \mathbf{y}) = H(\mathbf{y}) - H(\mathbf{n}), \quad (4.6)$$

where \mathbf{n} denotes a zero mean circularly symmetric complex Gaussian (ZMCSCG) noise vector with noise variance σ_n^2 per element and diagonal covariance matrix $\mathbf{R}_{\mathbf{nn}} = \mathbf{E}\{\mathbf{n}\mathbf{n}^\dagger\} = \sigma_n^2 \mathbf{I}_N$.

In consequence, average mutual information can be maximized if both \mathbf{y} and \mathbf{x} are made ZMCSCG variables [Tel99] (due to the fact that normal distributions are entropy maximizers [CT91]). In this way their distribution becomes fully characterized by their covariance matrices $\mathbf{R}_{yy} = \mathbb{E}\{\mathbf{y}\mathbf{y}^\dagger\}$ and $\mathbf{R}_{xx} = \mathbb{E}\{\mathbf{x}\mathbf{x}^\dagger\}$. Noting therefore that the covariance of the received signal \mathbf{y} results from the sum of the covariance of the desired received signal \mathbf{d} , $\mathbf{R}_{dd} = \mathbf{H}\mathbf{R}_{xx}\mathbf{H}^\dagger$, and the noise covariance \mathbf{R}_{nn}

$$\mathbf{R}_{yy} = \mathbf{R}_{dd} + \mathbf{R}_{nn} = \mathbf{H}\mathbf{R}_{xx}\mathbf{H}^\dagger + \mathbf{R}_{nn}, \quad (4.7)$$

it follows from

$$H(\mathbf{y}) = \log_2(\det(\pi e \mathbf{R}_{yy})) \quad (4.8)$$

$$H(\mathbf{n}) = \log_2(\det(\pi e \mathbf{R}_{nn})) \quad (4.9)$$

that (4.4) can be expressed with the aid of (4.6) [FFLV01] as

$$C = \max_{\{\mathbf{R}_{xx}: \text{Tr}(\mathbf{R}_{xx}) \leq P_{Tx}\}} \log_2 \left(\frac{\det(\mathbf{R}_{dd} + \mathbf{R}_{nn})}{\det(\mathbf{R}_{nn})} \right). \quad (4.10)$$

In this way it is seen that the capacity expression in (4.10) has been maximized over the covariance \mathbf{R}_{xx} , since it fully describes $f(\mathbf{x})$, and limited to the maximum available transmit power P_{Tx} , not affected by the number of transmit antennas. Finally, after some simplifications (4.7) is rewritten as

$$C = \max_{\{\mathbf{R}_{xx}: \text{Tr}(\mathbf{R}_{xx}) \leq P_{Tx}\}} \log_2 \det(\mathbf{R}_{dd}(\mathbf{R}_{nn})^{-1} + \mathbf{I}_N). \quad (4.11)$$

Furthermore, considering that \mathbf{R}_{nn} , as previously mentioned, is a diagonal matrix with available power per antenna equal to the noise variance σ_n^2 , (4.11) becomes

$$C = \max_{\{\mathbf{R}_{xx}: \text{Tr}(\mathbf{R}_{xx}) \leq P_{Tx}\}} \log_2 \det(\mathbf{I}_N + \frac{\mathbf{H}\mathbf{R}_{xx}\mathbf{H}^\dagger}{\sigma_n^2}), \quad (4.12)$$

as it is most commonly found in the literature, or as

$$C = \max_{\{\mathbf{R}_{xx}: \text{Tr}(\mathbf{R}_{xx}) \leq P_{Tx}\}} \log_2 \det(\mathbf{I}_M + \frac{\mathbf{H}^\dagger \mathbf{H} \mathbf{R}_{xx}}{\sigma_n^2}) \quad (4.13)$$

from the determinant identity

$$\det(\mathbf{I} + \mathbf{AB}) = \det(\mathbf{I} + \mathbf{BA}). \quad (4.14)$$

From the previous derivation follows that obtaining the system capacity is equivalent to maximizing the distribution of \mathbf{x} , i.e. selecting a $\mathbf{R}_{\mathbf{xx}}$ that maximizes (4.13). Furthermore from (4.13) follows that the signal to noise ratio (SNR) seen at the receiver, results from the second term of the determinant. If however a Frobenius normed channel is considered then SNR at the receiver is given by $\mathbf{R}_{\mathbf{xx}}/\sigma_n^2$. This is usually assumed, even when arbitrarily normalized channels are used. For real applications, use of a Frobenius normed channel makes sense when the channel is subject to a perfect power control scheme.

Based on (4.13) and depending on whether channel state information (CSI) is assumed to be known at the transmitter (CSIT), at the receiver (CSIR), at both or at none, different $\mathbf{R}_{\mathbf{xx}}$ can be used leading to different capacity computations as well. In general, CSI results from the estimation of the channel matrix \mathbf{H} and depends on additional coding and feedback. It thus follows that CSI comes at the expense of information throughput. In this work, since only the communication channel effects are of interest the impact of CSI on capacity will be omitted.

In this work, CSIR and in some cases CSIT will be assumed. As result, based on the channel knowledge, different power distributions at the transmitter will be used. In the following the capacity computation schemes for each case will be discussed.

4.2.1 Uniform Power Distribution

In the case that no CSIT is available it was shown for the first time in [FG98], that the $\mathbf{R}_{\mathbf{xx}}$ that maximizes (4.12) is $(P_{\text{Tx}}/M)\mathbf{I}_N$ thus resulting in

$$C = \log_2 \det(\mathbf{I}_N + \frac{P_{\text{Tx}}}{\sigma_n^2 M} \mathbf{H} \mathbf{H}^\dagger), \quad (4.15)$$

where the transmit power to noise power seen at the receiver relation is equivalent to the SNR of the Frobenius normed SISO channel ρ . In this way ρ can be written as

$$\rho = P_{\text{Tx}}/\sigma_n^2 \quad (4.16)$$

and (4.15) can be rewritten as

$$C = \log_2 \det(\mathbf{I}_N + \frac{\rho}{M} \mathbf{H} \mathbf{H}^\dagger). \quad (4.17)$$

In this way it is seen that for systems with uniform power distribution both the diversity and multiplexing effects go into the computation of the capacity. However, due to the lack of CSIT no optimum power distribution is done and therefore multiplexing gain is not fully exploited.

4.2.2 Waterfilling

If the channel is known at the transmitter, then the \mathbf{R}_{xx} that maximizes (4.12) can be shown to be a positive semi-definite matrix [Tel99] resulting out of the eigenvalue decomposition of the complex normal matrix $\mathbf{H}\mathbf{H}^\dagger$

$$\mathbf{H}\mathbf{H}^\dagger = \mathbf{U}\Lambda\mathbf{U}^\dagger, \quad (4.18)$$

where \mathbf{U} is a unitary matrix, whose column vectors are the eigenvectors of $\mathbf{H}\mathbf{H}^\dagger$ and Λ is a diagonal matrix, the entries of which are the eigenvalues of $\mathbf{H}\mathbf{H}^\dagger$, that when inserted into (4.12) can be expressed as

$$C = \max_{\{\mathbf{R}_{xx}: \text{Tr}(\mathbf{R}_{xx}) \leq P_{Tx}\}} \log_2 \det(\mathbf{I} + \frac{\mathbf{U}\Lambda\mathbf{U}^\dagger\mathbf{R}_{xx}}{\sigma_n^2}), \quad (4.19)$$

where $\mathbf{U}\Lambda\mathbf{U}^\dagger\mathbf{R}_{xx}$ must be a diagonal matrix in order to maximize the expression. Rewriting (4.19), with the use of (4.14), yields

$$C = \max_{\{\mathbf{R}_{xx}: \text{Tr}(\mathbf{R}_{xx}) \leq P_{Tx}\}} \log_2 \det(\mathbf{I} + \frac{\Lambda^{1/2}\mathbf{U}^\dagger\mathbf{R}_{xx}\mathbf{U}\Lambda^{1/2}}{\sigma_n^2}). \quad (4.20)$$

Now $\mathbf{U}^\dagger\mathbf{R}_{xx}\mathbf{U}$ can be substituted by a diagonal power distribution matrix $\mathbf{D} = \text{diag}(p_1, \dots, p_K)$, where $p_i (i = 1, 2, \dots, K)$ are the power coefficients for each eigenvector i and K is equal to the rank of matrix $\mathbf{H}\mathbf{H}^\dagger$ given by the minimum number of antennas available either at transmit or receive, i.e. $K \leq \min(M, N)$. In consequence, (4.20) simplifies to

$$C = \log_2 \det(\mathbf{I} + \frac{\mathbf{D}\Lambda}{\sigma_n^2}), \quad (4.21)$$

where \mathbf{R}_{xx} is implicitly considered to be a positive semi-definite matrix, as originally stated, of the form $\mathbf{U}^\dagger\mathbf{D}\mathbf{U}$. Expressing \mathbf{D} in terms of the power coefficients $p_i (i = 1, 2, \dots, K)$ and Λ with the eigenvalues $\lambda_i (i = 1, 2, \dots, K)$ of $\mathbf{H}\mathbf{H}^\dagger$, additional representations of (4.21) can be given:

$$C = \log_2 \prod_{i=1}^K (1 + \frac{p_i \lambda_i}{\sigma_n^2}), \quad (4.22)$$

$$C = \sum_{i=1}^K \log_2 (1 + \frac{p_i \lambda_i}{\sigma_n^2}). \quad (4.23)$$

In this way the capacity of the MEA channel is expressed as the sum of the individual parallel SISO subchannel capacities, resulting from the channel eigenmodes. Furthermore, since the

transmitter can access the spatial subchannels, it can allocate variable energy across the subchannels to maximize the mutual information. Therefore, both beamforming and multiplexing gains go into the computation of capacity and, contrary as with a uniform power distribution, the maximum multiplexing gain is achieved. In order to better illustrate this with respect to the antennas, an alternative approach to finding the optimal channel capacity under the assumption of full channel knowledge at the transmitter will be shown.

Ideally the channel matrix \mathbf{H} will be a vector Gaussian channel since it will result from several parallel, independent links subject to gaussian noise. Therefore, a factorization for the \mathbf{H} matrix, i.e. matrix decomposition, should exist that intuitively depicts the behavior of the individual Gaussian subchannels. The singular value decomposition (SVD) is such a factorization, where the basis directions of a matrix are found, along which matrix multiplication is equivalent to scalar multiplication. In the case of the channel matrix \mathbf{H} this yields

$$\mathbf{H} = \mathbf{U}\mathbf{S}\mathbf{V}^\dagger, \quad (4.24)$$

where the diagonal entries of \mathbf{S} are the non-negative square roots of the eigenvalues of $\mathbf{H}\mathbf{H}^\dagger$, whereas the columns of the unitary matrix \mathbf{U} are the eigenvectors of $\mathbf{H}\mathbf{H}^\dagger$ and the columns of the unitary matrix \mathbf{V} are the eigenvectors of $\mathbf{H}^\dagger\mathbf{H}$. In this way, the channel matrix is rewritten in terms of a rotation operator \mathbf{U} , a scaling operation \mathbf{S} and another rotation operator \mathbf{V} . This means that the columns of \mathbf{V} form a set of orthonormal "input" or "analysing" basis vector directions for \mathbf{H} and the columns of \mathbf{U} form a set of orthonormal "output" basis vector directions for \mathbf{H} , whereas the diagonal elements of \mathbf{S} yield the energy distributed to each pair of basis vectors, i.e. subchannels (also called eigenmodes).

If now, the channel information available is used and the input, output and noise vectors are accordingly changed to $\tilde{\mathbf{y}} = \mathbf{U}^\dagger\mathbf{y}$, $\tilde{\mathbf{n}} = \mathbf{U}^\dagger\mathbf{n}$ and $\tilde{\mathbf{x}} = \mathbf{V}\mathbf{x}$ then the original channel of (2.6) yields an equivalent channel

$$\tilde{\mathbf{y}} = \mathbf{S}\tilde{\mathbf{x}} + \tilde{\mathbf{n}}, \quad (4.25)$$

from which a set of independent channels is easily seen. Thus, (4.25) is just a compact way of describing the parallel SISO subchannels implicitly present in \mathbf{H} . In real applications where CSIR and CSIT are known this is achieved with pre and post-processing stages as the ones shown in Figure 4.2.

Once the channel has been pre-processed the problem reduces to assigning the necessary power to each eigenmode in order to exploit the channel properties. The latter can be done iteratively via waterfilling as was originally presented in [RC98],[Tel99],[KBJR01] and [And00] by

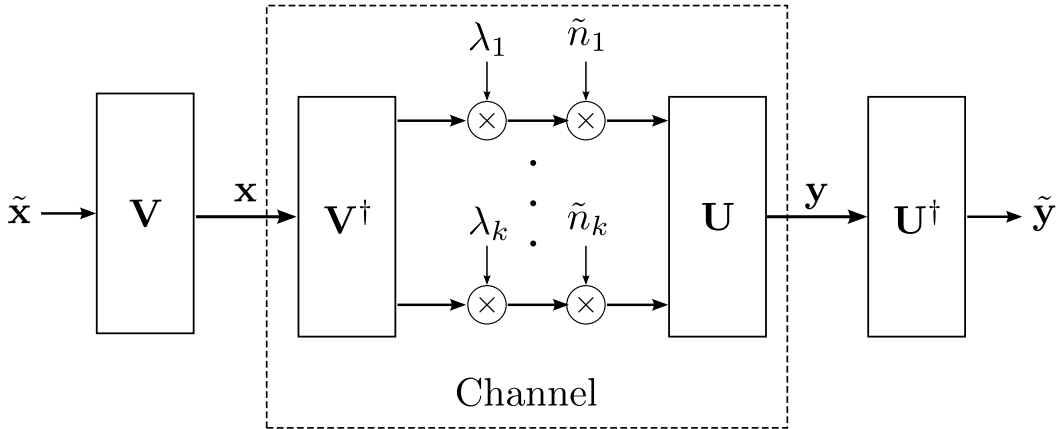


Figure 4.2: Block model of pre- and post-processing stages for a MIMO channel under assumption of perfect CSIR and CSIT [TV05].

choosing the i_{th} power coefficient to be

$$p_i = \left(\nu - \frac{1}{\lambda_i} \right)^+, \quad (4.26)$$

where $(x)^+$ implies

$$(x)^+ = \begin{cases} 0 & \text{if } x < 0 \\ x & \text{if } x \geq 0 \end{cases} \quad (4.27)$$

and the constant ν is chosen such as to preserve the total transmit power P_{Tx} , i.e. $\sum p_i = P_{Tx}$ and represents the “water level” that determines the amount of power poured into the “vessels” formed by the $1/\lambda_i$ functions. It follows that the smaller the SNR at the receiver, the larger the portion of the transmit power allocated to the best subchannel. In terms of ρ , i.e. the SNR at the receiver of the Frobenius normed SISO channel, one can define the i -th SNR coefficient as $\rho_i = p_i/\sigma_n^2$ subject to constraint $\sum p_i = \rho$, so that a simplified version of (4.23) results

$$C = \sum_{i=1}^K \log_2(1 + \rho_i \lambda_i). \quad (4.28)$$

4.2.3 Beamforming on transmit

Beamforming is closely related to waterfilling since channel knowledge at the transmitter is also presumed. However, in beamforming no optimum power allocation scheme among the available subchannels is done, but instead a simple selection of the best subchannel available.

In this manner (4.13) becomes

$$C = \log_2\left(1 + \frac{P_{\text{Tx}}\lambda_{\max}}{\sigma_n^2}\right) = \log_2(1 + \rho\lambda_{\max}), \quad (4.29)$$

where all the power P_{Tx} is allocated to the subchannel with the highest eigenvalue.

Therefore, it is seen that for such a power distribution only diversity effects are of significance. This is evidenced by the fact that only the most significant eigenvalue is used for the capacity computation, which therefore implies that only one transmitting and receiving eigenvector will be used. From an antenna perspective and following the discussion at the beginning of this chapter this means that the antenna will employ only one beamforming configuration. In consequence no multiple spatial signatures result and thus no multiplexing gain is achieved.

4.3 Channel capacity of temporal and spatial bandlimited systems

At the beginning of this chapter the concept of spatial gain as result from the beamforming and multiplexing effects in the channel were introduced. Then the theoretical basis for evaluating the performance of MEA communication systems with regard to maximum information throughput was given. Moreover, it was seen how the spatial properties of the channel determine the power allocation schemes that result most successful. Yet, no concrete way for quantifying the available spatial resources was given. For temporal band-limited systems [Pro01], however, the bandwidth B yields a measure of the available frequency resource so that the capacity

$$\hat{C} = B \log_2(1 + \text{SNR}) \quad (4.30)$$

results [Sha48]. In the following an expression that extends this capacity formulation by summarizing the available spatial resources will be derived in order to: 1) demonstrate the duality between the temporal and spatial domains and 2) show that space as a communication resource is also subject to optimization.

The capacity C in (4.13), even though widely used in the context of MEA and MIMO systems, is also often referred as the error-free spectral efficiency, or the data rate per unit bandwidth that can be sustained reliably over the MIMO link [PNG03] and differs from that originally given in [Sha48], where capacity \hat{C} is given in terms of bits/s as

$$\hat{C} = \lim_{T \rightarrow \infty} \max_{f(x)} \frac{1}{T} I(\mathbf{x}_t; \mathbf{y}_t). \quad (4.31)$$

The key difference between (4.4) and (4.31) is not the total transmission time T used for averaging but the average mutual information considered in each case. In (4.4) mutual information results from the average of spatial signal vectors (MEA channel at a single instant of time), whereas in (4.31) the average of temporal signal vectors \mathbf{x}_t and \mathbf{y}_t is done, thus the time t subscript. To distinguish these two cases the notations $\text{ave}_a\{\cdot\}$ and $\mathbb{E}_a\{\cdot\}$ to denote the average and expected value with respect to variable a are introduced.

When dealing with time signals, the average mutual information $\text{ave}_t\{I(\mathbf{x}_t; \mathbf{y}_t)\}$ in (4.31) for signal vectors \mathbf{x}_t and \mathbf{y}_t of N_S statistically independent random variables x_i and y_i , can be written as

$$\text{ave}_t\{I(\mathbf{x}_t; \mathbf{y}_t)\} = \sum_{i=1}^{N_S} \text{ave}_{p(x_i; y_i)}\{I(x_i; y_i)\}, \quad (4.32)$$

i.e. the sum of the average mutual information with respect to the probability of the occurrence of each joint event $(x_i; y_i)$. Where, the use of Nyquist sampling rate for a channel with bandwidth B yields an optimum number of (time) samples $N_S = 2BT$, i.e. $2B$ samples per second or its equivalent one sample every $T = 1/(2B)$ seconds. Therefore, for (real) zero-mean Gaussian random variables x_i with variance $\sigma_{x_i}^2$, ensemble average signal power P_{ave} (in time) and spectral noise power density $N_0/2 = \sigma_{n,i}^2$ for all i in (4.32), capacity, as defined in [Sha48], becomes [Pro01]

$$\hat{C} = \frac{1}{T} \sum_{i=1}^{N_S} \frac{1}{2} \log_2 \left(1 + \frac{\sigma_{x_i}^2}{\sigma_{n,i}^2} \right) = \frac{1}{T} \sum_{i=1}^{N_S} \frac{1}{2} \log_2 \left(1 + \frac{P_{\text{ave}}}{2B(N_0/2)} \right), \quad (4.33)$$

where $P_{\text{ave}} = N\sigma_{x_i}^2/T = 2B\sigma_{x_i}^2$ was used. Further simplifications finally yield

$$\hat{C} = B \log_2 \left(1 + \frac{P_{\text{ave}}}{BN_0} \right), \quad (4.34)$$

which is the basic formula for the capacity of the classical band-limited SISO channel with Additive White Gaussian Noise (AWGN).

In order to find a similar expression for a band-limited AWGN MEA channel, $I(x_i; y_i)$ in (4.32) has to be replaced with (4.6). This gives

$$\text{ave}_t\{I(\mathbf{X}; \mathbf{Y})\} = \sum_{i=1}^{N_S} \text{ave}_{p(x_i; y_i)}\{I(x_i; y_i)\}, \quad (4.35)$$

where \mathbf{X} and \mathbf{Y} can be seen as ensembles of temporal and spatial signal vectors (for practical purposes, though, \mathbf{X} and \mathbf{Y} can be seen as matrices of elements $X_{k,i}$ and $Y_{k,i}$, where the subscripts k and i denote the spatial and temporal sampling respectively). For the multiple antenna

case here considered use of (4.31) would yield

$$\hat{C} = \lim_{T \rightarrow \infty} \max_{f(x)} \frac{1}{T} I(\mathbf{X}; \mathbf{Y}) = \frac{1}{T} \sum_{i=1}^{N_S} \log_2 \det(\mathbf{I}_M + \frac{\mathbf{H}^\dagger \mathbf{H} \mathbf{R}_{\mathbf{x}\mathbf{x},i}}{\sigma_{n,i}^2}). \quad (4.36)$$

In this way an analogous expression to (4.33) is found, however, with a discrepancy in a missing $1/2$ factor in (4.36) due to the nature of the signals. In arriving to (4.33) real signals were assumed, whereas for (4.36) complex multivariate normal distributions (ZMCSCG variables) were used. Considering now that 1) noise variance is the same for all i time samples, 2) power is uniformly distributed among the K available subchannels (i.e. not over all transmitting antennas) and 3) all subchannels can be expressed in terms of an average eigenvalue λ_{ave} , (4.36) can be rewritten as

$$\hat{C} = \frac{1}{T} \sum_{i=1}^{N_S} \log_2 \prod_{k=1}^K \left(1 + \frac{P_{Tx} \lambda_{ave}}{K \sigma_n^2}\right) = \frac{N_S}{T} K \log_2 \left(1 + \frac{P_{Tx} \sigma_{ave}^2}{K \sigma_n^2}\right), \quad (4.37)$$

where $\lambda_{ave} = \sigma_{ave}^2$ was used. Then, based on the average power in time $P_{ave,k}$ for each k subchannel

$$P_{ave,k} = \frac{P_{Tx}}{KT} \int_0^T \mathbf{E}_t(\mathbf{x}_{t,k}^2) dt = \frac{P_{Tx}}{KT} \sum_{i=1}^{N_S} \mathbf{E}(x_{k,i}^2) = 2B \frac{P_{Tx}}{K} \sigma_{ave}^2, \quad (4.38)$$

leading to the total average power in time

$$P_{ave} = K P_{ave,k} = 2B P_{Tx} \sigma_{ave}^2, \quad (4.39)$$

the following spatial channel capacity expression results

$$\hat{C} = 2BK \log_2 \left(1 + \frac{P_{ave}}{2BK \sigma_n^2}\right). \quad (4.40)$$

This result is of great importance since it summarizes the spatial degrees of freedom of the channel into the available number of subchannels K . Providing, therefore, a way to predict in both space and time the capacity achievable by a certain MEA channel in the same manner that (4.34) did for SISO AWGN channels. Moreover, as it was the case for the temporal band-limited channels, (4.40) represents only an upper bound on capacity.

In spite of its importance, though, expression (4.40) is relatively unknown, having been only recently suggested in [CF06, Mig06c, Mig08]. In both [CF06] and [Mig06c] the symmetry between the space and time domains in terms of a concise measure for spatially describing the

channel is discussed. In addition, in [CF06, Mig08] this symmetry is further exploited as K is replaced by the space bandwidth product to yield

$$\hat{C} = (\Omega L)2B \log_2 \left(1 + \frac{P_{\text{ave}}}{(\Omega L)(2B\sigma_n^2)} \right), \quad (4.41)$$

where Ω represents the angular distribution of the incoming signals, i.e. the spatial bandwidth of the communication channel, and L is the normalized array length with respect to the wavelength², i.e. observation length. In this way the product ΩL represents the space bandwidth product analogous to the time bandwidth product BT . As result, also by analogy, one can argue that the optimal number of spatial samples is ΩL which is rigorously shown in [CF06]. Even though this interpretation of K is somewhat involved at this point, its physical meaning will become more clear in chapter 7.

Finally, with this new capacity expression comprising the space and time resources, the total number of transmitted bits can be found multiplying (4.41) with T

$$\text{Number of Bits} = \hat{C}T = (\Omega L)(2BT) \log_2 \left(1 + \frac{E_{\text{ave}}}{(\Omega L)(2BT)\sigma_n^2} \right), \quad (4.42)$$

which after replacing $(\Omega L)(2BT)$ with Υ gives

$$\text{Number of Bits} = \hat{C}T = \Upsilon \log_2 \left(1 + \frac{E_{\text{ave}}}{\Upsilon \sigma_n^2} \right). \quad (4.43)$$

This result shows that the channel can be operated in either time or space and that Υ constitutes the total number of degrees of freedom available for communication, i.e. the optimal sampling rate in both space and time. As result, space is now mathematically expressed as an information bearing object subject to optimization, as happens with codewords in time. Therefore, the rather passive interpretation that space is usually given as the byproduct of a certain scenario and antenna configuration becomes sub-optimal. Instead, in this work the investigation and optimization of the spatial degrees of freedom will be pursued as seen in chapter 7.

4.4 Final remarks

In this chapter the foundations for the study of MEA systems in terms of maximum information throughput were presented. In this regard, the channel effect in improving the amount of information conveyed between two points was explained along with the concepts of diversity and multiplexing gain. In addition, normalization and comparison issues were discussed.

² L could be replaced with the normalized area or volume depending on the geometry considered.

With this background, the concept of channel capacity as a measure of the maximum allowable amount of information that can be transmitted in a communication system was explained. Furthermore, its computation was derived for three different power allocation schemes: uniform power distribution, waterfilling and beamforming. It was seen, that for both uniform and waterfilling capacities diversity and multiplexing effects are considered, but in the case of uniform power distribution a sub-optimum use of the system richness is made. On the other hand, a beamforming power allocation scheme benefits from increased diversity gain, but remains insensitive to changes in the multipath richness. Therefore, multiplexing and diversity contributions could be understood out of the cross-comparison of the beamforming and waterfilling capacities, as will be done in chapter 5 for different antenna configurations. Later on, in chapter 6 a novel and improved evaluation metric that effectively separates diversity and multiplexing effects and eases the analysis will be introduced.

Finally, this chapter closes with a discussion on the duality of the Shannon capacity and the capacity of MEA systems, in order to express capacity in terms of the communication channel spatial resources. Thus it is emphasized that for maximum capacity in MEA channels to be achieved, an optimal arrangement and current distribution of the multiple antennas used is necessary. Therefore, finding the optimum antenna arrangements as well as exploring the spatial communicational limits for the "Karlsruhe" communication channel will be a center theme during this work and will be thoroughly discussed and investigated in chapter 7.

5 Capacity study of the “Karlsruhe” communication channel

The motivation of this work is two-fold; MEA systems analysis and design. In the following the former will be addressed based on the theoretical background described up to this point. Hence, relying on the simulation framework introduced in chapter 3, in this chapter the optimality of current antenna systems in maximizing capacity will be discussed. With this purpose commercial base station antennas will be tested with different ideal receiving configurations at the mobile station. As evaluation criteria the channel capacity with the different power allocation schemes discussed in chapter 4 will be used. The conclusions obtained will contribute in extending the understanding of the antennas and channel interaction within a urban context.

5.1 Antennas and antenna arrays under study

To investigate the antenna effect on capacity in urban channels, different antennas and antenna configurations will be investigated. At the base station, the 3D radiation patterns in ϑ and ψ polarization of two commercial Kathrein antennas [KG06] will be used: the 742445 vertically polarized antenna (V) and the 742215 $\pm 45^\circ$ polarized antenna. The latter, the 742215 $\pm 45^\circ$ polarized antenna, will be studied in two polarization modes: single (/, only $+45^\circ$ polarization) and dual (X) polarization mode. All base station antennas result from (complex) measured radiation patterns at a frequency of 1980 MHz (nearest available to the 2 GHz simulation frequency). It should be noted that a modal description of the base station antennas as given in section 3.2.4 yields almost identical results and will therefore be omitted for brevity.

At the receiver, on the other hand, mostly a modal description of arbitrarily oriented dipoles will be used (see section 3.2.3). However, two dipole setups will be mainly discussed: two vertically polarized dipoles (VV) and two $\pm 45^\circ$ oriented dipoles (X). All used configurations are shown in Table 5.1, where the name, dimensions and description for all antenna setups studied are shown. Here, setup dimension expresses the $M \times N$ relation between transmitting and receiving antennas M and N . Since focus is given to the base station, only the downlink case is considered, i.e. when the base station antennas are used in transmit mode and a certain mobile station as receiver. As result $M \times N$ systems result contrary to the uplink case where the setup dimension is expressed as $N \times M$.

Table 5.1: Simulated Antenna Setups

Name	Setup dimension	Description
VV×VV	2×2	Two 742445 vertically polarized Kathrein antennas as transmitters and two vertical dipoles as receivers
VV×X	2×2	Two 742445 vertically polarized Kathrein antennas as transmitters and $\pm 45^\circ$ polarized dipoles as receivers
VVVV×VV	4×2	Four 742445 vertically polarized Kathrein antennas as transmitters and two vertical dipoles as receivers
VVVV×X	4×2	Four 742445 vertically polarized Kathrein antennas as transmitters and $\pm 45^\circ$ polarized dipoles as receivers
///×VV	2×2	Two 742215 $\pm 45^\circ$ polarized Kathrein antennas in single polarization mode as transmitters and two vertical dipoles as receivers
///×X	2×2	Two 742215 $\pm 45^\circ$ polarized Kathrein antennas in single polarization mode as transmitters and $\pm 45^\circ$ polarized dipoles as receivers
////×VV	4×2	Four 742215 $\pm 45^\circ$ polarized Kathrein antennas in single polarization mode as transmitters and two vertical dipoles as receivers
////×X	4×2	Four 742215 $\pm 45^\circ$ polarized Kathrein antennas in single polarization mode as transmitters and $\pm 45^\circ$ polarized dipoles as receivers
X×VV	2×2	One 742215 $\pm 45^\circ$ polarized Kathrein antenna as transmitter and two vertical dipoles as receivers
X×X	2×2	One 742215 $\pm 45^\circ$ polarized Kathrein antenna as transmitter and $\pm 45^\circ$ polarized dipoles as receivers
XX×VV	4×2	Two 742215 $\pm 45^\circ$ polarized Kathrein antennas as transmitters and two vertical dipoles as receivers
XX×X	4×2	Two 742215 $\pm 45^\circ$ polarized Kathrein antennas as transmitters and $\pm 45^\circ$ polarized dipoles as receivers
XXXX×VV	8×2	Four 742215 $\pm 45^\circ$ polarized Kathrein antennas as transmitters and two vertical dipoles as receivers
XXXX×X	8×2	Four 742215 $\pm 45^\circ$ polarized Kathrein antennas as transmitters and $\pm 45^\circ$ polarized dipoles as receivers

5.2 Antenna placement effects on system capacity

In addition to the different antenna setups to be studied focus will be given to antenna spacing. In all cases base station inter-element spacing s_{Tx} and mobile station inter-element spacing s_{Rx} will be varied. Changes in s_{Tx} will be identified with marker, whereas changes in s_{Rx} will be shown with different line styles. In the following subsections every configuration, grouped based on base station antenna type, will be discussed.

As evaluation criteria the relative ergodic capacity gain with respect to the SISO capacity C/C_{SISO} is selected for a fixed ρ of 10 dB. For the setups with a vertically polarized antenna at the base station the SISO setup used for reference was that of one vertically polarized antenna at the base station and one vertically polarized dipole at the mobile station. In all other cases a Xs, +45° polarized, antenna at the base station and a Vd antenna at the mobile station were used. Moreover, the three different transmitting power schemes introduced in section 4.2 will be used: uniform, beamforming and waterfilling (see Eqs. (4.17),(4.28) and (4.29)).

In addition, the channel matrix \mathbf{H} is normalized with respect to a reference channel \mathbf{H}_{REF} , as explained in section 4.1.4. Here, the reference channel chosen is the equivalent isotropic MEA channel, i.e. the channel resulting from replacing the antennas under study with omnidirectional radiators. Choice of C/C_{SISO} as evaluation criteria and the equivalent isotropic MEA channel as the reference channel, follows the need to quantify the improvement due to a certain setup independent of channel effects with respect to a fixed value. Therefore, by normalizing with an equivalent isotropic MEA channel the correlation/decorrelation of the signals due to the channel contribution is removed, so that any additional correlation or gain effects result from the antennas (i.e. setup) under study. And, by studying the relative ergodic capacity gain, the improvement with respect to the fixed SISO capacity is highlighted.

It should be noted though that the use of ergodic capacity instead of the outage capacity [TV05] is due to the fact that: 1) the channel matrices are known at each realized position and 2) the interest of this work lies in knowing the maximum attainable average capacity over a long term period. Outage capacity, on the other hand, is used when: 1) the channel has only access to the statistical characterization of the channel matrix \mathbf{H} and/or 2) a communication rate has to be assured to each mobile station (not currently in outage).

In the following, results for all setups of interest for the downlink case will be presented. In addition, the effects of polarization at the mobile station will be discussed. In all cases the relative ergodic capacity gain with respect to a SISO configuration will be investigated for a fixed Signal to Noise Ratio (SNR) of 10 dB with channel matrices normalized with respect to a reference MEA System as previously explained.

5.2.1 Vertically polarized antennas

In this section 2×2 and 4×2 systems with two or four 742445 vertically polarized Kathrein antennas at the base station will be discussed. At the mobile station arrangements of two vertically or X polarized dipoles will be used.

VV×VV

In Figure 5.1, the relative ergodic capacity gain for the VV×VV setup of Table 5.1 is shown. It is observed that both waterfilling and uniform power distributions exhibit the same trends with respect to s_{Tx} and s_{Rx} : higher capacity with larger s_{Tx} and s_{Rx} . The beamforming capacity, on the other hand, remains relatively constant (varies less than 1%). Since beamforming is a diversity dominated approach this suggests that changes in antenna spacing have little impact in improving system diversity. As result the capacity improvement due to s_{Tx} and s_{Rx} for the waterfilling and uniform power distributions are solely due to improvement in the spatial degrees of freedom of the system, i.e. better multiplexing. Furthermore, as the channel richness is improved, changes in s_{Rx} have a more pronounced effect in improving capacity at $s_{Tx} \geq 2\lambda$ (spreading of the capacity curves). However, overall, s_{Rx} has only a marginal effect in improving the multiplexing gain of the channel. The highest achievable capacity for this configuration is found with $s_{Tx} = 5\lambda$ and $s_{Rx} = 0\lambda$.

VV×X

Capacity for the VV×X setup of Table 5.1 at different antenna inter-element spacings is shown in Figure 5.2. The overall behavior seems similar to the VV×VV case with capacity gain slightly reduced due to polarization mismatch. Yet, some important differences are noticed. In this case for both waterfilling and uniform power distributions larger s_{Tx} increases capacity, but larger s_{Rx} decreases it. In the beamforming case, on the other hand, s_{Tx} has no impact on capacity and s_{Rx} seems to improve it. In consequence and given the fact that in the evaluation of the beamforming capacity no multiplexing effects are considered, it can be concluded that at smaller s_{Rx} diversity is improved (which didn't occur in the VV×VV setup). However, this improvement is reduced at larger s_{Tx} (bundling of the capacity curves). The same occurs for the waterfilling and uniform power distributions. In addition, since in these cases multiplexing becomes a significant factor, it can be added that the impact of s_{Tx} due to multiplexing is more significant than the impact of s_{Rx} due to the combined effect of diversity and multiplexing. The highest achievable capacity for this configuration is found with $s_{Tx} = 5\lambda$ and $s_{Rx} = 0\lambda$, i.e. maximum capacity is achieved when the dipoles are placed at the same spot.

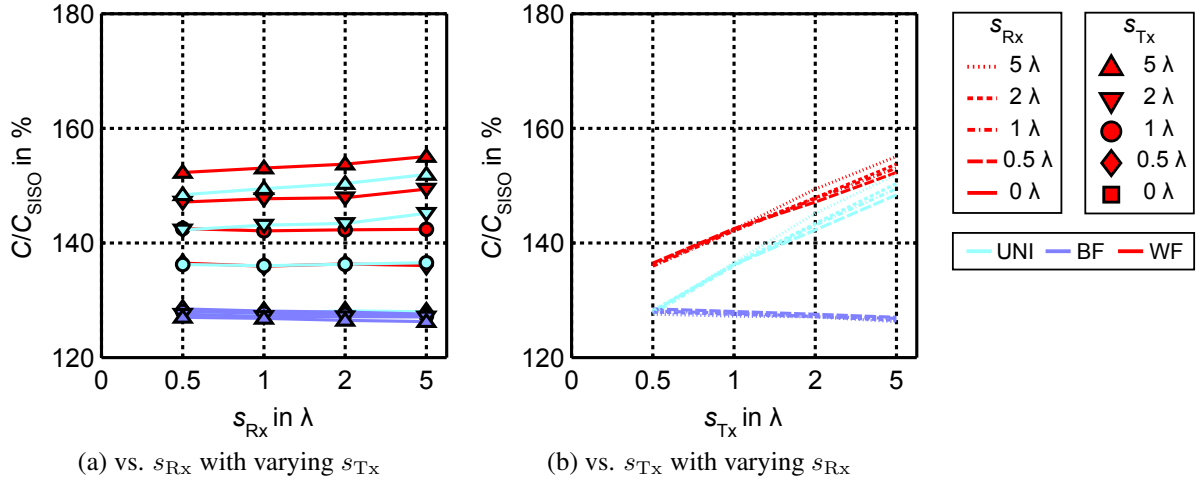


Figure 5.1: Relative ergodic capacity gain for $\text{VV} \times \text{VV}$ configuration with varying s_{Tx} and varying s_{Rx} (2×2 setup).

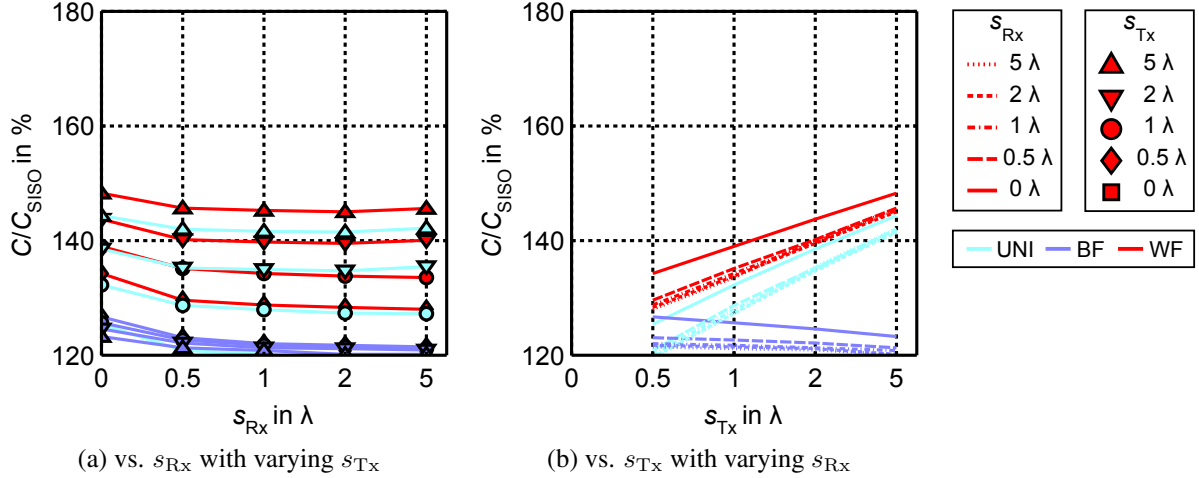


Figure 5.2: Relative ergodic capacity gain for $\text{VV} \times \text{X}$ configuration with varying s_{Tx} and varying s_{Rx} (2×2 setup).

VVVV \times X and VVVV \times X

Figures 5.3a and 5.3b show the results for VVVV \times VV and VVVV \times X setups of Table 5.1. Here, only one curve per power distribution is shown, namely that of $s_{\text{Tx}} = 0.5\lambda$ since the use of four antennas at greater s_{Tx} is impractical in light of current and planned future standards. As a result conclusions regarding the impact of s_{Tx} on the channel performance due to the antennas can not be drawn. It is seen that all power distribution schemes exhibit the same capacity trends for both receiving configurations. In the case of vertically oriented dipoles s_{Rx} has no impact on capacity. With $\pm 45^\circ$ oriented dipoles, however, a 5% capacity decrease with increasing s_{Rx} is noticed. Since all capacity curves exhibit the same trend, it can be furthermore stated that this dependence on s_{Rx} is solely due to diversity effects. Moreover, changes in s_{Rx} do not

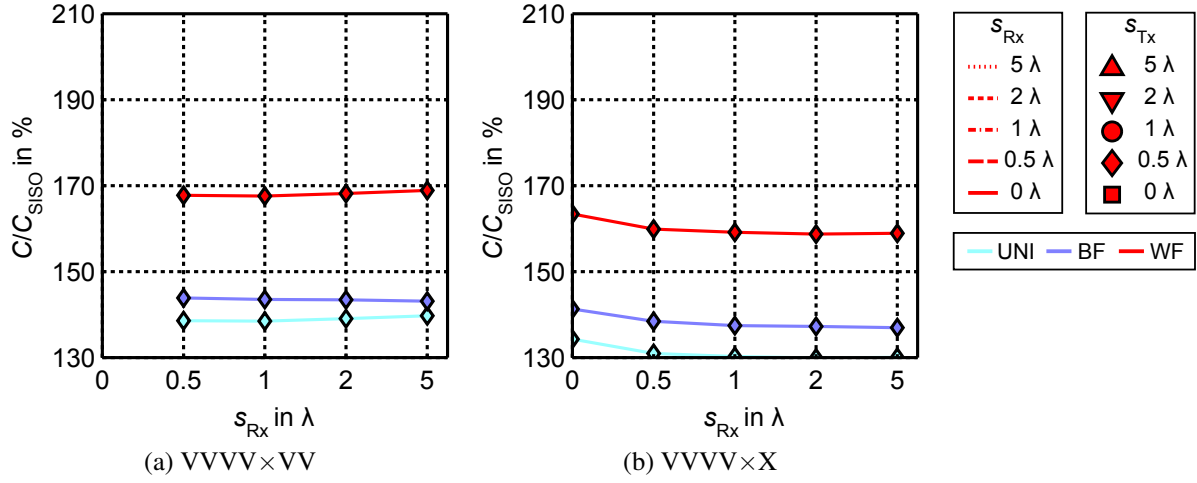


Figure 5.3: Relative ergodic capacity gain vs s_{Rx} for four vertically polarized base station antennas (4×2 setups) with $s_{\text{Tx}} = 0.5\lambda$.

seem to improve the multiplexing properties of the channel. As result, for both VVVV×VV and VVVV×X setups uniform power distribution capacity is smaller than the one attained with a beamforming power scheme. In addition, the VVVV×X setup exhibits an overall inferior performance with respect to the VVVV×VV one. The highest achievable capacity is found with $s_{\text{Rx}} = 5\lambda$ and $s_{\text{Rx}} = 0\lambda$ for the VVVV×VV and VVVV×X setups, respectively.

5.2.2 Dual polarized antennas in single polarization mode

In this section 2×2 and 4×2 systems with two or four $742215 \pm 45^\circ$ polarized Kathrein antennas in single polarization mode at the base station will be discussed. This means that in all cases each 742215 antenna will be considered as only one antenna with $+45^\circ$ polarization. At the mobile station arrangements of two vertically or X polarized dipoles will be used.

$\diagup \times \text{VV}$ and $\diagup \times \text{X}$

Figure 5.4 shows the relative ergodic capacity gain for a $\diagup \times \text{VV}$ configuration of Table 5.1. At first glance a very similar capacity dependence on used power scheme and antenna inter-element spacing to that in Figure 5.1 is seen. In addition, a slight overall capacity decrease with respect to Figure 5.1 is also observed. On the contrary, Figure 5.5, showing the $\diagup \times \text{X}$ setup of Table 5.1, gives evidence of a small overall capacity increase in spite of showing the same trends of Figure 5.2. These observations suggest that single (parallel) polarized antennas at the base station show very similar dependence on antenna placement regardless of orientation (polarization), whereas small differences on system performance can be attributed to polarization mismatch.

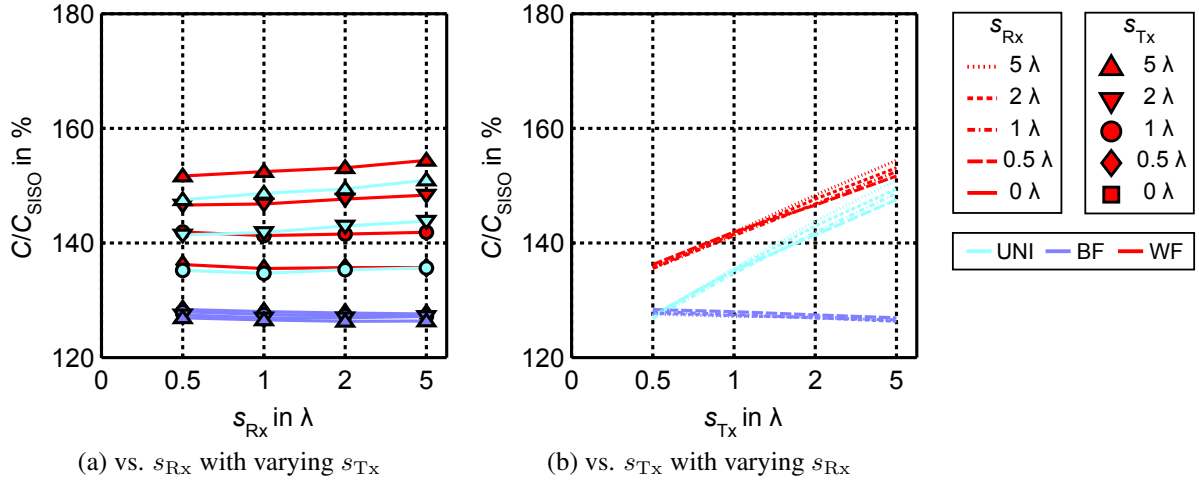


Figure 5.4: Relative ergodic capacity gain for $//\times VV$ configuration with varying s_{Tx} and varying s_{Rx} (2×2 setup).

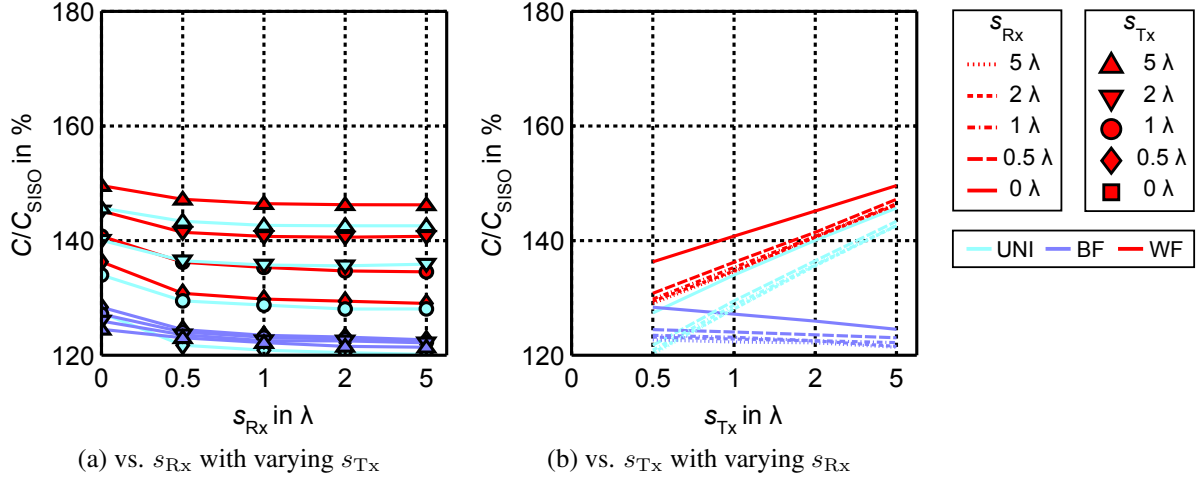


Figure 5.5: Relative ergodic capacity gain for $//\times X$ configuration with varying s_{Tx} and varying s_{Rx} (2×2 setup).

$////\times VV$ and $////\times X$

Figure 5.6 shows the relative ergodic capacity gain for the $////\times VV$ and $////\times X$ setups of Table 5.1. Here similar results as with four 742245 vertically polarized antennas are observed. In this way, higher system capacity is obtained when two vertically polarized dipoles are used at the mobile station thus confirming that the use of orthogonal polarized antennas at the mobile station when having parallel polarized antennas at the base station results in information loss. For this $////$ configuration, as was the case for VVVV, beamforming outperforms a uniform power distribution. In addition, the previous trend for the $\pm 45^\circ$ polarized dipoles is verified, i.e. a capacity maximum is obtained at $s_{Rx} = 0\lambda$. The highest achievable capacities are found with $s_{Rx} = 5\lambda$ and $s_{Rx} = 0\lambda$ for the $////\times VV$ and $////\times X$ setups.

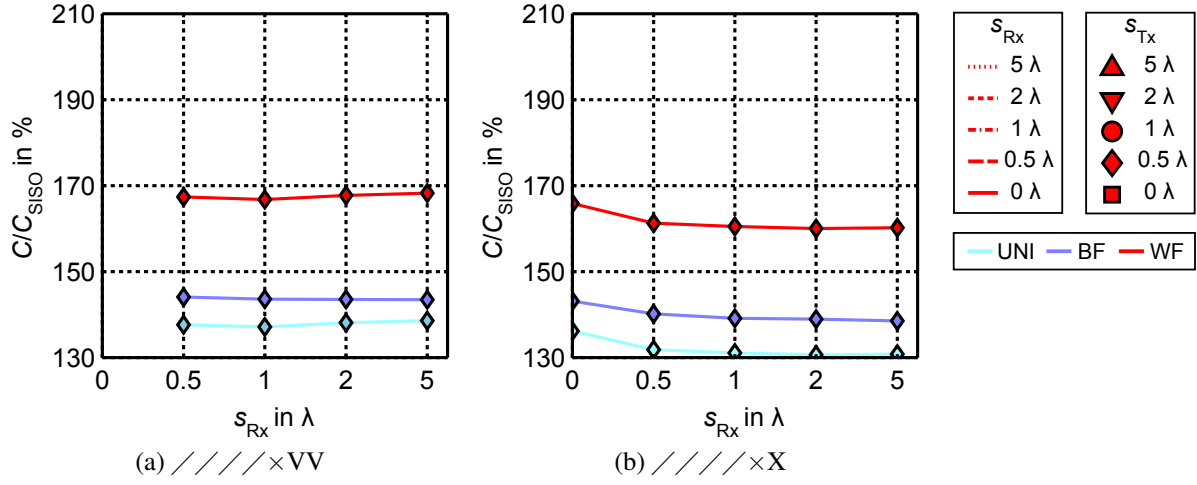


Figure 5.6: Relative ergodic capacity gain vs s_{Rx} for four $+45^\circ$ polarized base station antennas (4×2 setups) with $s_{Tx} = 0.5\lambda$.

5.2.3 Dual polarized antennas in dual polarization mode

In this section 2×2 , 4×2 and 8×2 systems with one, two and four $742215 \pm 45^\circ$ polarized Kathrein antennas at the base station will be discussed. At the mobile station arrangements of two vertically or X polarized dipoles will be used.

X×VV

In Figure 5.7, the relative ergodic capacity gain for the X×VV setup of Table 5.1 is shown. It is seen that once more both waterfilling and uniform power distributions exhibit similar trends as was the case of single polarized antennas at the base station. Furthermore, in this case, the capacity values exhibited by both power schemes are more similar. In particular it is seen that in this case relative ergodic capacity gain dependence on s_{Rx} is dominant with respect to s_{Tx} . The beamforming capacity curves, on the other hand, exhibit little change due to variations on the antennas inter-element spacing. From the previous observation it can be concluded that s_{Tx} and s_{Rx} do not significantly impact the channel diversity, whereas s_{Rx} does seem to improve the channel richness. s_{Tx} on the contrary has almost no effect on the channel multiplexing gain. In addition, neither s_{Tx} nor s_{Rx} increases the capacity dependence on antenna inter-element spacing at the other communicating end (cf. Figure 5.1). The highest achievable capacity for this configuration is found with $s_{Tx} = 0\lambda$ and $s_{Rx} = 5\lambda$.

It should be noted that in this case higher capacities with respect to VV and // configurations at the base station (equal number of active antennas) are seen for the waterfilling and uniform power distributions. Beamforming capacity, however, evidences little improvement. The latter indicates that orthogonal polarization at the base station can contribute to increased capacity if

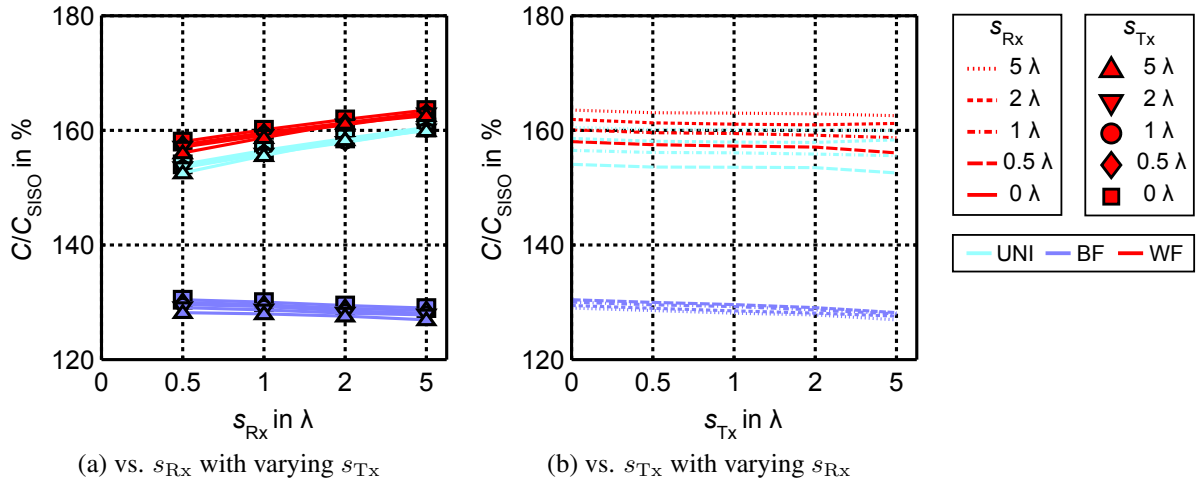


Figure 5.7: Relative ergodic capacity gain for $X \times VV$ configuration with varying s_{Tx} and varying s_{Rx} (2×2 setup).

the channel multiplexing properties are exploited. This also explains the very good performance of the uniform power scheme, which approximates the waterfilling case (optimum).

$X \times X$

In Figure 5.8 the relative ergodic capacity gain for the $X \times X$ setup of Table 5.1 is depicted. In this case, differences in the capacity performance with respect to power distribution scheme and antenna inter-element spacing is verified in all cases. Once more, the performance of the waterfilling and uniform power distributions is very similar, thus suggesting the existence of very strong multiplexing in the channel. This is corroborated by the fact that this setup leads to the highest capacities of all 2×2 configurations. Furthermore, a dependence on both s_{Tx} and s_{Rx} exists in the beamforming case which suggests increased channel diversity at smaller spacings. The same trend is also recognized for the waterfilling and uniform power distributions. This suggests that antenna spacing effects on diversity are more noticeable than those due to changes in the multiplexing properties of the channel. In addition it is seen that at smaller s_{Tx} and s_{Rx} changes in antenna spacing at the other communicating end have a greater impact on the capacity of the system (lines bundle at large s_{Tx} and s_{Rx}). Moreover, it seems that the impact of s_{Tx} on capacity is more dependent on s_{Rx} than otherwise. In other words diversity improvements due to s_{Tx} are mostly noticeable at $s_{\text{Rx}} = 0$ and less remarkable at all other spacings. The highest achievable capacity for this configuration is found with $s_{\text{Tx}} = 0\lambda$ and $s_{\text{Rx}} = 0\lambda$.

$XX \times VV$

In Figure 5.9 the relative ergodic capacity gain for the $XX \times VV$ setup of Table 5.1 is depicted. Since this is a 4×2 system a considerable capacity increase with respect to the previous 2×2

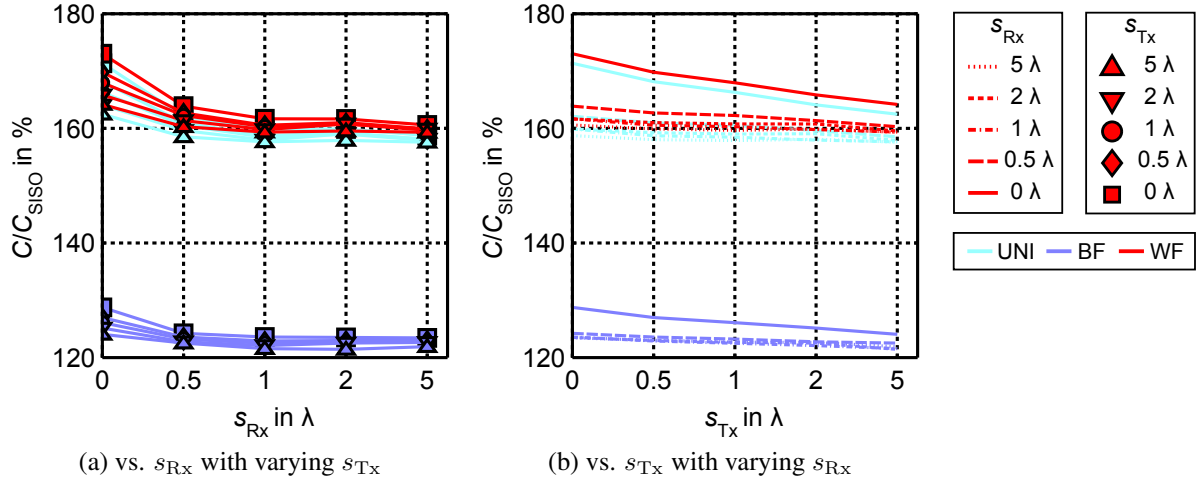


Figure 5.8: Relative ergodic capacity gain for $X \times X$ configuration with varying s_{Tx} and varying s_{Rx} (2×2 setup).

configurations is noted. However, an important capacity increase with respect to the 4×2 systems of the previous sections is also seen for the waterfilling and uniform power distributions (see Figures 5.3 and 5.6). In addition, both power schemes achieve different capacity gains, yet the same dependence to changes on s_{Tx} and s_{Rx} is noted. Beamforming capacities, however, are unaffected by variations in antenna spacing at both the base and mobile station and show similar values to those of previous 4×2 setups. As result it can be stated that the XX configuration at the base station does not improve the system diversity with respect to VVVV or $\diagup\diagup\diagup$ cases. Therefore, capacity changes in the waterfilling and uniform power distributions are solely due to increased multipath richness (since diversity effects seen at hand from the beamforming case are negligible). Concentrating thus in these two cases shows that both s_{Tx} and s_{Rx} improve the channel richness in a similar manner: at larger s_{Tx} and s_{Rx} capacity improves. Moreover, neither s_{Tx} nor s_{Rx} have a dominant effect. In the same manner neither one has an effect on the other one (no capacity bundling or spread). Finally, comparing Figure 5.9 with Figure 5.7 and the single polarized setups of the previous sections it seems that when more than one antenna of a certain polarization type is used both s_{Tx} and s_{Rx} increase capacity at larger spacings. Furthermore, in the case of s_{Tx} its impact on the channel becomes more significant. The highest achievable capacity for this configuration is found with $s_{\text{Tx}} = 5\lambda$ and $s_{\text{Rx}} = 5\lambda$.

XX×X

The relative ergodic capacity gain for the $XX \times X$ setup of Table 5.1 is shown in Figure 5.10. Overall, the capacity levels attained by each power scheme are comparable to those of Figure 5.9. An important difference is that for the beamforming case a slight capacity decrease is noticed. Because of these observations it can be stated that for this setup, diversity gain is reduced but multiplexing gain is comparable to that of the $XX \times VV$ configuration. Considering

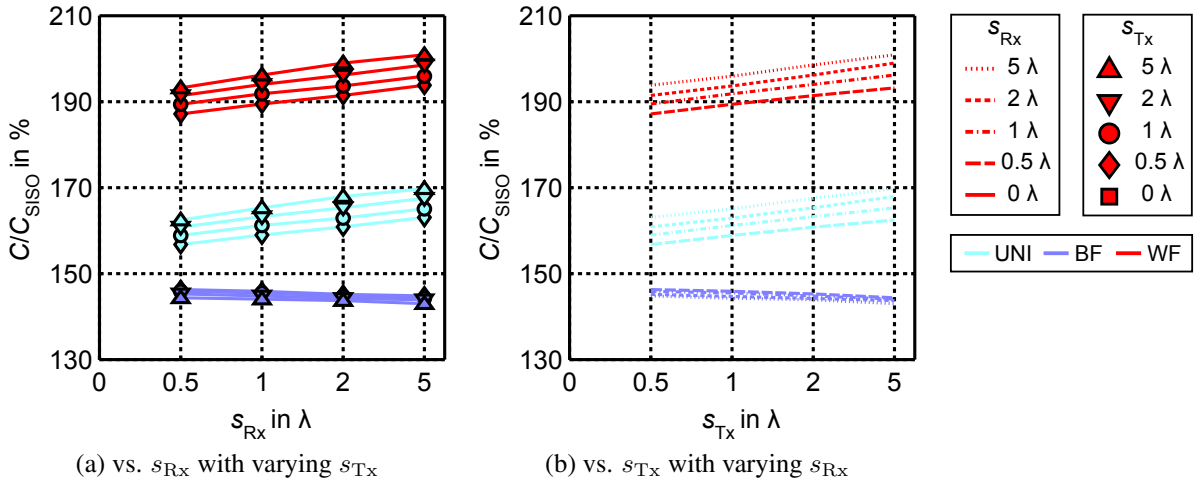


Figure 5.9: Relative ergodic capacity gain for XX×VV configuration with varying s_{Tx} and varying s_{Rx} (4×2 setup).

now the impact of s_{Tx} and s_{Rx} on the capacity of the different power schemes it is noted that: smaller s_{Rx} slightly improves the beamforming capacity, whereas s_{Tx} does the same for the multiplexing gain. As result impact of s_{Rx} on capacity is reduced at larger s_{Tx} (cf. Figure 5.2b). In the same manner, impact of s_{Tx} on capacity is reduced at smaller s_{Rx} (cf. Figure 5.2a). The highest achievable capacity for this configuration is found with $s_{\text{Tx}} = 5\lambda$ (only marginal difference with respect to other configurations) and $s_{\text{Rx}} = 0\lambda$.

XXXX×VV and XXXX×X

Figure 5.11 shows the XXXX×VV and XXXX×X setups of Table 5.1. Given that these are the only 8×2 setups, higher capacities are obtained. However, in this case impact of s_{Tx} on channel performance can't be assessed since only one antenna inter-element spacing at the base station is used. Overall, improvement with respect to the previous setups is noticed mostly by the waterfilling and beamforming power distributions. The uniform power distribution capacities evidence no improvement due to this new configuration. Dependence on s_{Rx} on the other hand is the same as that of Figures 5.3 and 5.6 for both receiving configurations. The only difference with respect to these previous setups is that in this case, impact of s_{Rx} on the channel capacity of the waterfilling and uniform power distributions is more pronounced for the case of vertical polarized dipoles at the mobile station. The highest achievable capacities are found with $s_{\text{Rx}} = 5\lambda$ and $s_{\text{Rx}} = 0\lambda$ for the XXXX×VV and XXXX×X setups, respectively.

5.2.4 Influence of mobile unit rotation on antenna placement

The previous results have been novel in the sense that they extend previous network modeling efforts to urban scenario with 3D measured patterns. Nonetheless, up to this point, in spite of

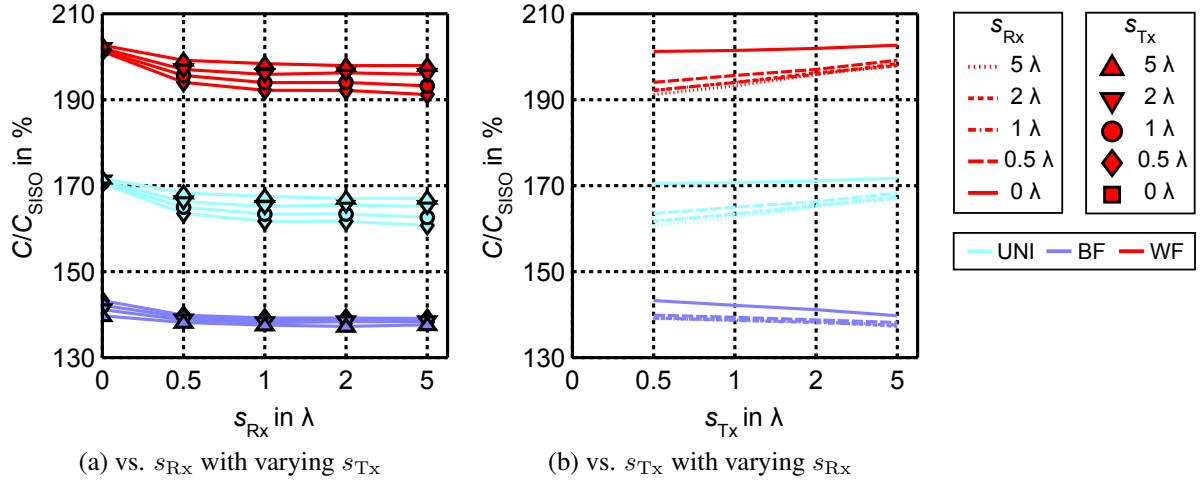


Figure 5.10: Relative ergodic capacity gain for XX×X configuration with varying s_{Tx} and varying s_{Rx} (4×2 setup).

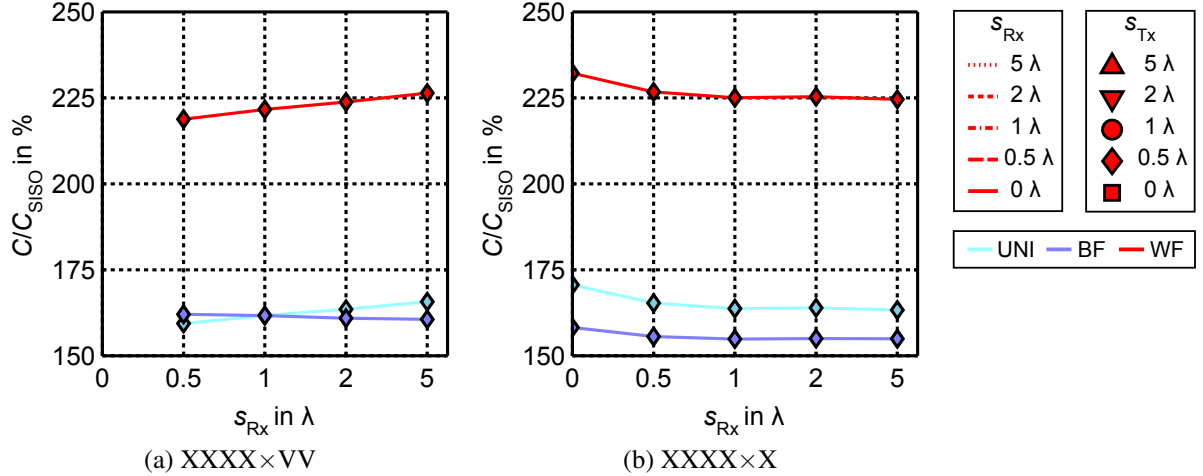


Figure 5.11: Relative ergodic capacity gain vs s_{Rx} for four ±45° polarized base station antennas (4×2 setups) with $s_{\text{Tx}} = 0.5\lambda$.

the results obtained, no additional benefit seems to have been gained from the modal approach with respect to the known network model. This follows from the fact that in the previous section three different modes and three different antenna orientations, vertical and ±45°, were used per base station antenna, which results in approximately the same number of computations for both network modeling approaches. The key difference is, however, that with the modal method it is now possible to describe all possible antenna orientations, since all modes needed to describe an arbitrarily oriented dipole have already been computed, i.e. all $\tilde{\gamma}_{r,nm}$ in (3.13) are known. Therefore, here the relative capacity gain plotted against rotation angle α for the vertical and ±45° polarized base station antennas will be shown. In addition the two different mobile station antenna setups seen in Figure 5.12 will be used: a) two parallel dipoles rotated

with respect to the z -axis and b) two perpendicular dipoles rotated with respect to their starting position as vertically and horizontally polarized dipoles. Finally, the impact of antenna spacing in each case will be also investigated. Overall, with the modal approach, simulation time was reduced to half the simulation time of the traditional network model.

In Figure 5.13a the 742445 vertically polarized Kathrein antenna is studied together with two parallel dipoles rotated around the z -axis. It is seen that there is a cosine-like dependence on the angle α resulting in decreased capacity gain for all angles greater than 0° . Nevertheless, no significant influence of rotation angle on the behavior of s_{Tx} and s_{Rx} is seen. In Figure 5.13b the same base station antenna with two perpendicular dipoles is studied. In this case, the capacity dependence on varying s_{Tx} and s_{Rx} remains to great extent constant (a smaller dependence on s_{Rx} at $\alpha = 45^\circ$ is however noted). Most importantly great robustness toward changes in rotation angle α is seen.

Figures 5.14a and 5.14b show similar results for the $742215 \pm 45^\circ$ polarized Kathrein antenna. Contrary to the vertically polarized base station, for the case of two parallel dipoles at the mobile station a slight maximum appears at a rotation angle of 30° for almost all s_{Tx} and s_{Rx} configurations. This suggests that the channel propagation effects induce a concentration of electric fields polarized around 30° . Even though this is a channel specific phenomenon it is not expected to vary drastically in other urban scenarios. A setup of two perpendicular dipoles, on the other hand, yields a similar performance as in Figure 5.13b with almost no dependence of capacity on rotation angle.

5.3 Setup comparison

At this point, in order to have a better overview of how each configuration performs with respect to the others, when compared with regard to s_{Rx} and s_{Tx} , a comparison of all setups is

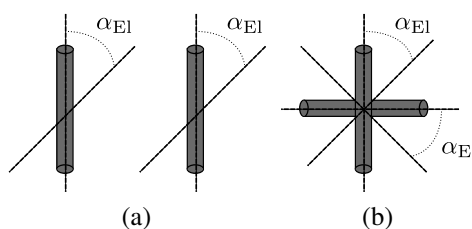


Figure 5.12: Mobile station antenna setups. (a) Two parallel dipoles rotated with respect to the z -axis and (b) two perpendicular dipoles rotated with respect to their starting position as vertically and horizontally polarized dipoles.

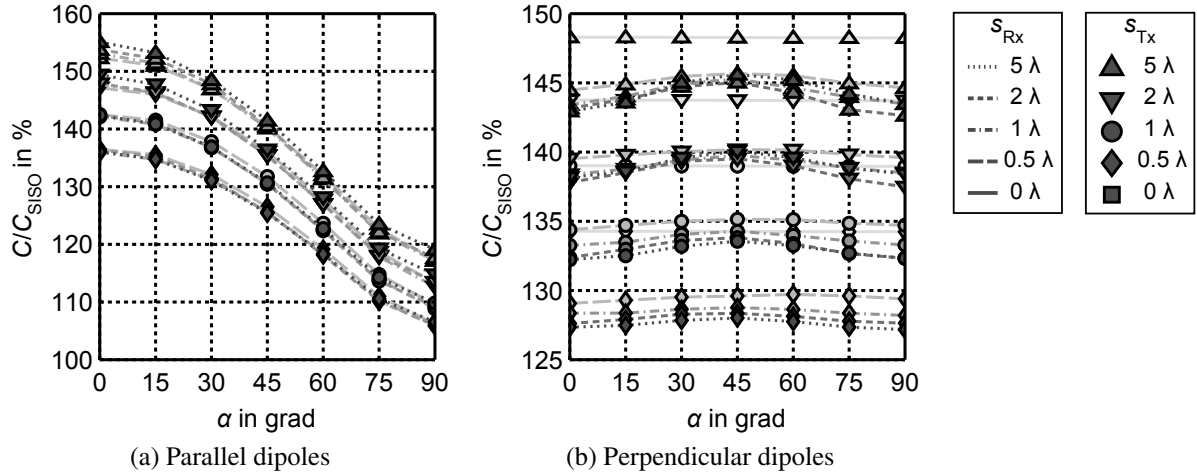


Figure 5.13: Relative ergodic capacity gain with varying s_{Tx} and varying s_{Rx} for configurations of two vertically polarized base station antennas and two rotated dipoles (2×2 setups).

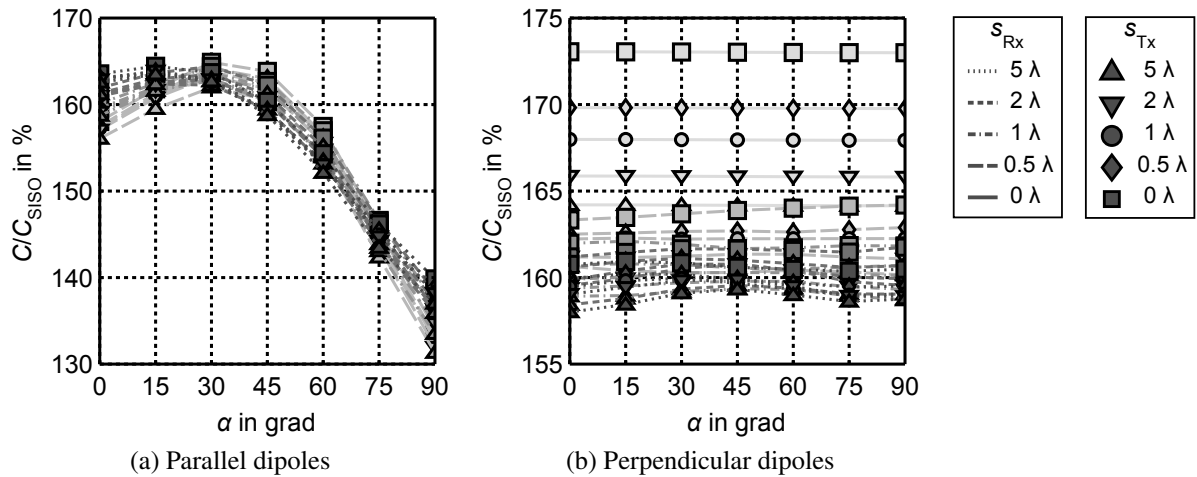


Figure 5.14: Relative ergodic capacity gain with varying s_{Tx} and varying s_{Rx} for configurations of two vertically polarized base station antennas and two rotated dipoles (2×2 setups).

performed. For this purpose the waterfilling capacity for vertically and perpendicularly polarized dipoles at the mobile station is shown in Figures 5.15a and 5.15b respectively. In this way the overall diversity and multiplexing effects for each configuration can be assessed. For compactness s_{Rx} is varied, whereas s_{Tx} is chosen to be the inter-element spacing at the base station yielding the highest capacity. It should be noted though that for those configurations with more than two physical antennas at the base station, i.e. VVVV, // / / and XXXX, only inter-element spacings of 0.5λ are considered. Setups are ordered based on the MIMO system dimensions, i.e. number of active transmit and receive antennas as shown in Table 5.1. The abscissa axis is labeled after the base station antenna type used in each case.

In general, from Figure 5.15 it is confirmed that multiple antennas of the same type achieve the greatest capacities at $s_{Tx} = 5\lambda$, i.e. in the VV, //, XX setups (VVVV, //// and XXXX setups would probably yield the same results but weren't simulated). Furthermore, it is noticed that in configurations of equal dimensions (VV, //, X) the use of $\pm 45^\circ$ polarized antennas at the base station results in higher capacities, especially in the case of two $\pm 45^\circ$ polarized dipoles at the mobile station. In addition, it is also observed that for configurations with X polarized receiving antennas dependence on s_{Rx} is small. On the other hand, for vertically polarized dipoles at the mobile station the capacity performance among single polarized configurations is very similar.

5.4 Final remarks

In the previous sections the analysis of antenna systems was undertaken and several assessments toward the efficiency of each configuration and the capacity improvement it represented for the communication channel were made. The goal of this analysis was to understand how the channel-antennas interaction results in better capacities, in order to improve the design of antenna systems. In particular two effects were of interest: 1) capacity increase in response to antenna diversity at different antenna positions and 2) increased multiplexing gain as result of more decorrelated setups. In the following the most important conclusions of the previous analysis will be summarized:

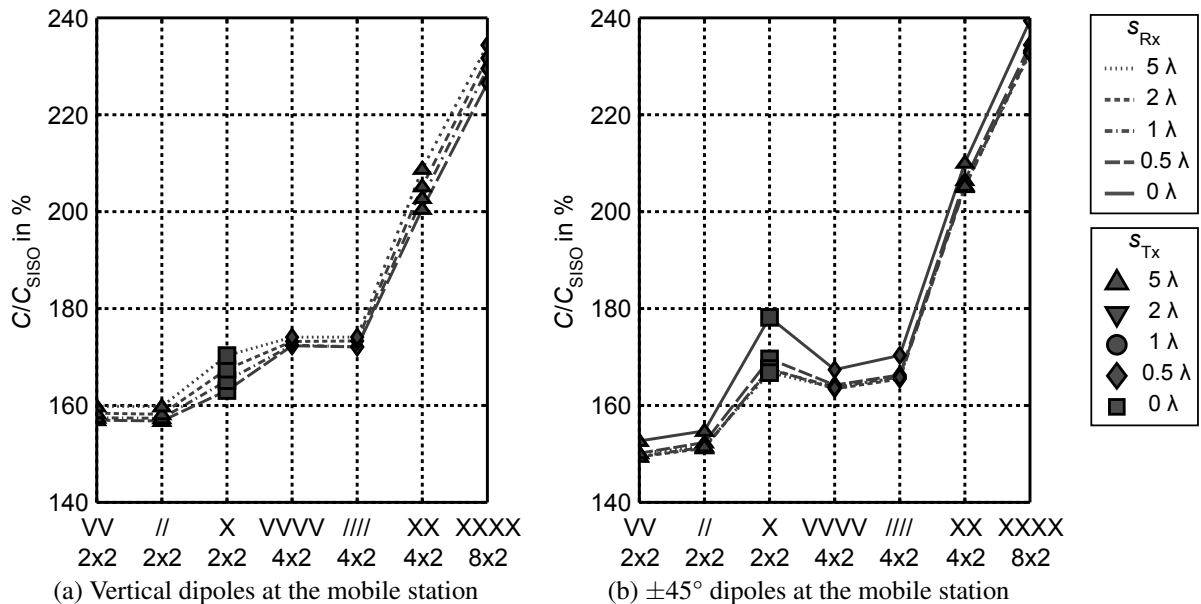


Figure 5.15: Relative ergodic capacity gain for different base station configurations with varying s_{Rx} and optimum s_{Tx} .

- Diversity, seen through the capacity gain of the beamforming power scheme, is in most configurations insensitive to changes in s_{Rx} or s_{Tx} . However, $\pm 45^\circ$ polarized antennas at the mobile station improved diversity gain at $s_{Rx} = 0\lambda$.
- Capacity of single polarized antenna systems is directly dependent on antenna inter-element spacing at both the base station and mobile station. Dependence on s_{Tx} is however larger due to the fact that the incoming signals at the mobile station arrive sufficiently decorrelated. Because of this, larger antenna inter-element spacings do not further decorrelate the signals.
- Perpendicular polarized antennas (no repeated polarization) show that polarization diversity results in a capacity maximum when the antennas are placed at the exact same position. In other words, X polarized antennas exhibit their largest diversity gain at 0λ . From this follows that $\pm 45^\circ$ polarized antennas capacity is inversely proportional to antenna inter-element spacing.
- Polarization diversity in the form of $\pm 45^\circ$ polarized antennas at the base station improves capacity regardless of the receiving configuration.
- Polarization diversity in the form of $\pm 45^\circ$ polarized antennas at the mobile station can result in lower capacity values when used together with single polarized setups at the base station.
- If more than one set of perpendicular polarized antennas is used at the base station, for example XX, capacity curves resemble those of single polarized antennas, even though higher capacity values are obtained. This means that repetition of a certain antenna type (polarization) worsens signal correlation so that larger s_{Tx} improves the multiplexing gain.

From the previous capacity study the complexity behind the analysis of multiple element antennas has been grasped. It is seen that the understanding of such systems is a multi dimensional problem that requires extensive cross-comparison and experience. Because of this, the choice of new antenna configurations poses a serious difficulty to system engineers trying to understand the true nature of the contribution a certain antenna setup might have on the system. In this chapter an extensive comparison of possible antenna setups has been made that strives to ease the selection process of future antenna configurations based on the diversity and multiplexing effects verified here for the previously discussed setups. The fact, however that no clear measure for each of this contribution other than an experienced analysis of different capacity curves is still an open problem. Therefore, in the next chapter, a solution to this problematic will be introduced.

6 Improved evaluation metric for multiple element antenna systems

In the previous chapter the analysis of MEA systems in an urban setting was approached. It was seen that for such an extensive study important difficulties in the evaluation and understanding of antenna systems exist that demand both experience and a great deal of cross-comparison. Therefore, this chapter contribution will focus mainly on improving the evaluation framework of MEA systems. With this purpose an evaluation metric will be provided that addresses the following two issues:

- **Comparison ease between published works.** In the previous section capacity results for several antenna setups were shown and compared for the urban communication channel. As benchmarking criteria the relative ergodic capacity of the normalized channel (with respect to the equivalent isotropic MIMO channel) was chosen. This criteria was justified by the need to understand the relative improvement of a certain antenna configuration with respect to the SISO case. At the same time the choice of an equivalent isotropic MIMO channel for normalizing the channel matrix meant to exclude diversity effects proper to the channel. By doing so, no universal comparison was given, but rather a very specific one. As result, the fact that different needs require different norms consists in the biggest problem faced when trying to compare different works regarding MEA systems.
- **Analysis of diversity and multiplexing trade-off.** Through the results presented in chapter 5 it was seen that in some cases it is not clear by which mechanisms a certain antenna configuration may contribute to improve the capacity of a system. Usually being able to discern between the multiplexing and diversity benefits of two antenna configurations based on capacity curves alone requires a great deal of experience. This is mostly so, due to the fact that both effects go simultaneously into the channel matrix, which is then used to compute the system capacity as shown in section 4.2. In consequence it is very difficult to quickly and unequivocally identify the mechanism by which a certain configuration or setup might help improve system performance.

In this chapter an evaluation metric for multiple element antenna systems will be provided that addresses the two previously discussed issues. More specifically, an implementation of an eigenvalue based evaluation framework is detailed. The main idea behind this metric is to introduce a measure of performance independent to changes in normalization scheme and SNR

regime, that separates diversity and multiplexing effects. In this way it would be possible to use the results of previous works where the capacity is evaluated for an arbitrarily normalized system, e.g. Frobenius normalized, to obtain the capacity of the same system under another norming scheme, that wasn't originally considered. Furthermore, it would be also possible to more easily understand the mechanism (i.e. diversity or multiplexing gain) in which a certain antenna arrangement impacts the system performance for communicating. In the following a general description of this metric for arbitrary sized channels will be derived. The metric presented here is a modified and extended version of the one used in [SSV⁺08]. Throughout this chapter the most relevant setups from chapter 5 will be used.

6.1 Eigenmode-based metric for Frobenius-normalized channels

It has already been shown that there is a considerable amount of information to be processed when dealing with multipath propagation channels and multiple channel realizations. Out of this raw data useful information about the system or channel performance can be obtained, such as information throughput. The problem is that in doing so several assumptions are done, such as constant transmit power, constant SNR or reference system, which result in different normalizations. Therefore, once the data has been processed and presented in form of capacity curves it is difficult to display it in some other way. As result, a cross comparison of published results becomes a very difficult (if not impossible) task. To overcome this problem an intermediate metric is needed that is both compact and allows reconstruction of capacity and other performance measures with ease. In this work an eigenvalue analysis is used to address these issues.

Several works have previously suggested the use in some way of the eigenvalues to analyze the informational theoretical limits of MIMO systems. Furthermore, exact solutions for capacity based on moment generating functions (MGF) of the distribution of the mutual information [SW08, SMM06, KA06, WG04] have been proposed. However, in spite of the fact that both ergodic and outage capacities can be obtained through direct differentiation and integration, these MGF are involved, non-intuitive for system developers and based on assumptions about the statistics of the channel matrix. Furthermore, no straightforward information regarding the diversity and multiplexing characteristics of the system is given. Therefore, even though a wide knowledge of the eigenvalues statistical properties, summarized in [OPF09], is readily available, a general framework for a channel independent and accurate description of mutual information for both simulations and measurements is still missing.

On the search for a better evaluation framework for the capacity performance, in this section a set of evaluation criteria is introduced based on the concept of eigenvalue dispersion to be derived in the following. Furthermore, since the approach proposed is valid for communication channels or communication systems as a whole, mention to the communication system will be made instead of to the communication channel. In addition, for brevity, only the uniform power distribution will be considered.

Derivation of an eigenmode-based metric will begin by first considering the instantaneous capacity of a Frobenius normalized system with uniform power distribution (4.17) expressed as

$$C(\mathbf{H}, \rho) = \log_2 \left| \mathbf{I}_N + \frac{\rho}{M} \left(\frac{\mathbf{W}}{1/MN} \right) \right|, \quad (6.1)$$

with $\mathbf{W} = \mathbf{H}\mathbf{H}^H / \|\mathbf{H}\|_F^2$. This can now be rewritten to

$$\begin{aligned} C(\mathbf{H}, \rho) &= \log_2 |\mathbf{I}_M + \rho N(\mathbf{W})| \\ &= \log_2 \left[\prod_{k=1}^K (1 + \zeta \lambda_k) \right], \end{aligned} \quad (6.2)$$

where $\zeta = \rho N$, $K = \min(M, N)$ and where the matrix \mathbf{W} determinant has been expressed in form of its characteristic polynomial, i.e. its eigenvalues λ_k .

6.1.1 Rank-2 systems

Evaluating (6.2) for a rank-2 system, i.e. a system with two antennas at either the receiver or transmitter so that $K = 2$, gives

$$\begin{aligned} C(\mathbf{H}, \rho) &= \log_2 [(1 + \zeta \lambda_1)(1 + \zeta \lambda_2)] \\ &= \log_2 [(1 + \zeta(\lambda_1 + \lambda_2) + \zeta^2 \lambda_1 \lambda_2)], \end{aligned} \quad (6.3)$$

which can be rewritten as function of the eigenvalues sum and product to

$$C(\mathbf{H}, \rho) = \log_2 \left[(1 + \zeta \left(\sum_{k=1}^2 \lambda_k \right)) + \zeta^2 \left(\prod_{k=1}^2 \lambda_k \right) \right]. \quad (6.4)$$

Observing that in this last equation the sum term is related to the arithmetic mean of the eigenvalues of the matrix \mathbf{W} , whereas the product term is related to the geometric gain, a geometrical

measure relating both results could exist. A literature survey pointed to the eigenvalue dispersion criterion defined in [SSV⁺08] and originally proposed in [SSESV04]

$$\xi = \frac{\left(\prod_{k=1}^K \lambda_k\right)^{\frac{1}{K}}}{\frac{1}{K} \sum_{k=1}^K \lambda_k}. \quad (6.5)$$

In [SSESV04] and [SSESV06b] this sphericity measure of multivariate statistic [And03] was proposed for finding a lower bound for the ergodic capacity in the high SNR regime. In these works it was also shown that the ratio of the geometric and arithmetic means ξ constitutes a scale-invariant measure of the system dispersion. Due to this fact it was proposed as evaluation metric in [SSV⁺08] and will be fundamental in providing an intuitive evaluation metric, in contrast to very similar diversity measures already proposed in the past, such as that of [IN03].

Having found a measure for the relationship of the geometric and arithmetic means this new measure is now incorporated within the capacity expression by first solving (6.5) for the product of the eigenvalues with $K=2$

$$\prod_{k=1}^2 \lambda_k = \left(\frac{\xi \sum_{k=1}^2 \lambda_k}{2} \right)^2 \quad (6.6)$$

and then using the result in (6.4) yields

$$\begin{aligned} C(\mathbf{H}, \zeta(\rho)) &= \log_2 \left[\left(1 + \zeta \left(\sum_{k=1}^2 \lambda_k \right) + \zeta^2 \left(\frac{\xi \sum_{k=1}^2 \lambda_k}{2} \right)^2 \right) \right] \\ &= \log_2 \left[\left(1 + \zeta + \left(\frac{\zeta \xi}{2} \right)^2 \right) \right], \end{aligned} \quad (6.7)$$

where for the Frobenius normalized system $\sum_{k=1}^K \lambda_k = 1$. It should be noted that the system dimension, i.e. the total number of receiving and transmitting antennas MN , 4 in this case, is already accounted for in (6.1).

(6.7) is of great importance since the capacity of rank-2 systems is now expressed in a separable form as a function of SNR and of the multipath richness expressed through the eigenvalue dispersion. This means that it is now possible to compare different Frobenius normalized MIMO systems based only on SNR regime and its eigenvalue dispersion. This is a great advantage towards other metrics like effective degrees of freedom [SFGK00], which is SNR dependent, or condition number [ESBP02], dependent only on the largest or smallest eigenvalue (which for the case of a rank-2 system may suffice, but lacks information for higher ranked systems).

6.1.2 Rank-K systems

A more general expression of (6.4) for rank-K systems based on (6.5) can be expressed as

$$C \geq \log_2 \left[(1 + \zeta \left(\sum_{k=1}^K \lambda_k \right) + \zeta^K \left(\prod_{k=1}^K \lambda_k \right) \right]. \quad (6.8)$$

Expression (6.8) becomes an equality for the case of K=2. For higher ranked systems, though, it fails to reproduce the true system capacity. This leaves the need for a metric as insightful as (6.5) but with much higher fidelity. Therefore, in order to understand how can the eigenvalue dispersion metric adapt to higher ranked systems, a rank-3 system is now investigated. Obtaining a similar expression to (6.3) for rank-3 systems results in

$$\begin{aligned} C(\mathbf{H}, \rho) &= \log_2 [(1 + \zeta \lambda_1)(1 + \zeta \lambda_2)(1 + \zeta \lambda_3)] \\ &= \log_2 [1 + \zeta(\lambda_1 + \lambda_2 + \lambda_3) + \\ &\quad \zeta^2(\lambda_1 \lambda_2 + \lambda_1 \lambda_3 + \lambda_2 \lambda_3) + \zeta^3(\lambda_1 \lambda_2 \lambda_3)] \\ &= \log_2 [1 + \zeta(\text{tr}_1(\mathbf{W})) + \zeta^2(\text{tr}_2(\mathbf{W})) + \zeta^3(\text{tr}_3(\mathbf{W}))], \end{aligned} \quad (6.9)$$

where in the last step of (6.9) the definition of elementary symmetric functions of \mathbf{W} given in [Mat97] is used. Here, the k -th elementary symmetric function is given by

$$\text{tr}_k(\mathbf{W}) = \sum_{i_1 < i_2 < \dots < i_k} \lambda_{i_1} \cdots \lambda_{i_k} \quad (6.10)$$

and the sum is over all $\binom{K}{k}$ combinations of k indices with $i_1 < \dots < i_k$.

The use of elementary symmetric functions within the context of mutual information is not novel. In [MSV04] elementary symmetric functions were used in obtaining a tight upper bound on the average mutual information, i.e. ergodic capacity. Furthermore, [MSV04] also explains its relation to complex zonal polynomials which were also used in [SMV04] to obtain an upper bound on ergodic capacity. Here, it is departed from the common approach of defining capacity bounds valid under certain assumptions to explore the physical significance of restructuring the instantaneous mutual information expression in terms which can be easily understood. The goal is then to use these terms as a general metric regardless of SNR regime, norm and evaluation sense (ergodic or outage). With this in mind, the instantaneous capacity for the general case of rank-K systems can be rewritten as follows

$$C(\mathbf{H}, \rho) = \log_2 \left[1 + \sum_{k=1}^K \zeta^k \text{tr}_k(\mathbf{W}) \right]. \quad (6.11)$$

This equation, also valid for the case of rank-2 systems, can now be compared with the one found previously in (6.7) based on the eigenvalue dispersion ξ . An attempt to rewrite (6.7) in a similar form of (6.11) as a sum of terms, fails because of the absence of ξ in the second term of the logarithm. However, it is seen that if it were possible to do such an analogy the elementary symmetric functions could be rewritten in terms of physical meaningful system quantities. In the search of an equivalent expression of (6.11), related in some form to ξ , (6.9) is approximated by considering only the most meaningful eigenvalues in each elementary symmetric function, leading to

$$C(\mathbf{H}, \rho) \approx \log_2 [1 + \zeta(\lambda_1) + \zeta^2(\lambda_1\lambda_2) + \zeta^3(\lambda_1\lambda_2\lambda_3)]. \quad (6.12)$$

It is seen that each k-term corresponds to the k -th elementary symmetric function of a rank- k system, with $k \leq K$, i.e.

$$\begin{aligned} C(\mathbf{H}, \rho) \approx \log_2 & [1 + \zeta(\text{tr}_1(\mathbf{W}_1)) + \\ & \zeta^2(\text{tr}_2(\mathbf{W}_2)) + \zeta^3(\text{tr}_3(\mathbf{W}_3))] , \end{aligned} \quad (6.13)$$

where \mathbf{W}_k represents the k -th ranked submatrix from the rank-K matrix \mathbf{W} with

$$\text{tr}_1(\mathbf{W}_1) = \lambda_1, \quad (6.14)$$

$$\text{tr}_2(\mathbf{W}_2) = \lambda_1\lambda_2, \quad (6.15)$$

$$\text{tr}_3(\mathbf{W}_3) = \lambda_1\lambda_2\lambda_3, \quad (6.16)$$

i.e.

$$\text{tr}_{\mathcal{K}}(\mathbf{W}_{\mathcal{K}}) = \prod_{k=1}^{\mathcal{K}} \lambda_k. \quad (6.17)$$

In addition, from (6.7) it is known that for rank-2 systems the 2-nd elementary symmetric function can be related directly to ξ . Therefore, a revision of the eigenvalue dispersion definition to consider sub-ranked systems might give insight into a more intuitive characterization of communication systems. It follows that the new eigenvalue dispersion $\phi_{\mathcal{K}}$ of the \mathcal{K} -th sub-ranked system can be written as

$$\phi_{\mathcal{K}} = \frac{\left(\prod_{k=1}^{\mathcal{K}} \lambda_k\right)^{\frac{1}{\mathcal{K}}}}{\frac{1}{\mathcal{K}} \sum_{k=1}^{\mathcal{K}} \lambda_k} = \frac{(\text{tr}_{\mathcal{K}}(\mathbf{W}_{\mathcal{K}}))^{\frac{1}{\mathcal{K}}}}{\frac{1}{\mathcal{K}} \sum_{k=1}^{\mathcal{K}} \lambda_k} \quad \mathcal{K} = 1, \dots, K, \quad (6.18)$$

where the following very attractive properties of the original eigenvalue dispersion [SSESV06a, SSESV06b] are maintained:

- Its logarithm can be interpreted as the information loss owing to the sub-ranked eigenvalue dispersion.

- Its value lies between $0 \leq \phi_{\mathcal{K}} \leq 1$, where 1 is the case when the channel is decorrelated the most and 0 is the case where there is only one eigenvalue.
- It is scale-invariant measure with respect to system (channel) norm and SNR, thus depicting the multipath richness of the channel.
- It can be readily applied to any known (published) system (channel), without restrictions towards its statistical properties, i.e. correlated or non-correlated, Rayleigh or Rician, etc.

Given that $\sum_{k=1}^{\mathcal{K}} \lambda_k \approx 1$ is valid in underspread channels (channels with poor to moderate multipath richness), it is possible to reshape (6.18) into

$$\prod_{k=1}^{\mathcal{K}} \lambda_k = \left(\frac{\phi_{\mathcal{K}}}{\mathcal{K}} \right)^{\mathcal{K}}, \quad \mathcal{K} = 1, \dots, K. \quad (6.19)$$

In this way an eigenvalue-based expression for each k -th elementary symmetric function of the k -th ranked submatrix \mathbf{W}_k is found, where the \mathcal{K} -th eigenvalue dispersion is identical to the eigenvalue dispersion ξ defined in (6.5). For very rich channels some error will be made. However, since the urban communication channel is also underspread the error done by this approximation can be assumed to be small and will not be further discussed. Introducing (6.19) in (6.13) the instantaneous system capacity can now be rewritten to

$$\begin{aligned} C(\mathbf{H}, \rho) &\approx \log_2 \left[1 + \sum_{\mathcal{K}=1}^K \zeta^{\mathcal{K}} \left(\frac{\phi_{\mathcal{K}}}{\mathcal{K}} \right)^{\mathcal{K}} \right] \\ &= \log_2 \left[1 + \sum_{\mathcal{K}=1}^K (\rho N)^{\mathcal{K}} \left(\frac{\phi_{\mathcal{K}}}{\mathcal{K}} \right)^{\mathcal{K}} \right]. \end{aligned} \quad (6.20)$$

(6.20) is a very compact and powerful expression that reshapes the capacity as a function of a set of scale-invariant measures: the family of $\phi_{\mathcal{K}}$ resulting from all sub-ranked systems. This means that the behavior of the Frobenius normalized communication system has been decomposed into: its eigenvalue dispersion, its SNR operating point and the number of antennas used. Furthermore, it is seen from the special case of rank two systems, for which an exact expression of instantaneous mutual information is given in (6.7), that only one eigenvalue dispersion is relevant. Extended to higher K -th ranked systems, this means that there are $K - 1$ meaningful indicators of the system capacity performance. It will be shown though, that for 4×4 systems the first two eigenvalue dispersions suffice (or even just $\phi_{\mathcal{K}=3}$).

6.2 Eigenmode-based metric for arbitrarily normalized systems

Up to this point only Frobenius normalized systems have been discussed. However, in general, different system normalizations might be of interest as previously discussed. In [SSV⁺08] G_{sys} , a measure of instantaneous transferred signal power (TSP), was defined for systems normalized with respect to a reference system \mathbf{H}_{REF} , with which they were able to express the instantaneous mutual information of the arbitrarily normalized system as a function of the normalized matrix \mathbf{W}

$$C(\mathbf{H}, \rho) = \log_2 |\mathbf{I}_M + \rho N G_{\text{sys}} \mathbf{W}|, \quad (6.21)$$

where G_{sys} gives the relationship between the studied channel and a reference one

$$G_{\text{sys}} = \frac{\|\mathbf{H}\|_F^2}{\|\mathbf{H}_{\text{REF}}\|_F^2}. \quad (6.22)$$

This recast of the instantaneous channel information, similarly used in [SSV07, SSKV05], expresses the system capacity in a very intuitive manner since the distribution of the G_{sys} term results from the power contributions of the complete communication system. In consequence G_{sys} becomes at the same time a measure of diversity, which contrary to similar measures as the one shown in [IN03, Özc04] has a physical interpretation for the computation of capacity. Multipath richness of the system under study, on the other hand, is given solely by the eigenvalue dispersions $\phi_{\mathcal{K}}$. Furthermore, since $\phi_{\mathcal{K}}$ are scale-invariant, then the previously derived metric remains valid for the general case. Therefore, combining the results obtained in the previous sections with this reshaped instantaneous capacity yields

$$\begin{aligned} C(\mathbf{H}, \rho) &= \log_2 \left[\prod_{k=1}^K (1 + G_{\text{sys}} \zeta \lambda_k) \right] \\ &\approx \log_2 \left[1 + \sum_{\mathcal{K}=1}^K \left(G_{\text{sys}} \cdot \rho N \cdot \left(\frac{\phi_{\mathcal{K}}}{\mathcal{K}} \right) \right)^{\mathcal{K}} \right], \end{aligned} \quad (6.23)$$

where the λ_k eigenvalues in the first part of (6.23) constitute the eigenvalues of the Frobenius normalized system. This thus justifies the assumption $\sum_{k=1}^K \lambda_k \approx 1$ implicitly made in (6.23). In addition, for medium to high SNR-regimes (6.23) can be further simplified into:

$$C(\mathbf{H}, \rho) \approx \log_2 \left[\sum_{\mathcal{K}=1}^K \left(G_{\text{sys}} \cdot \rho N \cdot \left(\frac{\phi_{\mathcal{K}}}{\mathcal{K}} \right) \right)^{\mathcal{K}} \right]. \quad (6.24)$$

Both expressions are now general in the sense that they separate the effects of normalization, SNR regime and multipath richness in the terms G_{sys} , ρN and $\phi_{\mathcal{K}}$. Moreover, the diversity and multiplexing effects of the system are now isolated in different terms. $\phi_{\mathcal{K}}$ expresses the multiplexing or degrees of freedom gain, whereas G_{sys} expresses the diversity gain along with the propagation channel gain. In comparison, other measures such as signal correlation [Lee82, KCVW03] provide less insight. In consequence, with this metric easy evaluation and straightforward characterization of MIMO systems results.

For ease of notation the following variable

$$\Phi_{\mathcal{K}} = \frac{\phi_{\mathcal{K}}}{\mathcal{K}} \quad (6.25)$$

will be used in some cases instead of $\phi_{\mathcal{K}}$. In the upcoming section it will be shown how these criteria are sufficient to thoroughly describe MIMO systems.

6.3 Capacity analysis with eigenmode-based metric

To prove the usefulness of the eigenvalue dispersion and the TSP in the evaluation of MIMO systems the capacity of a path-based macro-cellular channel will be studied for 2×2 and 4×4 MIMO systems. In the case of 2×2 systems only the most relevant results from chapter 5 will be used.

6.3.1 Rank-2 systems

In (6.7) an expression for the system capacity was given for systems with two antennas either on transmit, on receive or both. Later on, in (6.20), an approximation for the capacity of Frobenius normalized systems regardless of system rank was proposed. Both expressions showed that capacity could be expressed as the product of independent terms. In this section it will be demonstrated how these terms can be used to describe the system in a more general sense out of which different capacity analysis can be performed. Furthermore, it will be exemplified how the newly defined metric allows for better comparison of real communication systems for different antenna configurations. With this purpose, the communication channels resulting from the $VV \times VV$, $VV \times X$, $X \times VV$ and the $X \times X$ configurations of Table 5.1 will be analyzed in light of the achievable system capacity in both the ergodic and outage sense.

Proof that (6.20) is very accurate for rank-2 systems results from the fact that ϕ_1 is equal to one (see (6.18)). Hence, the same capacity is obtained with both (6.1) and (6.20), namely the capacity of the Frobenius normalized system. Moreover, the same occurs for the arbitrarily

normalized channel, given by (6.23). This fact is of great interest because it means that the proposed metric is exact for 2×2 systems, the most common ones in the literature and the most likely to be implemented in the near future because of cost issues. Therefore, the communication system can be analyzed in a very exact manner as a function of SNR regime ρN , multipath richness ϕ_K and TSP G_{sys} . Here, as was also the case in chapter 5, in computing G_{sys} an isotropic system of antennas radiating equal power in all directions is used. However, since the choice of reference channel is arbitrary, different types of comparisons are possible (e.g. the normalizations found in [SSV07]).

The goal at this point is to analyze the most relevant antenna setups mentioned in the previous section in light of the metric proposed. The first metric of interest is ρN . However, since the SNR regime of interest is a system independent criterion, it doesn't play any role in the evaluation of different antenna types and will not be discussed at this point.

The second metric of interest is the family of eigenvalue dispersions ϕ_K . For rank-2 systems this reduces to the study of only ϕ_2 , since $\phi_1 = 1$. In Figure 6.1 the second order eigenvalue dispersion ϕ_2 for the $VV \times VV$, $X \times VV$ and $X \times X$ setups is shown alongside with the one of an independent identically distributed (iid) channel [PNG03]. The eigenvalue dispersion of the $VV \times X$ setup is omitted for brevity, since it yields almost identical results to the $VV \times X$ one.

From Figure 6.1 it is seen that ϕ_2 is greatly dependent on antenna type, and on the antenna inter-element spacing s_{Tx} and s_{Rx} at the transmitter and at the receiver. A brief comparison of these two setups shows that the use of $\pm 45^\circ$ polarized antennas greatly benefits the system performance, being the performance of the $X \times X$ setup the most similar of all 2×2 setups to the iid case. The $VV \times VV$ setup, on the other hand, is the most dissimilar regardless of antenna inter-element spacing. In addition to this, depending on the antenna type used, different impact of s_{Tx} and s_{Rx} on the system is seen.

In the case of the $VV \times VV$ setup a clear dependence on s_{Tx} is observed, where $s_{\text{Tx}} = 5\lambda$ resulted in the most proximate curves to the iid channel (multipath rich environment). s_{Rx} , on the other hand, also showed improved multipath richness at bigger inter-element spacings, even though only marginally when compared to s_{Tx} . For the $X \times VV$ setup a significant multiplexing gain with respect to the $VV \times VV$ one was seen, but the same trends regarding s_{Tx} and s_{Rx} were verified. However, it was noted that in this case, changes in s_{Rx} have a larger influence on the eigenvalue dispersion than changes in s_{Tx} . Finally, in Figure 6.1c it is shown how the inter-element spacing effect on eigenvalue dispersion is marginal for the $X \times X$ setup. In this case as well larger s_{Tx} leads to more decorrelated signals, i.e. better multiplexing behavior. Yet, at smaller s_{Rx} the multiplexing gain is improved. To summarize Figure 6.1 depicts the multiplexing behavior of the channel and adds to the conclusions drawn in the previous chapter:

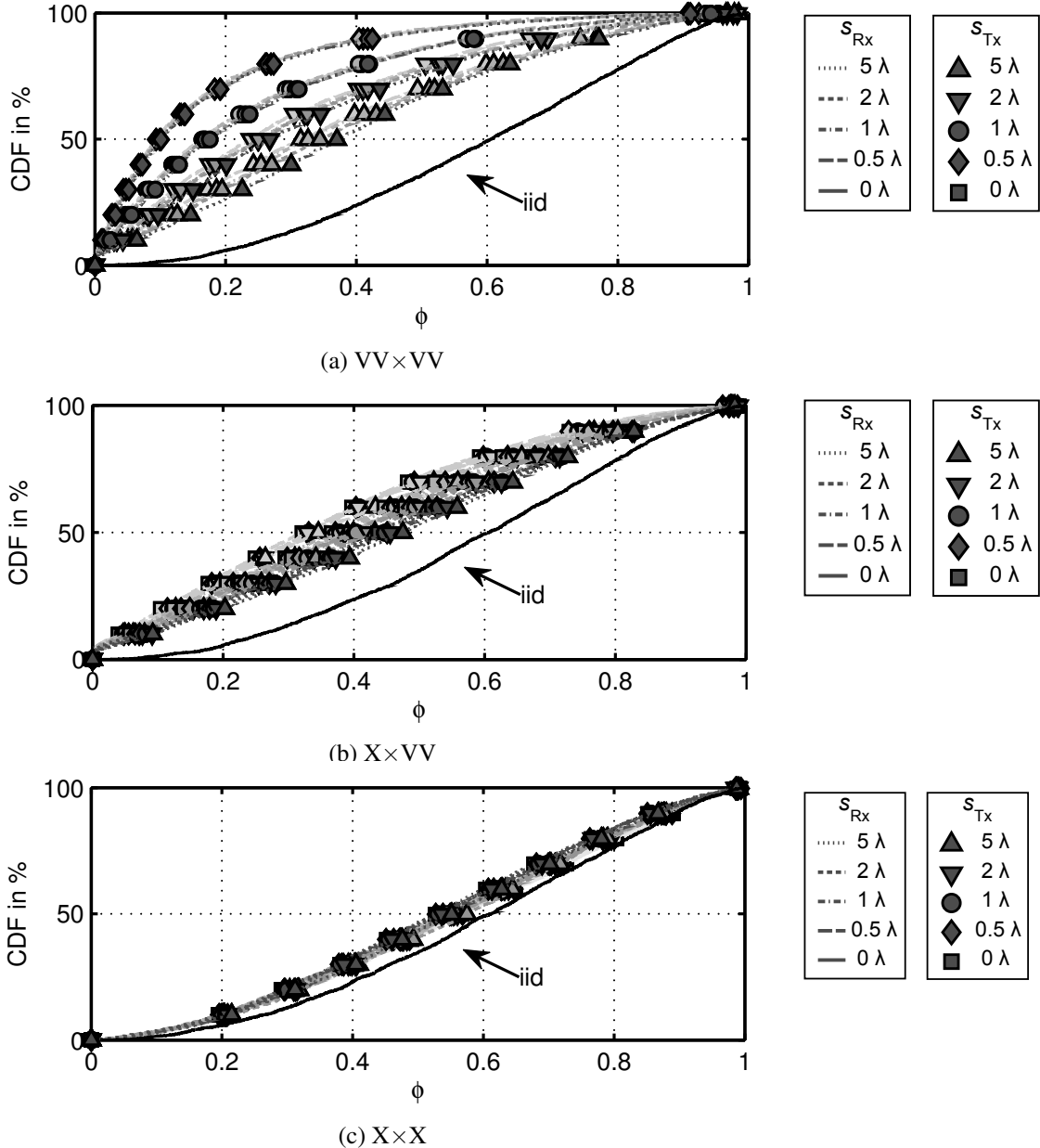


Figure 6.1: CDF of second eigenvalue dispersion ϕ_2 for the “Karlsruhe” communication channel with different 2×2 setups.

- Orthogonal polarized setups at the base station are capable of better exploiting the available spatial degrees of freedom of the channel.
- Larger antenna spacings at the base station always improve the multiplexing gain of 2×2 systems.
- Larger antenna spacings at the mobile station help decorrelate the received signals in all but one configuration: the X \times X setup.
- The most iid-like performance is achieved with the X \times X setup.

The remaining metric to be evaluated is TSP, which as was the case of eigenvalue dispersion is also dependent on the antenna setup used. However, in this case the setup impact on diversity rather than multiplexing is seen. Moreover, since an isotropic equivalent channel is used as reference, only the diversity effects due to different antenna types are noticed (not those of the propagation channel). In Figure 6.2 a comparison of G_{sys} for all 2×2 studied antenna configurations is shown based on their cumulative distribution function (CDF). Here, for clarity, only the cases of $s_{\text{Tx}} = 0.5\lambda$ and $s_{\text{Rx}} = 5\lambda$ are shown. In Figure 6.2, on the other hand, all curves are plotted together. It is seen that G_{sys} does not change greatly based on the antenna type used. Comparison with [SSV⁺08] also shows lesser dependence of G_{sys} on antenna type. This can be due to the scenario considered and the sliding norm (normalization in time) used in [SSV⁺08]. It is seen that among all 4 configurations a maximum of 1 dB variation is observed for changes at the receiver. More specifically, two vertically polarized dipoles exhibit greater TSP (diversity gain) than X polarized dipoles, regardless of base station antenna. However, X polarized dipoles increase the effect of different antenna spacings on TSP. In particular it is verified that smaller s_{Tx} increases TSP in those setups with X polarized dipoles. Altogether, regarding the diversity behavior of all 2×2 setups these observations indicate that:

- The use of different antenna types at the base station, where multipath effects are less noticeable, result in little change in TSP. At the mobile station, however, vertically polarized dipoles outperform X polarized dipoles in terms of diversity.
- With vertically polarized antennas at the mobile station changes in s_{Tx} do not have an impact on diversity.
- In setups with X polarized antennas at the mobile station changes in antenna spacing can impact the system diversity. More specifically, smaller s_{Tx} achieve greater diversity gain.

Now that the newly defined metric has been discussed for all 2×2 setups the way different capacity curves can be obtained from it will be demonstrated. Here, (6.20) and (6.23) are used to obtain the capacity of the Frobenius normalized channel and the reference normalized channel (isotropic equivalent channel, see chapter 5). All capacity curves for the four 2×2 configurations previously discussed are shown in Figure 6.4. In addition the capacity of the iid channel is also given.

From Figure 6.4 it is seen that the capacity curves of the Frobenius normalized channel have the same dependence on s_{Tx} and s_{Rx} as the eigenvalue dispersions. This is a reasonable result since in the instantaneous capacity of (6.20) SNR is only an additive and multiplicative term to ϕ . This means that in Frobenius normalized channels only the antennas multiplexing contribution is reproduced. In the capacity of reference normalized channels, however, both diversity and multiplexing effects are present. Yet it is not straightforward how each effect impacts the overall performance. This was the case of all results presented in chapter 5. Therefore the adoption of this metric allows to easily interpret the nature of the spatial benefit a certain antenna

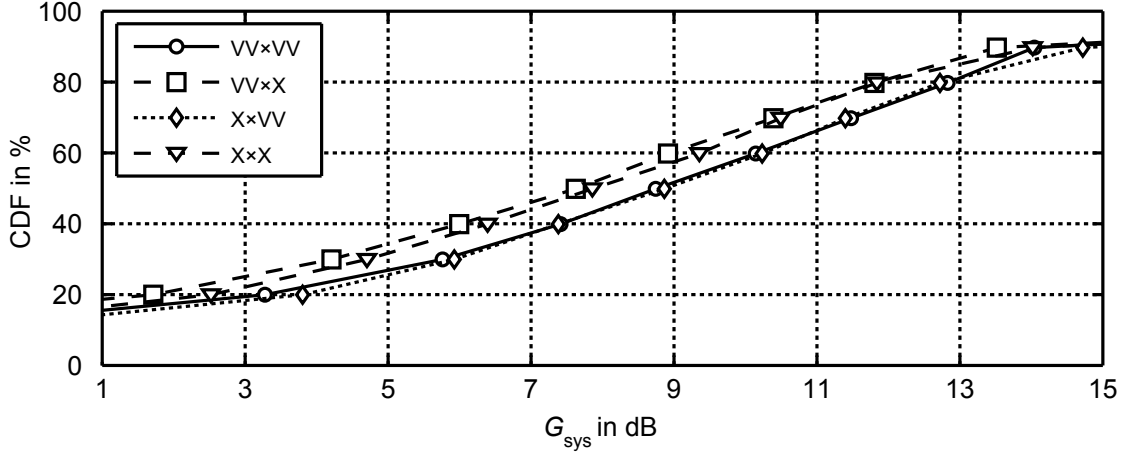


Figure 6.2: CDF of TSP for different 2×2 MIMO setups with $s_{\text{Tx}} = 0.5\lambda$ and $s_{\text{Rx}} = 5\lambda$.

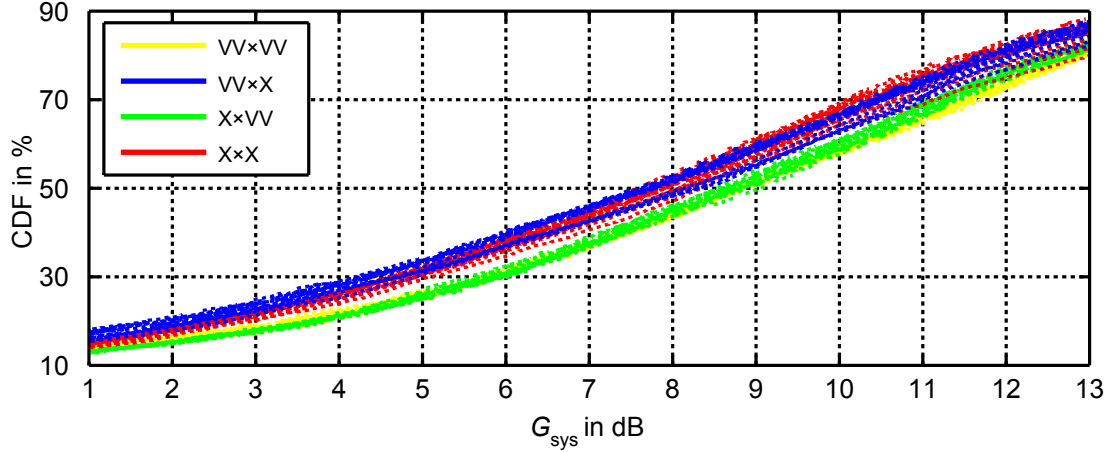


Figure 6.3: CDF of TSP for different 2×2 MIMO setups with varying s_{Tx} and s_{Rx} .

configuration brings to the system performance. Since the curves of the reference normalized channel are identical to those presented in chapter 5 a discussion at this point on the antenna spacing effect on ergodic capacity will be omitted.

Regarding the capacity curves of the reference normalized channels in Figure 6.4 it is noticed that, due to the Gaussian nature of G_{sys} (see Figure 6.2), eigenvalue dispersion impact on capacity at small to medium outage probabilities ($\leq 50\%$), even though considerably reduced with respect to mean values, is augmented with respect to the Frobenius normalized channel. This, therefore, explains why low outage capacities have less dispersion for Frobenius normalized channels. The latter has thus lead to the conclusion that Frobenius normalized channels not only compensate for fading but also for the antennas and therefore are not a good basis of comparison for antenna systems in general [WSW04]. Here it is corroborated that this is not necessarily the case, since the use of the Frobenius norm while compensating for G_{sys} does not mitigate the antenna induced eigenvalue dispersion. What happens is that non-Frobenius normalized channels, exhibiting Gaussian distributions, augment ϕ . It follows that antenna effects

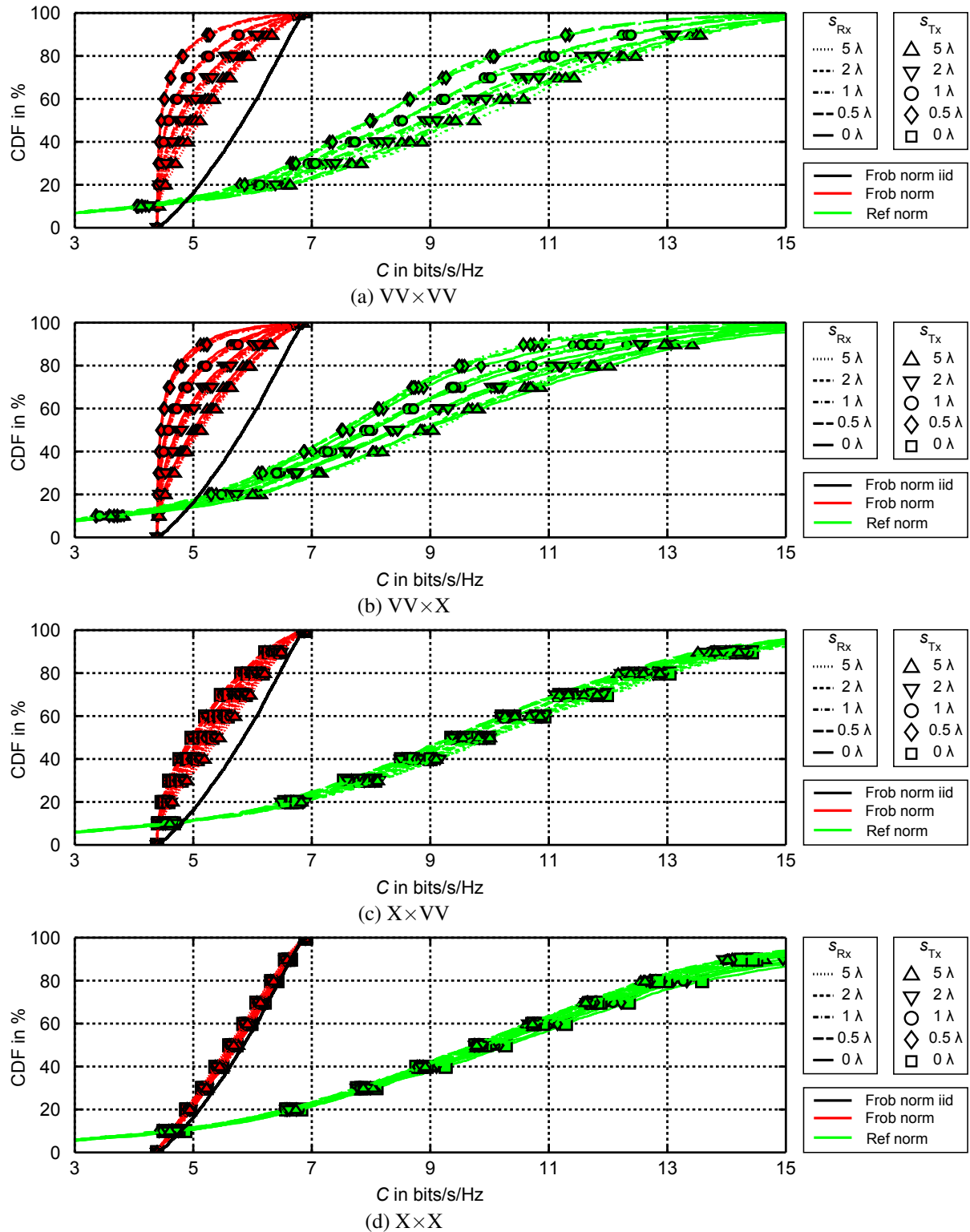
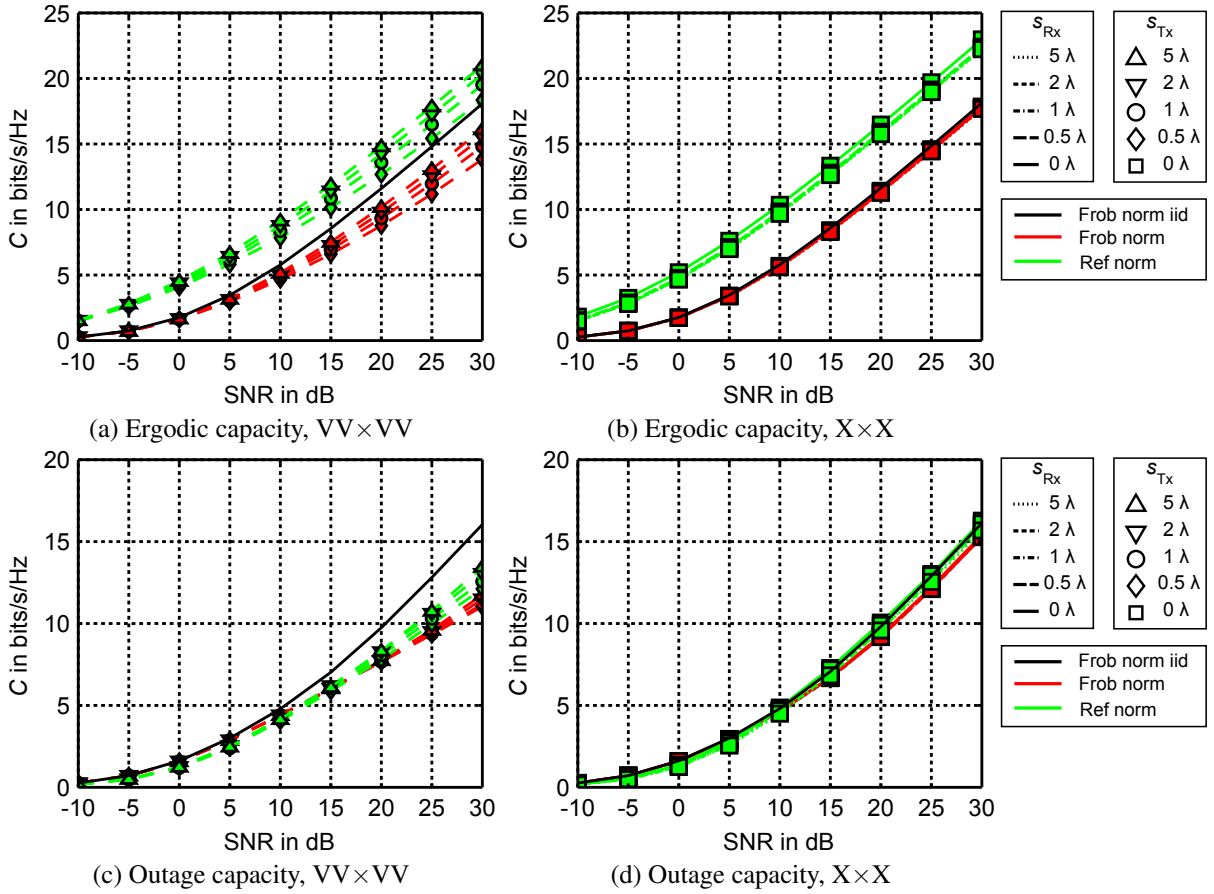


Figure 6.4: Cumulative distribution function of capacity for different 2×2 setups.

Figure 6.5: Ergodic and outage capacity vs SNR for $VV \times VV$ and $X \times X$ setups.

in general are less noticeable at low outage capacities while maintaining the same tendencies of capacities in the ergodic sense. In the same manner, at lower SNR (power) regimes multi-path richness becomes less noticeable. This is of great importance for system developers, since based on the SNR regime of operation of any given application, significant efforts on antenna design might not be worthwhile.

In order to better understand this metric influence on the study of capacity, a study of capacity vs. SNR in the ergodic and outage sense [TV05] is given in Figure 6.5 for the $VV \times VV$ and $X \times X$ setups. For the $VV \times VV$ configuration $s_{Rx} = 0.5\lambda$ and varying s_{Tx} are used. For the $X \times X$ case, on the other hand, $s_{Tx} = 0\lambda$ and varying s_{Rx} are considered. Selection of this working points, i.e. s_{Rx} and s_{Tx} was arbitrary and was done in the interest of clarity, since all other spacings result in almost identical curves with small deviations. Here, the capacities of both the Frobenius normalized and reference normalized channel are once more given along with the Frobenius normalized capacity of the iid channel. Moreover, all curves are evaluated for mean capacity and outage level of 10%.

By looking first at the ergodic capacity curves a visual insight into the functioning of the proposed metric is gained. It is noticed that the deviation between the capacity of the iid channel and the Frobenius normalized one represents the mutual information loss due to the non-ideal richness of that particular setup. Moreover, this deviation becomes less significant at the low SNR regimes. In the same manner, looking at the reference normalized curve it is seen that the capacity increase due to the mean TSP is more noticeable at all SNR values than the eigenvalue dispersion (see Figure 6.5b). This corroborates the known fact that diversity gain is more significant at low-SNR regimes, whereas multiplexing gain is important for high SNR regimes.

For the outage capacities a similar behavior is verified. One significant difference, however, is that the impact of the total spatial gain decreases for both setups. As result, capacity deviation among these two channels becomes less significant in the same manner. In addition it is seen that the $X \times X$ setup succeeds in reproducing the capacities of scatterer rich environments for all SNR regimes. In general it is demonstrated, that the multiplexing and diversity effects of the channel can be predicted from the previous metric for all SNR-regimes.

The previous results show that an analysis of the eigenvalue dispersion and TSP suffices to understand the impact of a certain antenna configuration on the system. Furthermore it is shown that this can be done regardless of antenna spacing and antenna polarization. In addition, out of these measures any capacity evaluation of any arbitrarily normalized channel can be performed. Here, this was demonstrated for the equivalent isotropic channel of chapter 5. To further prove the usefulness of this metric in higher ranked systems now 3×3 and 4×4 systems will be investigated.

6.3.2 Rank-K systems

When dealing with higher ranked systems the first thing to validate in the proposed metric is its accuracy. As was previously discussed, (6.23) is only an approximation of the true instantaneous capacity of a system. Therefore, investigating the accuracy of the eigenvalue dispersion metric is of great importance. In order to do this 3×3 and 4×4 ideal channel based systems will be investigated. Such systems represent a good criteria for comparison because of their greater channel richness. Afterwards the proposed metric will be validated for real channels, as done in the previous section, for 4×4 systems.

Figures 6.6 and 6.7 show the comparison between the exact

$$\phi_{\mathcal{K},\text{exact}} = \frac{(\text{tr}_{\mathcal{K}}(\mathbf{W}))^{\frac{1}{\mathcal{K}}}}{\frac{1}{\mathcal{K}} \sum_{k=1}^{\mathcal{K}} \lambda_k} \quad \mathcal{K} = 1, \dots, K \quad (6.26)$$

and approximated (6.18) family of eigenvalue dispersions for 3×3 and 4×4 iid channels. Here, the CDF and probability density functions (PDF) of the eigenvalue dispersions are compared. The results confirm that with higher ranked channels the lower order eigenvalue dispersions become less accurate. Eigenvalue dispersions of the highest order possible per System, i.e. ϕ_3 for 3×3 systems and ϕ_4 for 4×4 systems, are, however, exact. This is of special importance because of the implicit exponent dependence of each eigenvalue dispersion, which yields higher ordered ϕ more important.

In addition, Figures 6.6 and 6.7 also give insight regarding the statistical properties of the family of eigenvalue dispersions. It is thus seen that all eigenvalue dispersion functions ϕ_K exhibit Gaussian-like distributions, whereas the family of eigenvalue dispersions given by (6.18) rep-

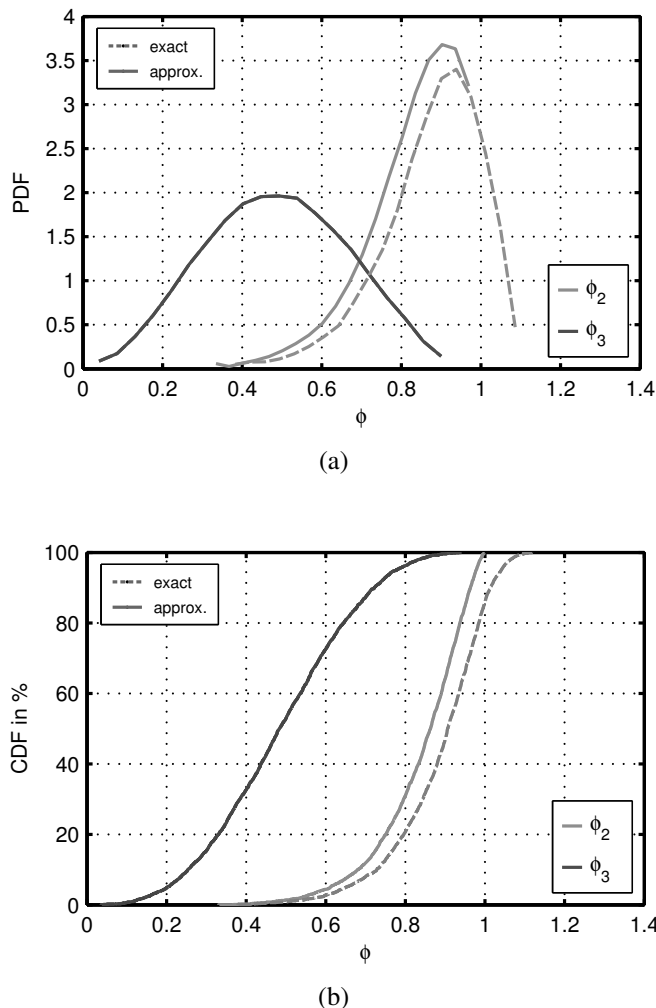


Figure 6.6: (a) Probability density function and (b) cumulative distribution function of the eigenvalue dispersions for a 3×3 MIMO iid channel.

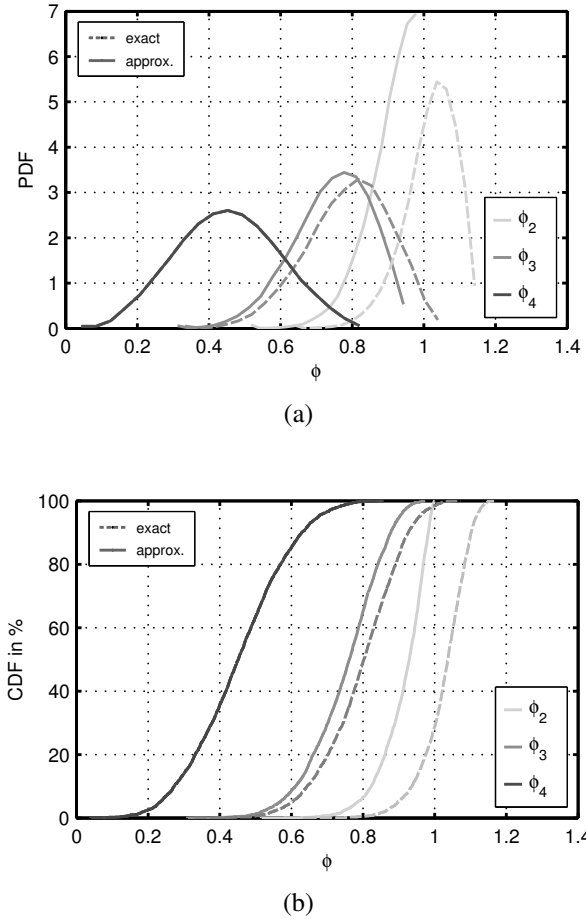


Figure 6.7: (a) Probability density function and (b) cumulative distribution function of the eigenvalue dispersions for a 4×4 MIMO iid channel.

resent truncated versions of the original ones. How exactly this affects the capacity evaluation of the system will be now discussed.

In order to prove the efficiency of the proposed eigenvalue-based metric focus is now given to 4×4 systems of a macro-cellular scenario with two antenna setups: 1) VVVV \times VVVV and 2) XX \times XX (same nomenclature and antennas as in chapter 5). Once more, as was done for the 2×2 systems considered in the previous section, antenna inter-element spacing is varied at both the receiver and transmitter. In this case s_{Tx} and s_{Rx} are varied between 0.5λ and 2λ . Results for G_{sys} are omitted for brevity, but similar curves as those of Figures 6.2 and 6.3 are observed.

Figure 6.8 shows for the VVVV \times VVVV setup the cumulative distribution functions for all eigenvalue dispersions ϕ_K together with the capacity curves of the Frobenius normalized channel and the reference normalized one. In this way it is intended to understand the impact that the

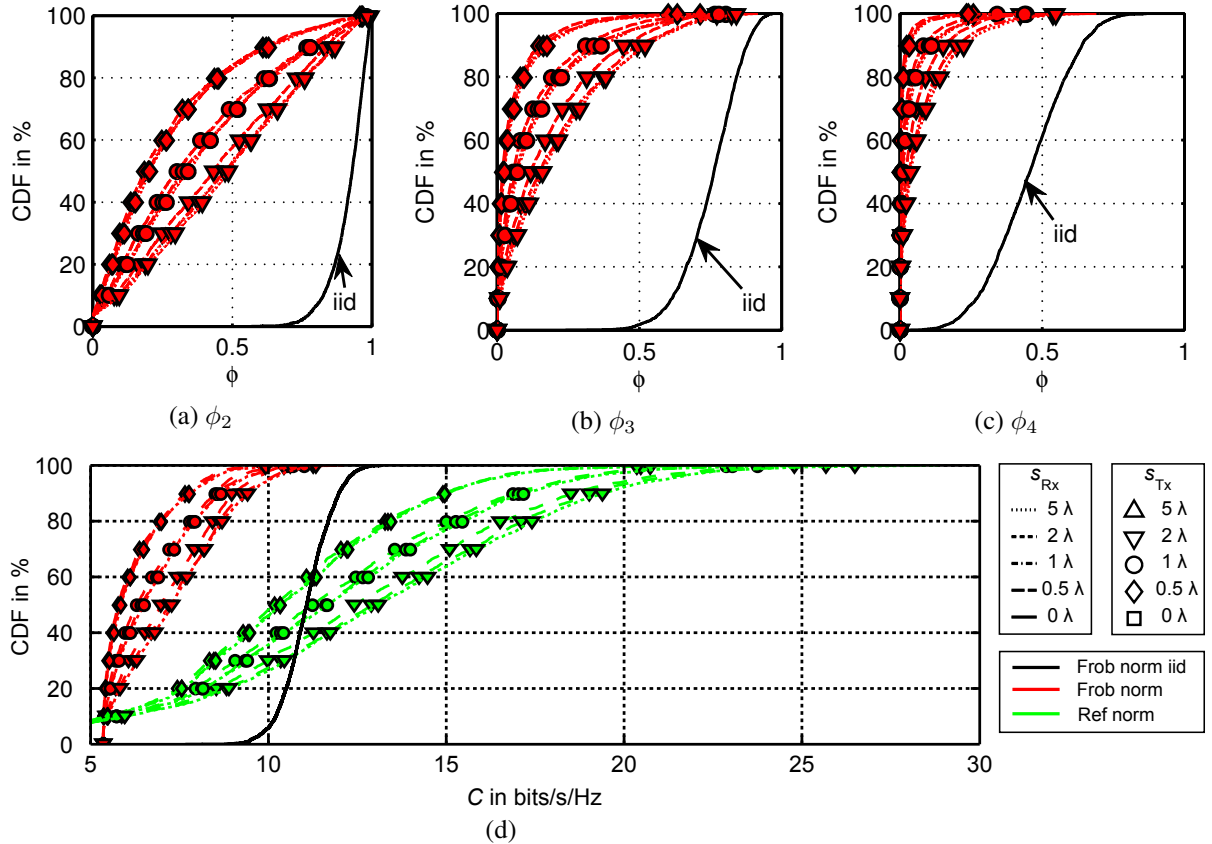


Figure 6.8: Cumulative distribution function of (a-c) the eigenvalue dispersions and (d) the capacity of a $VVVV \times VVVV$ setup.

different eigenvalue dispersions have on overall multiplexing gain. In addition the iid channel is also shown as reference. It is seen that each eigenvalue dispersion is a measure of the richness achieved with the studied setup, whereas the Frobenius normalized channel summarizes all eigenvalue dispersion contributions. Due to this behavior it seems that by determining which eigenvalue dispersion has the largest impact on capacity this eigenvalue dispersion can be used to predict the capacity of arbitrary normalized systems with the additional knowledge of TSP.

In the case of Figure 6.8 it is seen that both ϕ_2 and ϕ_3 resemble the behavior of the Frobenius normalized channel. However, it can't be determined which eigenvalue has a greater influence on the overall diversity performance. In general it can be said that, as was the case with the $VV \times VV$ setup, the eigenvalue dispersions exhibit significant multiplexing degradation with respect to the iid channel. Regarding the reference normalized channel, on the other hand, it is noticed that the same trends as for the Frobenius normalized channel take place. This means that for both channel normalizations larger s_{Tx} and s_{Rx} yields the largest capacities. In this way it can be stated that both diversity and multiplexing gains respond in the same manner to changes in the antennas inter-element spacings.

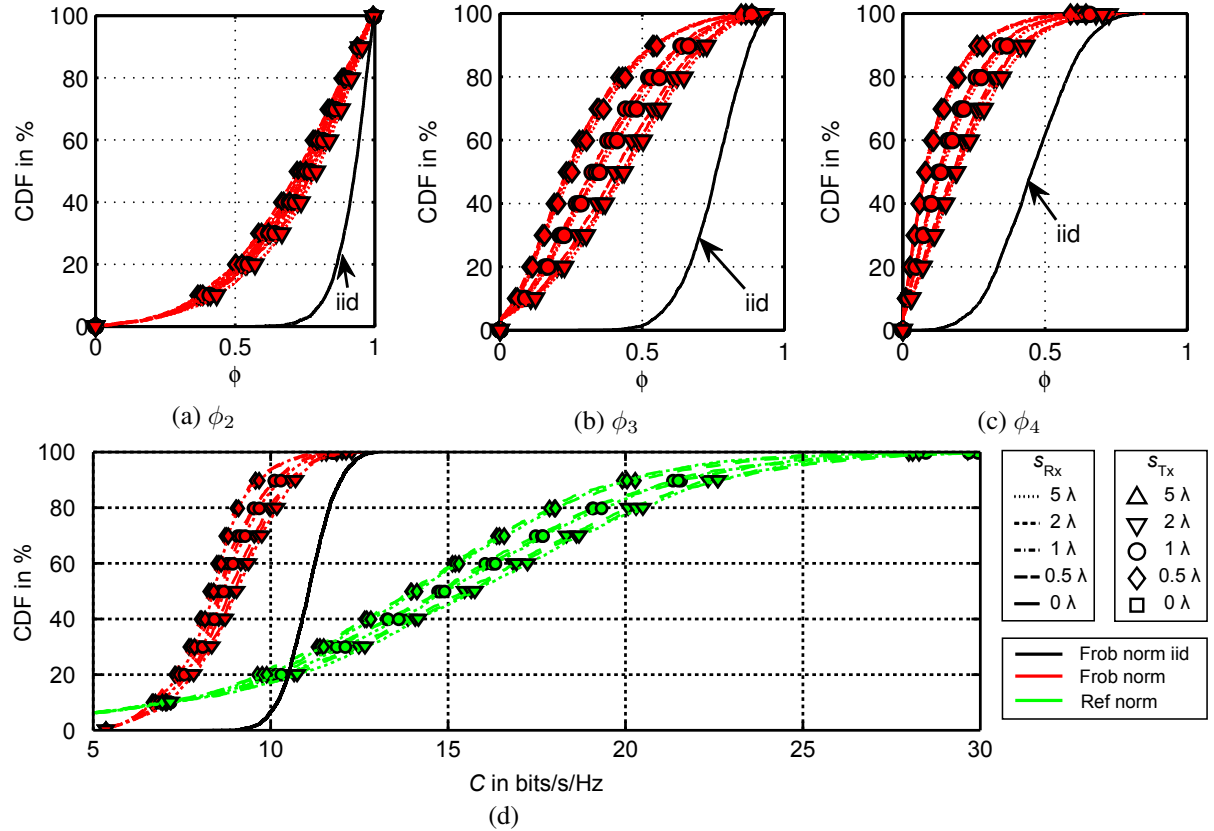


Figure 6.9: Cumulative distribution function of (a-c) the eigenvalue dispersions and (d) the capacity of a $XX \times XX$ setup.

In Figure 6.9 now the eigenvalue dispersions and capacity curves of the $XX \times XX$ setup are shown. Overall, contrary to Figure 6.8 all eigenvalue dispersions approximate better the eigenvalue dispersion of the iid channel. However, an important degradation in system richness is noted when compared to the almost ideal behavior of the $X \times X$ setup. Furthermore, in this case it is seen more clearly that ϕ_3 resembles best the overall multiplexing behavior.

In addition for this setup the same trends regarding antenna inter-element spacing as those in Figure 6.8 are verified. This means that at larger s_{Tx} and s_{Rx} better capacity values are obtained. In particular, this confirms the conclusion drawn in chapter 5, where it was stated that: by using multiple antennas of the same type (in this case same polarization) the behavior of single polarized systems was reproduced.

From Figures 6.8 and 6.9 it is seen that ϕ_3 resembles best, the overall multiplexing behavior of the system. However, the dependence on s_{Tx} and s_{Rx} of each eigenvalue dispersion remains the same for all, even though each eigenvalue dispersion exhibits different statistical properties. This dependence on s_{Tx} and s_{Rx} is also seen for the arbitrary normalized channel. This means

that, with respect to an equivalent isotropic channel, system diversity does not change the dependence on antenna inter-element spacing for none of the previous configurations. As result, the eigenvalue dispersion determines to great extent how the system will perform. Moreover, since in 4×4 systems a repetition of the same polarization type occurs, the channel multiplexing behavior will most likely be improved with larger s_{Tx} and s_{Rx} , regardless of polarization or antenna type.

6.4 Final remarks

In this chapter a new evaluation metric was introduced for communication channels and systems in general. The goal of the proposed metric was to ease comparison of simulations and measurements. To attain this goal an intermediate metric between the raw data in form of channel matrices and the final performance measures such as capacity was introduced. This preprocessed measure is defined as the eigenvalue dispersion and what sets it apart from other similar evaluation metrics is its compactness in describing the system. Furthermore, it has been shown that with this metric not only a very accurate description of the system is made, but a simple depiction of the system capacity with any given norm is achieved (only two figures of merit). As result an evaluation framework understandable for antenna designers and manufacturers, presented with the difficult task of sorting out optimum antenna configurations, has been laid out.

Deriving from the previous results, additional work should focus on exploring the information given in the different eigenvalue dispersions of rank-K systems in order to better understand their role in the overall system capacity. Its validity and effectiveness though has been proven here. Moreover, not only the impact of this metric in systems with no channel state information at the transmitter should be considered, but also waterfilling and beamforming power allocation schemes should be analyzed.

7 Communicational limits of linear multiple element antennas

In the previous chapters the modeling and evaluation of MEA systems was discussed. It was shown how diversity and multiplexing effects contribute to improve the system performance from an information point of view. Furthermore, certain trends regarding antenna type, orientation and polarization were verified with the aid of simulation results and a novel evaluation framework. However, no antenna setup was proven to provide the maximum attainable capacity and no investigation on the communicational limits of the system was performed. Therefore, the goal of this chapter is to find the communicational limits of linear arrays in general and within the “Karlsruhe” communication channel. Later, in chapter 9 antenna setups capable of achieving those limits will be investigated based on a novel synthesis method.

To determine the spatial degrees of freedom of linear arrays in the “Karlsruhe” communication channel, a progressive approach will be taken. First a methodology for investigating the maximum number of spatial degrees of freedom available in free space will be discussed. Then the proposed approach will be extended to the case of multipath scenarios. And finally, with this background, the attainable capacity limits under different SNR regimes for the non-ideal “Karlsruhe” communication channel will be investigated.

7.1 Spatial degrees of freedom in free space

The spatial degrees of freedom of a channel can be recognized by the number of parallel independent data streams that can be used in a certain scenario. In the context of information theory this is usually defined as the number of degrees of freedom (NDF). In free space NDF will depend on the geometry of the problem, i.e. how many spatial distinct communication links can be established. In the following, the case of linear arrays will be shown based on the approach taken in [TV05]. The case of two arrays placed at very large distances will be considered first. Based on the observations made for this case, the conditions for achieving multiplexing gain in free space will be derived.

For two linear vertically oriented arrays of single-polarized omni-directional antennas placed at a distance d_0 (see Figure 7.1) with transmitting and receiving inter-element spacings s_{Tx} and

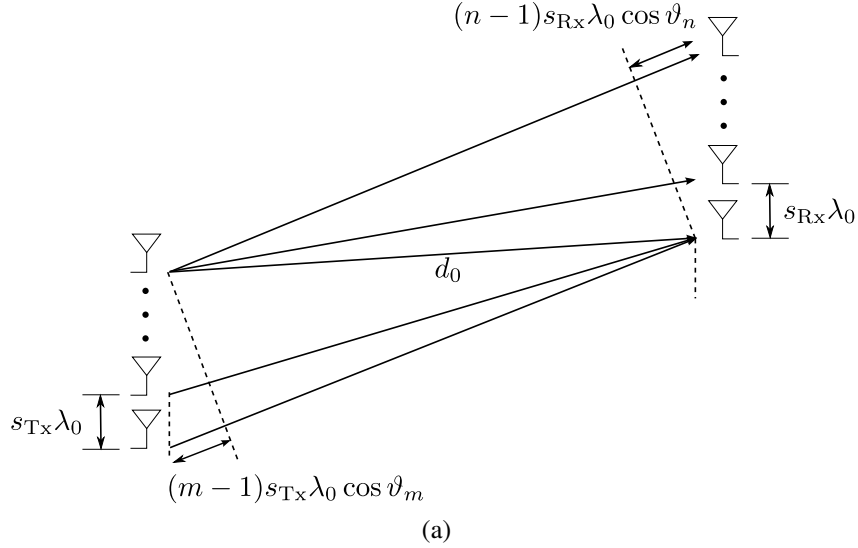


Figure 7.1: Multipath model for angular resolvability.

s_{Rx} (normalized with respect to wavelength λ_0), the channel coefficients given by (2.49) can be written as

$$H_{nm} = \sqrt{\frac{R_n^A}{R_m^A} \eta_n \eta_m D_n D_m} \left(\frac{\lambda}{4\pi} \right) \frac{e^{-j\beta d_{nm}}}{d_0}. \quad (7.1)$$

Considering that for $s_{Tx} \ll d_0$ and $s_{Rx} \ll d_0$, d_{nm} in (7.1) is equal to

$$d_{nm} = d_0 + (m-1)s_{Tx}\lambda_0 \cos \vartheta_m + (n-1)s_{Rx}\lambda_0 \cos \vartheta_n. \quad (7.2)$$

With (7.2) the resulting channel matrix \mathbf{H} of channel coefficients H_{nm} can now be rewritten as

$$\mathbf{H} = \sqrt{\frac{R_n^A}{R_m^A} \eta_n \eta_m D_n D_m} \left(\frac{\lambda}{4\pi} \right) \frac{e^{-j\beta d_0}}{d_0} \vec{e}_{Tx}^*(\vartheta_{Tx}) \vec{e}_{Rx}(\vartheta_{Rx}), \quad (7.3)$$

where $\vec{e}_{Tx}(\vartheta_m)$ and $\vec{e}_{Rx}(\vartheta_n)$ are given by

$$\vec{e}_{Tx}(\vartheta_{Tx}) = \begin{bmatrix} 1 \\ \exp(-j2\pi s_{Tx} \cos(\vartheta_{Tx})) \\ \exp(-j2\pi 2s_{Tx} \cos(\vartheta_{Tx})) \\ \vdots \\ \exp(-j2\pi (M-1)s_{Tx} \cos(\vartheta_{Tx})) \end{bmatrix}, \quad (7.4)$$

and

$$\vec{e}_{\text{Rx}}(\vartheta_{\text{Rx}}) = \begin{bmatrix} 1 \\ \exp(-j2\pi s_{\text{Rx}} \cos(\vartheta_{\text{Rx}})) \\ \exp(-j2\pi 2s_{\text{Rx}} \cos(\vartheta_{\text{Rx}})) \\ \vdots \\ \exp(-j2\pi(N-1)s_{\text{Rx}} \cos(\vartheta_{\text{Rx}})) \end{bmatrix}. \quad (7.5)$$

In this way the channel matrix is now expressed in term of the transmitting and receiving array steering vectors $\vec{e}_{\text{Tx}}(\vartheta_m)$ and $\vec{e}_{\text{Rx}}(\vartheta_n)$, which correspond to the looking directions of the transmitting and receiving arrays of size M and N respectively. Furthermore, since in this case only one ϑ_m and one ϑ_n are used, it follows that there is only one communication path and that the transmitted signals are all projected onto a single dimensional space. As result a channel matrix \mathbf{H} is obtained with approximately equal coefficients, which translates into a communication system with no degrees of freedom gain, but only diversity gain due to array beamforming. This behavior is expected for scenarios with strong line of sight (LoS) component in general.

In (7.3) it was assumed that all antennas see an outgoing or impinging plane wave, which is true if the distance d_0 between transmitting and receiving array is infinite. In reality, propagating waves are spherical and all antenna do see a slightly different outgoing or incoming angle, even in the case of $s_{\text{Tx}} \ll d_0$ and $s_{\text{Rx}} \ll d_0$. However, these small angular variations are not big enough to generate distinct spatial signatures. This means that rich channel matrices require, in addition, comparable energy distribution among all subchannels (eigenvalues). Otherwise, the channel matrix is said to be ill-conditioned [GL96] and not all communication paths are resolved. From this, two questions now arise: 1) how different should the angles be in order to achieve resolvable parallel data streams? and 2) based on the sufficient resolvability of all data streams, how many parallel links can be implemented? (what is the NDF of the system?).

The easiest way to answer these questions is to consider the case of two transmitting antennas, i.e. $M = 2$. Since in this case, the maximum number of resolvable paths, i.e. the rank of the system, is determined by the minimum number of antennas, it is a priori known that only two paths can be resolved. Therefore, by placing the two antennas at different spacings the existence and number of distinct communication links can be investigated.

From (7.3) and following the approach in [TV05], when two antennas are used as transmitters, the spatial signature that each transmit antenna impinges on the receiving array (if both antennas are located at a distance d_0 from the receiving array) is

$$\mathbf{H}_k = \sqrt{\frac{R_n^A}{R_m^A} \eta_n \eta_m D_n D_m} \left(\frac{\lambda}{4\pi} \right) \frac{e^{-j\beta d_0}}{d_0} \vec{e}_{\text{Rx}}(\vartheta_{\text{Rx},k}), \quad k = 1, 2, \quad (7.6)$$

Therefore, the channel matrix $\mathbf{H} = [\mathbf{H}_1, \mathbf{H}_2]$ will have independent columns as long as $\vec{e}_{\text{Rx}}(\vartheta_{\text{Rx},1}) \neq \vec{e}_{\text{Rx}}(\vartheta_{\text{Rx},2})$. Given the periodic nature of the steering vector (exponential functions) this is guaranteed to happen as long as the difference between directional cosines $\delta = (\cos(\vartheta_{\text{Rx},2}) - \cos(\vartheta_{\text{Rx},1}))$ differs from the period of \vec{e}_{Rx} , which for linear arrays is $1/s_{\text{Rx}}$ [TV05]. This means that based on resolvability the following constraints for δ exists

$$0 < \delta < \min\left(\frac{1}{s_{\text{Rx}}}, 2\right). \quad (7.7)$$

From (7.7) follows that if $s_{\text{Rx}} \leq 1/2$ is chosen, a full rank channel matrix results for all $\delta > 0$. Yet, this is not sufficient to guarantee multiplexing, since the matrix can still be ill-conditioned (cf. previous discussion when $s_{\text{Tx}} \ll d_0$ and $s_{\text{Rx}} \ll d_0$). Therefore the question remains as to which value should δ take in order to have both a full ranked and well conditioned channel matrix \mathbf{H} .

In order to study the minimum distance for resolvability between two paths, in [TV05] the alignment between the spatial signatures

$$f(\delta) = \vec{e}_{\text{Rx}}(\vartheta_{\text{Rx},1}) * \vec{e}_{\text{Rx}}(\vartheta_{\text{Rx},2}) \quad (7.8)$$

is studied. There it is found by direct computation that

$$|f(\delta)| = \left| \frac{\sin(\pi L_{\text{Rx}}\delta)}{\sin(\pi L_{\text{Rx}}\delta/N)} \right|, \quad (7.9)$$

i.e. $|f(\Delta\vartheta)|$ follows the absolute value of a sinc function. Therefore, given the fact that the condition number

$$\frac{\lambda_1}{\lambda_2} = \sqrt{\frac{1 + |f(\delta)|}{1 - |f(\delta)|}}, \quad (7.10)$$

directly depends on $|f(\delta)|$, the matrix will be ill-conditioned whenever $|f(\delta)| \approx 1$, which occurs for all δ lying within the main lobe of the sinc function in (7.9). From this, an additional constraint for δ results

$$\frac{1}{L_{\text{Rx}}} \leq \delta, \quad (7.11)$$

which yields the minimum angular resolvability. It is then found with (7.7), that the set \mathcal{S}

$$\mathcal{S} := \left\{ \vec{e}_{\text{Rx}}(0), \vec{e}_{\text{Rx}}\left(\frac{1}{L_{\text{Rx}}}\right), \dots, \vec{e}_{\text{Rx}}\left(\frac{N-1}{L_{\text{Rx}}}\right) \right\} \quad (7.12)$$

constitutes a basis of spatially orthogonal modes.

To evidence this fact, $|f(\delta)|$ is plotted as a function of δ in Figure 7.2 with $L_{Rx} = 1$ and $L_{Rx} = 2$. It is seen that in both cases only two distinct modes¹ exist ($\vartheta_{Rx} = 0, 1/L$) which comply with conditions (7.7) and (7.11). Yet, for $L_{Rx} = 1$ the whole visible δ range [-2,2] is used, whereas for $L_{Rx} = 2$ two distinct signatures exist already within [-1,1]. This means that multiple maxima of the same mode will occur if all possible δ values are considered. As result, in the blacked-out regions of Figure 7.2 the spatial signatures will be ambiguous.

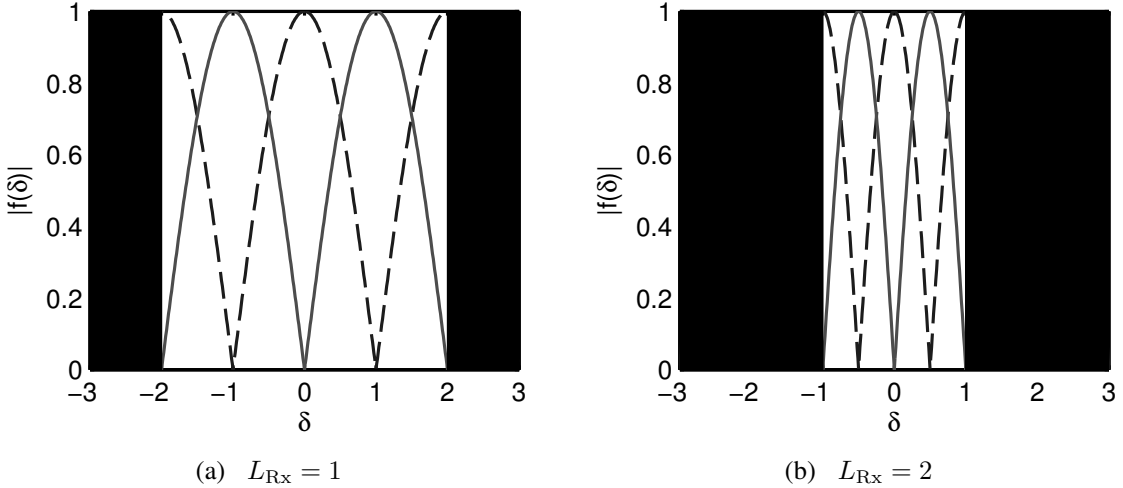


Figure 7.2: Spatial signature alignment for fixed number of receiving antennas $N = 2$.

From an antenna perspective this is equivalent to study the available beamforming vectors of the receiving array, since the spatial signature $|f(\delta)|$ gives also the attenuation seen by an incoming signal. This means that the radiation pattern $C(\vartheta)$ of the array factor [Bal97] with look direction ϑ_0 is equivalent to $|f(\cos(\vartheta) - \cos(\vartheta_0))|$. The corresponding beamforming patterns plotted in this manner are shown in Figure 7.3. Here, it is seen that in the case of $L_{Rx} = 1$, $s_{Rx} = 1/2$, only two main beams per mode result, whereas for $L_{Rx} = 2$, $s_{Rx} = 1$, four main beams for each mode are obtained (cf. 7.2b). Additionally, all patterns are symmetrical about the 0° - 180° and are spatially orthogonal.

Figures 7.2 and 7.3 show how conditions (7.7) and (7.11) guarantee the existence of orthogonal beamforming vectors and a well-conditioned channel matrix. The beamforming vectors for $N = 4$ and $N = 8$ are shown in Figures 7.4 and 7.5 in order to show the way these two constraints determine NDF at the receiver, NDF_{Rx} .

From Figures 7.3c, 7.3d, 7.4 and 7.5, where $L_{Rx} = 2$, it is seen that regardless of the number of antennas and modes, given a certain array length the same spatial signatures result (same main

¹Here, the term modes refer to the different orthogonal spatial signatures or beamforming vectors, not to be confused with the spherical modes introduced in chapter 3.

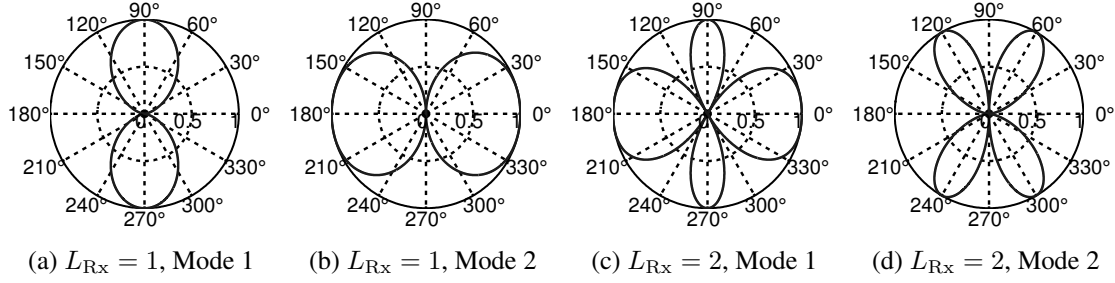


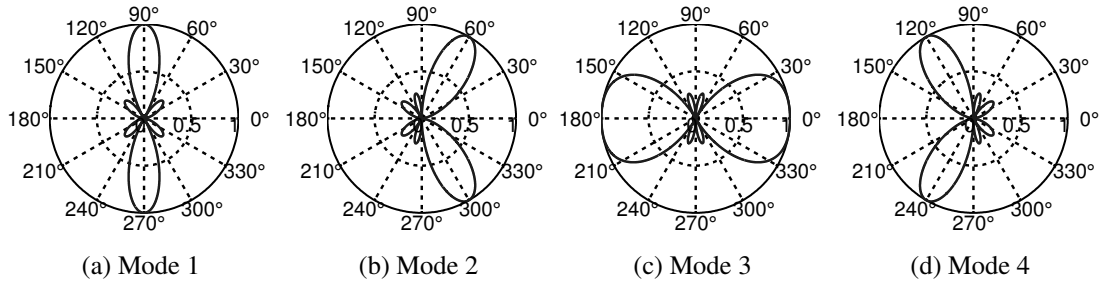
Figure 7.3: Receive patterns with varying length and 2 receiving antennas.

beams). This means that the number of orthogonal directions that can be used in free space is given solely by L_{Rx} . However, depending on whether a sufficient number of antennas is used or not, one or many looking directions are assigned to each mode. Ideally, one mode is assigned to each looking direction, as is the case in Figures 7.4 and 7.5. In the case of Figure 7.5 more antennas than available look directions are used. As result, most of the modes provide very little to no energy (cf. Figures 7.5d-7.5f), which means that together with conditions (7.7) and (7.11), the periodicity of the steering vector limits the largest angular distance between resolvable paths, regardless of N . It thus follows that if the minimum distance between resolvable paths is given by the angle δ then the following condition should be also enforced

$$\delta NDF_{Rx} \leq \frac{1}{s_{Rx}} \quad (7.13)$$

In consequence, the number of distinct communication links inherent to the system is determined by the periodicity of the steering vector, which depends on the total number of antennas N and the array length L_{Rx} ($s_{Rx} = L_{Rx}/N$). Therefore, replacing (7.11) into (7.13) and applying the constraint (7.7) a more general condition for NDF_{Rx} results

$$NDF_{Rx} \leq \min \left(\frac{L_{Rx}}{s_{Rx}}, 2L_{Rx} \right) = \min (N, 2L_{Rx}) . \quad (7.14)$$


 Figure 7.4: Receive patterns for fixed receiving length $L_{Rx} = 2$ and 4 receiving antennas.

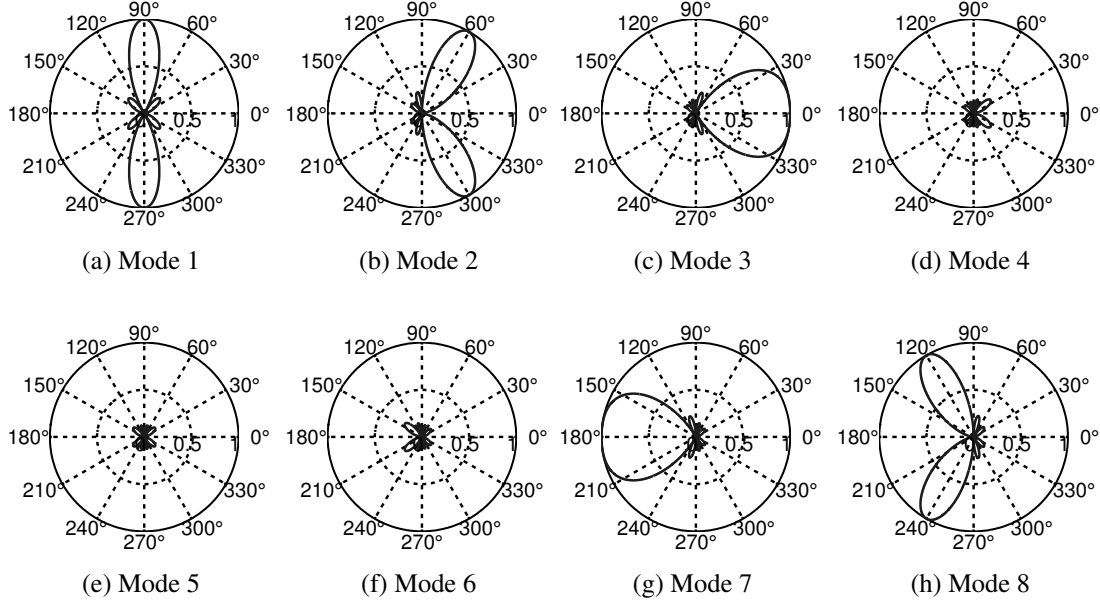


Figure 7.5: Receive patterns for fixed receiving length $L_{Rx} = 2$ and 8 receiving antennas.

(7.14) predicts the number of available subchannels that a linear system in free space can have. Moreover, the number of subchannels is limited by two times the array length², after which the inclusion of additional antennas only provides spatial signatures that are energetically weak (see Figures 7.5d-7.5f). In addition, an identical condition for a transmitting array can be found due to the reciprocity of antennas. Combining both conditions the total NDF is found to be

$$\text{NDF} \leq \min (\text{NDF}_{Tx}, \text{NDF}_{Rx}) = \min (M, N, \lceil 2L_{Tx} \rceil, \lceil 2L_{Rx} \rceil). \quad (7.15)$$

It should be noted that in (7.15) $\lceil \cdot \rceil$ has been included to denote the rounding up to the next integer, since NDF can only take integer values (no fractional subchannels possible). Furthermore, the minimum number of antennas at each communicating end determines the rank of the communication channel in the case that the $2L_{Tx}$ and $2L_{Rx}$ limits haven't been yet reached. Because of this, within the context of information theory, the term NDF refers rather to the maximum NDF and not to the current number of subchannels available. From now on, this definition of NDF will be adopted and applied to multipath propagation channels, and more specifically to the "Karlsruhe" communication channel.

²Due to the symmetry along the 0° - 180° axis, even though the number of main beams in one half-space is limited to $2L_{Rx}$, an additional spatial signature to that predicted by (7.14) results. This can be seen in Figure 7.5 where $2L_{Rx} + 1$ energetically strong modes were obtained. In general, though, (7.14) is an acceptable approximation [PBT05].

7.2 Spatial degrees of freedom in multipath channels

In the previous section, a resolvability criterion for the study of the maximal number of sub-channels that could be established in free space was discussed. It was shown, that the number of orthogonal steering vectors determines the resolvability of different angular regions. Therefore, regardless of the antenna radiation pattern, it is the array factor (in the form of steering vectors) what guarantees sufficient multipath richness. By means of both the array length and the number of antenna elements. The former determines the angular resolution, i.e. the spatial beamwidth (cf. (7.11)), while the latter shows the extent up to which each look direction can be individually resolved. Furthermore, since there can be only as many look directions as the number of main beams that result from a certain array length, the number of resolvable angular regions is constrained by the array length (cf. (7.15)). However, this requires comparable antenna inter-element spacings with respect to the distance between transmitting and receiving arrays, which is not the case in practical antenna systems. Nonetheless, significant multiplexing gains have been reported. Therefore, it will be shown how the existence of multiple propagation paths yields an analogous effect to that of largely spaced arrays. In particular equal received power for all paths will be assumed in order to omit effects due to uneven power distribution in the angular domain. These effects will be studied in more detail in section 7.3.

Extending (7.3) to multipath channels as done in section 2.3.2 it is seen that the expression of the channel matrix \mathbf{H} can be written as

$$\mathbf{H} = \sqrt{\frac{R_n^A}{R_m^A} \eta_n \eta_m D_n D_m} \left(\frac{\lambda}{4\pi} \right) \sum_{p=1}^P T_p \vec{e}_{Tx,p}^*(\vartheta_{Tx,p}) \vec{e}_{Rx,p}(\vartheta_{Rx,p}), \quad (7.16)$$

where T_p is the vertically polarized transmission coefficient (contrary to the full polarimetric matrix \mathbf{T} in (2.50)) of the p -th path. It is seen that, due to the multiple propagation paths, different outgoing and incoming angles at the transmitting and receiving antennas result. In consequence, different spatial signatures can be obtained. For the receiving array in (7.6), these different spatial signatures are associated with the angle at which the transmitting antennas are seen (i.e. look direction). In multipath environments, though, the different spatial signatures result from the look direction to/from which the path propagates. It follows that, as was the case in free space, an spatially orthogonal set of steering vectors can be also obtained for multipath propagation.

An ideal set of orthogonal steering vectors for multipath scenarios can be found based on the same constraints derived in the previous section. Hence, (7.12) is also a basis of spatially orthogonal vectors in multipath scenarios. However, since in this case the direction of the outgoing or incoming paths can't be varied, NDF will depend on the channel itself. This is to some

extent known from communication theory where the number of paths P determines the rank of \mathbf{H} . The novelty in this analysis lies in the fact that paths exhibiting very similar outgoing or incoming angles will reduce the number of subchannels to less than P . This situation is depicted in Figure 7.6 for $P = 3$. It is seen that paths A and B have a very similar spatial signature at the transmitter. As result any transmit beamforming scheme wouldn't be able to resolve for both paths since the resulting beams (with beamwidth $1/L_{Tx}$) would overlap to great extent. It follows that for a situation as the one shown in Figure 7.6 only two subchannels could be effectively used. Furthermore, as was the case in free space it suffices to have overlapping spatial signatures at either one communicating end, to limit the rank of the whole system.

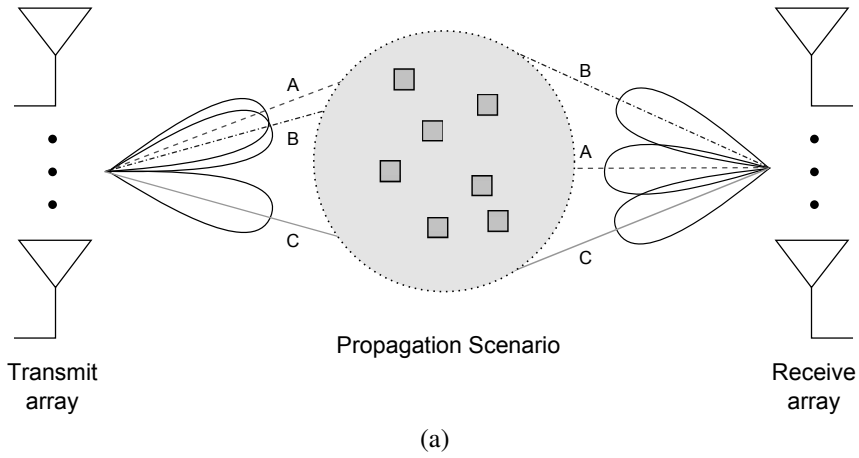


Figure 7.6: Multipath model for angular resolvability.

Assuming now an array length L at both transmitting and receiving arrays, it follows that at each communicating end a maximum of $2L$ subchannels can result (for sufficiently high number of antennas). Considering, in addition, an ideally scattered scenario, paths will be transmitted and received from all angular directions. Yet, paths will be only assigned to one of the $2L$ distinct beamforming vectors. This means that, even though the paths themselves are not all resolvable, they are grouped into resolvable regions by the antennas steering vectors.

As result, it can be said that, for scatterings scenarios, the antennas are responsible for spatially sampling the communication channel. Furthermore, it is the channel-antennas interaction what determines the resulting look directions. This refers to the fact that the way the propagation channel scatters the signals will determine which spatial signatures can be effectively used. In the case that most of the paths are localized within a certain angular region, very large arrays will be needed to distinguish between the very similar look directions of each path. Yet, the number of antennas used may remain small³.

³It should be noted that if a small number of antennas together with large overall array length is used, then an important number of grating lobes will result.

The influence of scattering on NDF was studied in [PBT05]. It was suggested that condition (7.15) for sparsely scattered scenarios can be given by

$$\text{NDF} \leq \min (\lceil L_{\text{Tx}} \Omega_{\text{Tx}} \rceil, \lceil L_{\text{Rx}} \Omega_{\text{Rx}} \rceil), \quad (7.17)$$

where Ω_{Tx} and Ω_{Rx} are

$$\Omega_{\text{Tx}} = \int_{\Theta_{\text{Tx}}} d \cos(\theta_{\text{Tx}}) \quad \text{and} \quad \Omega_{\text{Rx}} = \int_{\Theta_{\text{Rx}}} d \cos(\theta_{\text{Rx}}), \quad (7.18)$$

with Θ_{Tx} and Θ_{Rx} being the angular regions along which the paths propagate. In this manner, $\Omega_{\text{Tx}} = \Omega_{\text{Rx}} = 2$ results for scatterering rich scenarios with outgoing and incoming paths from all directions. In consequence, in multipath scenarios the antennas also act as sampling elements of space, but the number of spatial signatures that can be used is limited by the multipath richness.

From this sampling interpretation, it is now possible to imagine an angular domain representation for multipath communication channels. The idea is to decompose the channel matrix similar to the SVD decomposition as

$$\mathbf{H} = \mathbf{U}_a \mathbf{S}_a \mathbf{V}_a^\dagger, \quad (7.19)$$

where \mathbf{U}_a and \mathbf{V}_a are the unitary matrices responsible for the spatial to angular transformation, and \mathbf{S}_a is the angular channel matrix. The columns of \mathbf{U}_a and \mathbf{V}_a are given by the (possibly non-orthogonal) steering vectors inherent to the communication channel. It can be seen that the rank of the channel matrix is limited by the number of resolvable (i.e. spatially orthogonal) angular regions obtained from the previous factorization. Hence, (7.19) is a more intuitive angular domain representation of the channel to that given in [TV05] and is in good agreement with the channel model interpretation of [WHÖB06]. In the following no further details on the computations of \mathbf{U}_a , \mathbf{S}_a and \mathbf{V}_a will be given since this does not fall within the scope of this work. The interested reader is referred to the work in [WHÖB06].

From the previous angular domain representation, it is seen that the ideal waterfilling scheme of chapter 4 also yields the spatial orthogonalization of the transmitted signals, and that by doing so specific spatial signatures are used. For a waterfilling system of linear arrays these signatures are given by the columns of $\vec{e}_{\text{Tx}}(\vartheta) \mathbf{V} \mathbf{V}^\dagger$ and $\vec{e}_{\text{Rx}}(\vartheta) \mathbf{U} \mathbf{U}^\dagger$ for the transmitting and receiving cases respectively. Therefore, the singular value (and diagonal) matrix \mathbf{S} in (4.23) is also a measure of the number of spatial signatures that are effectively used by the system. Also, if a sufficiently large number of “sampling” antennas N_S is considered then the previous discussion confirms

that the system NDF will be reached. In other words, for $\min(N, M) > \text{NDF}$ there will be NDF non-zero eigenvalues and the rest will have near to no energy. Because of this, the eigenvalue analysis of over-dimensioned systems will be the core approach to be used in the following section in order to investigate the spatial degrees of freedom of the “Karlsruhe” communication channel. Additionally, condition (7.17) will be used to predict the channel behavior.

7.3 Spatial degrees of freedom of the “Karlsruhe” communication channel

Since 7.17 can predict NDF in multipath channels, this approach will be used in this section to investigate the NDF of the “Karlsruhe” communication channel. Focus will be given to the study of NDF in real systems and its dependence on SNR, as well as the validness of condition (7.17) in the prediction of NDF in real systems.

7.3.1 Degrees of freedom definitions for non-ideal channels

Up to this point the concept of degrees of freedom has been discussed for both free space and multipath scenarios. In this way, considerable insight into the communicational limits of these ideal channels was obtained. Yet, these scenarios do not reflect the complexity of real settings, such as the uneven (power) multipath propagation that takes place in an urban communication channel. Therefore, the number of degrees of freedom in such non-ideal channels will now be investigated based on the following two NDF definitions:

- **Traditional definition (NDF).** In the traditional definition of degrees of freedom the number of available orthogonal channels is determined by the angular domain representation of the communication channel as discussed in the previous sections. In this way, the communication channel (propagation channel + antennas) relates the spatial and angular domains to each other and the eigenvalues of the matrix \mathbf{H} yield a measure of the number of spatial signatures (looking directions) available to the system, namely the traditional NDF. Furthermore, since the number of beamforming vectors realizable in an ideal channel depends on the transmitting and receiving lengths (or areas), the addition of more antennas does not increase the number of orthogonal links. Therefore, the scenario dependent NDF can be determined by studying the number of eigenvalues in systems with a large number of transmitting and receiving antennas but fixed array length [Mig06b]. This is the traditional SNR independent NDF definition as found in information theory works and previously discussed for the free space and multipath channels [PBT05].

- **SNR dependent definition** ($\widehat{\text{NDF}}$). It is known from communication systems that, due to the uneven power distribution of the singular values, not all singular values greater than zero can be used with insufficient SNR. Therefore, SNR constraints the maximum number of subchannels that can be used if non-ideal channels, in the sense of non-equal power distribution among all paths, are considered. This can be seen at hand from systems using the waterfilling power allocation scheme. For such systems it was explained in section 4.2.2 that energy is distributed optimally along each subchannel. Hence, if there are subchannels with no energy, the waterfilling capacity will remain the same. From this follows that by increasing the number of sampling antennas N_S at both communicating ends, a certain threshold $N_S = \widehat{\text{NDF}}$ will be reached, after which capacity will no longer increase for a given SNR. $\widehat{\text{NDF}}$ then yields the maximum number of subchannels that can be found. However, contrary to the discussion of sections 7.1 and 7.2 not all subchannels need to correspond to orthogonal spatial signatures in this case.

Since both definitions depend on the channel matrix \mathbf{H} , two questions arise regarding the traditional NDF analysis and this new SNR dependent $\widehat{\text{NDF}}$ definition: 1) what is their relationship? and 2) what practical meaning do both definitions have in predicting the degrees of freedom of non-ideal channels? In the following this will be explained for single channel realizations of the “Karlsruhe” communication channel.

7.3.2 Degrees of freedom of single channel realizations

To begin the study of the relationship between the two degrees of freedom definitions and their practical meaning, first the traditional NDF interpretation will be investigated. For this purpose, the eigenvalues of the \mathbf{H} matrix are analyzed. Their distribution yields the critical number of subchannels S_C after which the energy of the remaining subchannels drops significantly. In free-space [Mig06b, Fig. 5] and multipath environments with equal power distribution in all angular directions, i.e. ideal scenarios, a knee-like behavior for the singular values of the communication channel results. In non-ideal multipath scenarios, however, a different behavior has been reported [HF06, XJ06]. For these cases, in spite of energy decrease in the singular values, no step-like behavior is obtained. Since the “Karlsruhe” communication channel falls within this category, a similar behavior is also expected. This is confirmed in Figure 7.7, where a 5λ array, located at coordinates (1637 m, 637 m), oriented in y -direction and with $N_S = 22$, has been considered. It is seen that, in spite of the downward trend of σ_k , no obvious step-like behavior is recognized. Yet, for $k > 4$ a significant decrease in the subchannels power is seen. This corroborates previous results and indicates that in non-ideal scenarios non-orthogonal spatial signatures result, due to the uneven power distribution among angular regions. This means that two non-(spatially-)orthogonal neighboring look directions might be favored over other better

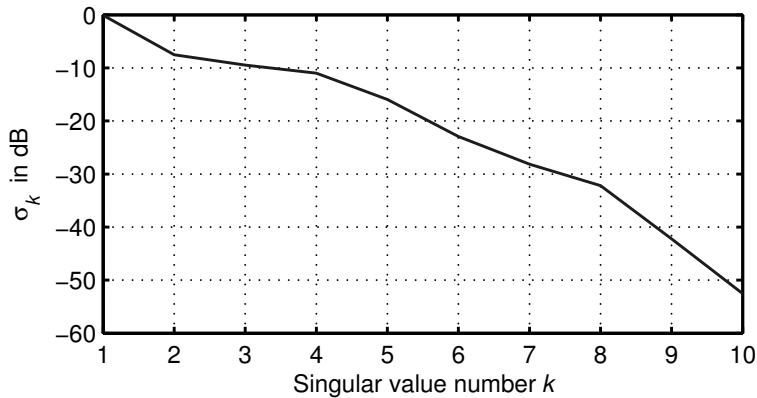


Figure 7.7: Singular values of 5λ array of $N_S = 22$ omni-directional antennas oriented in the y -direction. Only the first 10 eigenvalues are shown. Receiver is located at (1637 m, 637 m).

resolved ones, if the incoming energy at these two is sufficiently strong. In other words, when there is no angular constant power distribution, the propagation channel can concentrate energy in those directions where non-orthogonal spatial modes can be formed. As result, contrary to ideal systems that are SNR-insensitive (due to the step-like energetic differences between strong and weak spatial modes) SNR plays a significant role in non-ideal channels.

In order to see the impact of SNR on the number of available subchannels Figure 7.8 shows the relationship between \widehat{NDF} and SNR. As previously explained, \widehat{NDF} in Figure 7.8 corresponds to the number of subchannels after which, at a certain SNR regime, capacity no longer increases when a waterfilling scheme is used⁴. In other words, \widehat{NDF} is equal to the number of non-zero singular values⁵ of \mathbf{H} used by the waterfilling power allocation scheme. In this regard, it is seen from Figure 7.8 that \widehat{NDF} grows more rapidly at low SNR regimes. At mid to high SNR regimes ($SNR > 10$ dB) considerable larger SNR values are needed to improve \widehat{NDF} . This accelerated increased of \widehat{NDF} at low SNR regimes can be closely followed by a line up to the point where $\widehat{NDF} = NDF$. From this point on, the rate at which NDF increases decelerates considerably. Moreover, the same linear behavior could be verified at different channel locations with only changes in NDF and slight shifts towards lower or higher SNR values. From these observations, it is thus concluded that for relative small NDF values (≤ 4), in most cases, 10 dB SNR suffices to reach the NDF threshold.

For practical purposes, the behavior depicted in Figure 7.8 means that, even if higher SNR regimes are considered, the most “profitable” S_C subchannels are those where $S_C \leq NDF$.

⁴Waterfilling capacity curves are omitted for brevity. It should be noted though that the same normalization scheme of chapter 5 was used.

⁵In real channel realizations there might exist spurious singular values that have only marginal energy levels. Therefore singular values below -55 dB (eigenvalues below -110 dB) are considered to be equal to zero.

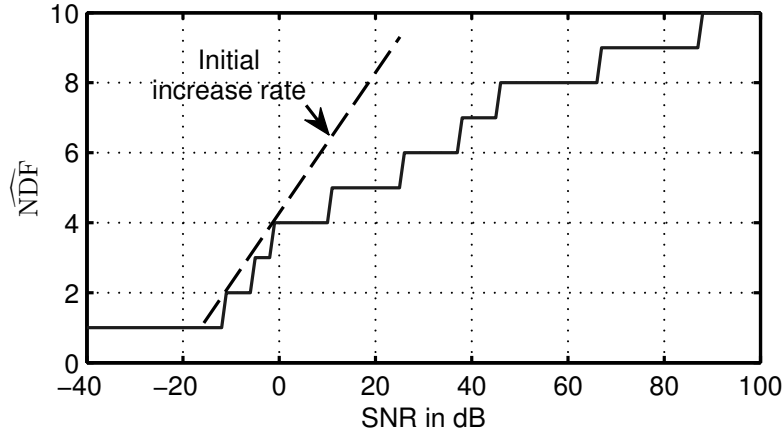


Figure 7.8: $\widehat{\text{NDF}}$ vs SNR of 5λ array of $N_S = 22$ omni-directional antennas oriented in y -direction. Receiver is located at (1637 m, 637 m).

Therefore, being able to predict NDF in the traditional sense is of great importance in the dimensioning of antenna arrays and can optimize the performance-cost tradeoff. In the following, NDF prediction based on (7.17) will be discussed.

It has been seen that approximation of NDF for multipath channels requires the knowledge of the angular distribution of the scattered signals. Hence, in order to understand the quality of the NDF estimation in (7.17), the angular distribution of the transmitted and received signals is needed. Since NDF for a receiver located at coordinates (1637 m, 637 m) has been already determined, the angular spectrum of the received power, P_r , for this very case is plotted in Figure 7.9. It should be noted that, in spite of ϕ ranging between 0 and 2π , ϕ has been remapped to the $(0, 2\pi)$ region in Figure 7.9 due to the symmetry of linear arrays (cf. 7.3). In this way, it is now possible to compute Ω_{Tx} and Ω_{Rx} , as given in (7.18), in order to predict the NDF of the communication channel for a given array length. From Figure 7.9 and (7.18), $\Omega_{Tx} \approx 0.75$ and $\Omega_{Rx} \approx 1.95$ result. In consequence by considering different array lengths the predicted NDF of Table 7.1 result. From Table 7.1 follows that the transmitter is responsible for limiting the NDF of the system for this particular channel realization. Furthermore, based on the simulation results and previous discussion, for the setup of Figures 7.7 and 7.8, $L\Omega$ correctly predicts the simulated value of NDF=4.

Now, in order to verify the ability of (7.17) in predicting the impact of L on NDF, Figure 7.10 shows the computed NDF for all cases in Table 7.1. This is a similar representation to that in Figure 7.8, where $\widehat{\text{NDF}}$ vs SNR is once more plotted, but in this case, the $\widehat{\text{NDF}}$ steps have been replaced with markers for visualization ease. From Figure 7.10 it is seen that, even though a clear trend towards higher NDF and $\widehat{\text{NDF}}$ with larger arrays exists, (7.17) is an inaccurate measure of the NDF of the channel. In consequence, at small array lengths (7.17) underestimates

Table 7.1: Predicted NDF for Figure 7.9

L	1λ	2λ	3λ	4λ	5λ	6λ	7λ
Tx	1	2	3	3	4	5	6
Rx	2	4	6	8	10	12	14

the channel NDF, whereas for larger arrays it overestimates it. In particular it is also noticed that for small array length a larger number of subchannels appears as those theoretically possible in free space (cf. $L = 2\lambda$ case with Figure 7.5). In the following the possible reasons for these discrepancies will be discussed.

Considering that results presented so far were based on the assumption that array dimensions vary simultaneously at transmitter and receiver, if transmitter and receiver are allowed to change independently from each other a different behavior to that observed so far might be found as reported in [XJ06]. These results showed that changes in the transmitter affected the eigenvalue distribution and system NDF, for a NDF_{Rx} limited system. To see if this holds true in the “Karlsruhe” scenario, a fixed transmitter length L_{Tx} of 3λ was chosen, whereas L_{Rx} , i.e. receiver length, was allowed to vary between 1λ and 7λ . The result is shown in Figure 7.11. It is seen that for $L_{Rx} = 1\lambda$ and 2λ the NDF curve changes slightly with respect to the $L = 3\lambda$ case of Figure 7.10. For all other cases only marginal changes are observed. Furthermore, only for $L_{Rx} = 1\lambda$ NDF is reduced. This shows that $NDF_{Tx} \leq NDF_{Rx}$ holds true for $L_{Tx} = 3\lambda$ when $L_{Rx} \geq 2\lambda$. In this way $NDF = \min(NDF_{Tx}, NDF_{Rx})$ is proven valid and excluded as possible cause for the discrepancies between Table 7.1 and Figure 7.10.

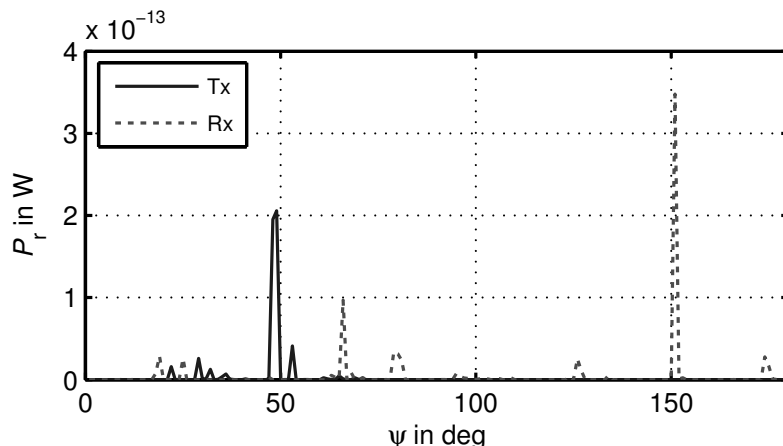


Figure 7.9: Received power vs angular distribution in azimuth. Receiver is located at (1637 m, 637 m).

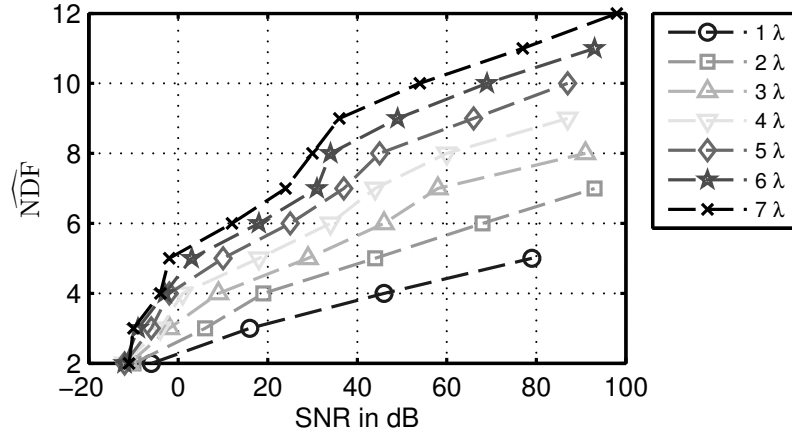


Figure 7.10: Number of available subchannels vs SNR for an array of varying length oriented in the y -direction and $N_S = 22$. Receiver is located at (1637 m, 637 m).

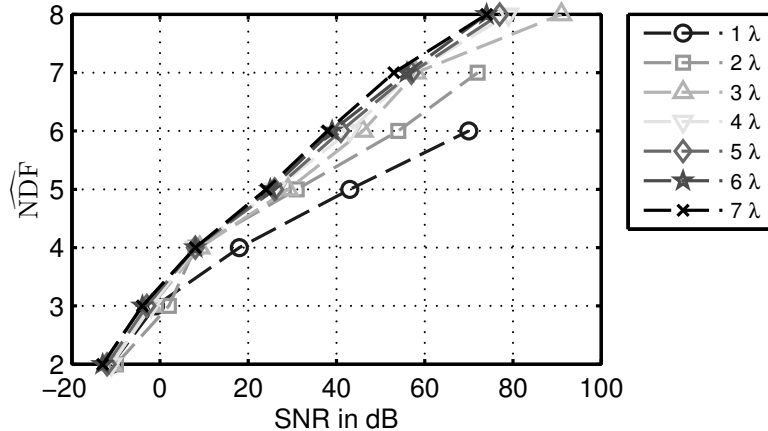


Figure 7.11: Number of available subchannels vs SNR for an array of varying length oriented in the y -direction and $N_S = 22$ with fixed antenna length $L_{Tx} = 3\lambda$. Receiver is located at (1637 m, 637 m).

Another possible cause for an inaccurate NDF prediction may be the use of a poorly scattered channel (i.e. very limited angular distribution). To exclude this possibility in Figure 7.12 a more scattered channel is considered resulting from a receiver located at (1400 m, 150 m). In this case $\Omega_{Tx} \approx 1.97$ and $\Omega_{Rx} \approx 2$ are obtained. The predicted NDF values with (7.17) for different L are given in Table 7.2. Here, once more no accurate prediction can be made as seen from Figure 7.13. Moreover, the same trends as with Table 7.1 are confirmed, i.e. at small array lengths NDF is underestimated, whereas at larger array lengths NDF is overestimated. In addition, a different behavior to that of Figure 7.10 is observed. In this case all curves exhibit a more pronounced rake-like shape with distinct regions. A first region in which \widehat{NDF} increases slowly with respect to SNR, a second region in which \widehat{NDF} increments occur much

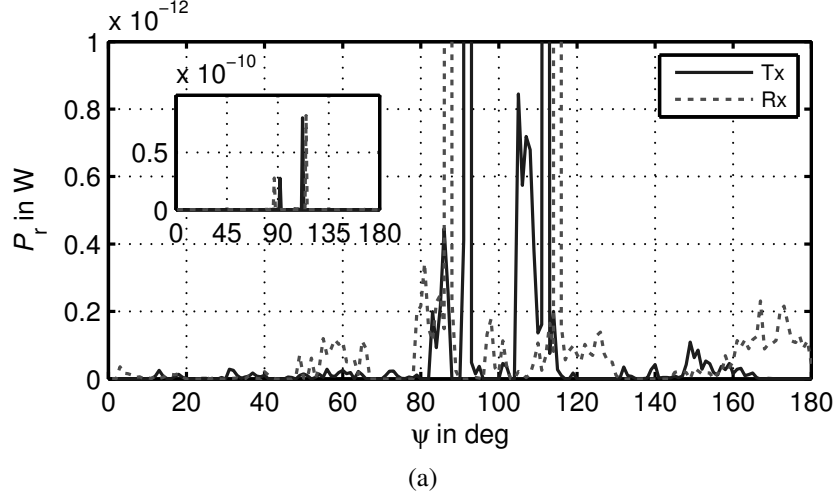


Figure 7.12: (a) Received power vs angular distribution in azimuth. Receiver is located at (1400 m, 150 m).

more rapidly and a third region in which $\widehat{\text{NDF}}$ growth decelerates once more. The transition point between the second and third region yields the system NDF. Finally, it can be concluded that even in scatterer-richer scenarios (7.17) still fails in predicting NDF.

From the previous discussion follows that in all cases NDF is proportional to array length and to some extent also on Ω . Yet, it seems that due to the fact that the transmitted power is not uniformly distributed along θ , Ω might have an SNR dependence. Therefore, depending on SNR a different angular region might be seen by the antennas. In addition the fact that in some cases

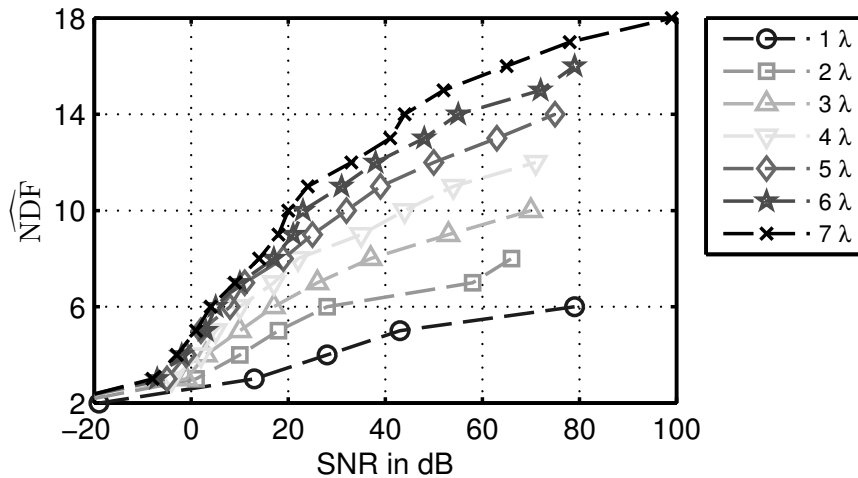


Figure 7.13: Number of available subchannels vs SNR for an array of varying length oriented in the y -direction and $N_S = 22$. Receiver is located at (1400 m, 150 m).

Table 7.2: Predicted NDF for Figure 7.13

L	1λ	2λ	3λ	4λ	5λ	6λ	7λ
Tx	2	4	6	8	10	12	14
Rx	2	4	6	8	10	12	14

(smaller array lengths) additional subchannels to those possible in free space result, is also due to the uneven power distribution. In this way, otherwise weak subchannels from an antenna perspective might receive sufficient energy as to contribute to $\widehat{\text{NDF}}$.

To summarize, even though the previously published formula $L\Omega$ for predicting NDF has been proven inadequate for the single channel realizations of the “Karlsruhe” communication channel, similar trends could still be observed:

- Angular spread at transmitter and receiver do limit NDF, and in consequence $\widehat{\text{NDF}}$.
- Array size directly influences both NDF and $\widehat{\text{NDF}}$.
- Even though higher SNR regimes can increase the degrees of freedom of the channel as evidenced by $\widehat{\text{NDF}}$, it is most convenient to design antenna systems with a maximum of NDF dimensions. Otherwise great amounts of energy might be needed to benefit from higher ranked systems.
- Finally, it seems that due to the non-uniform nature of the angular distribution of real environments SNR effects on Ω need to be considered.

With this knowledge, evaluation of the urban communication channel in a more general sense, i.e. as the statistic resulting of all links, can be approached.

7.3.3 Degrees of freedom of all channel realizations

The study of the urban communication channel in a statistical sense can only be done based on certain system assumptions. Here, the same assumptions as given in 3.3 are used. Furthermore, the same approach in the study of the degrees of freedom of the channel as the one given in the previous section is used. This means that $\widehat{\text{NDF}}$ vs SNR will be investigated for all channel realizations. Therefore, the total $\widehat{\text{NDF}}$ will result from the maximum $\widehat{\text{NDF}}_l$ among all L channel realizations, where the subscript l denotes the l -th channel realization.

Figure 7.14 shows the angular received power distribution and the corresponding $\widehat{\text{NDF}}$, for an array of 22 omni-directional antennas oriented in the y -direction. It is seen in Figure 7.14a that power is better distributed among all angles than it was the case for the single channel realizations considered in the previous section ($\Omega = 2$ at receiver and transmitter). In consequence

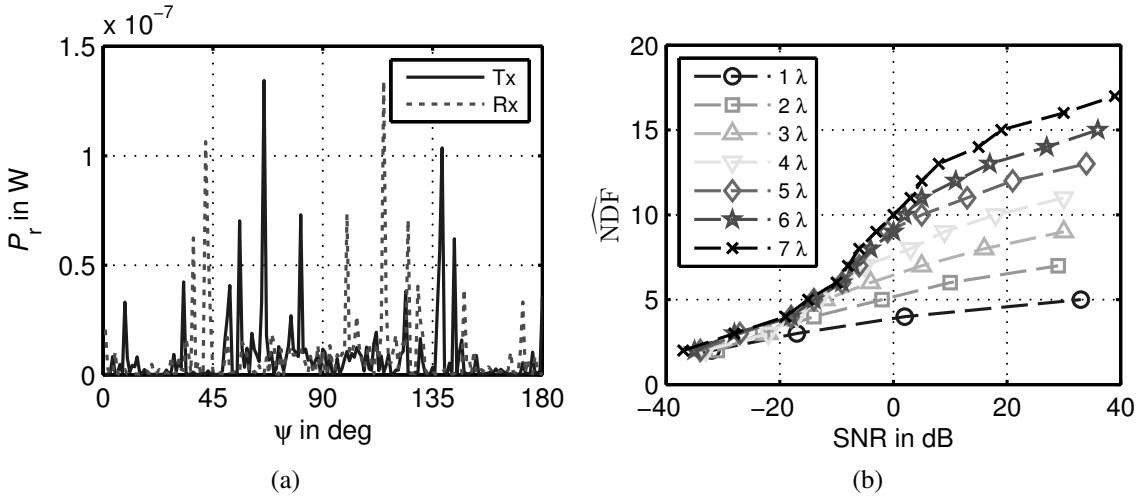


Figure 7.14: (a) Received power vs angular distribution in azimuth and (b) S_C vs SNR for an array of varying length oriented in the y -direction and $N_S = 22$ averaged over all receiver positions.

the same predicted NDF values of Table 7.2 result. Furthermore, an uneven power distribution is also noticed in this case. Therefore, as seen from the $\widehat{\text{NDF}}$ curve in Figure 7.14b, (7.17) fails once more in predicting $\widehat{\text{NDF}}$. Nonetheless, certain trends are recognized: 1) the channel as a whole exhibits higher $\widehat{\text{NDF}}$ values and 2) similar to Figure 7.12 a rake-like behavior for all curves was found. For SNR regimes below ≤ -10 dB $\widehat{\text{NDF}}$ increases slowly with SNR and continues to do so for $L < 3\lambda$. For $L \geq 3\lambda$, on the other hand, an accelerated growth rate is noted, from which according to the examples of the previous section, a NDF value can be estimated. For $L = 3\lambda-7\lambda$ NDF, as read from Figure 7.14b, is 5, 7, 9, 11 and 13 respectively. Here, once more a linear dependence of NDF on L is verified, yet only from a certain threshold length (in this case 3λ). In addition, when looking at a fixed SNR, i.e. 20 dB, also a linear dependence on L for $\widehat{\text{NDF}}$ is suggested.

For completeness, in Figure 7.15 also the received power angular distribution and the corresponding $\widehat{\text{NDF}}$, for an array of 22 omni-directional antennas oriented in the z -direction are shown. It is seen that in this case an uneven power distribution in the elevation also results⁶. Furthermore, in this case, a smaller angular region is used. In consequence, much smaller $\widehat{\text{NDF}}$ values are obtained, yet the same rake-like behavior of Figure 7.14b is seen. Finally, in this case (7.17) is also a poor approximation of the true NDF of the system.

⁶It should be noted that related angular distributions for the “Karlsruhe” communication channel have been already published [Sch07]. Yet, in this case the angular spectrum and not the number of received paths per angle are plotted. An histogram of all received paths (not shown) is very similar to the one in [Sch07]. However, such histograms are not a sufficient measure to understand the available spatial resources, since they might wrongly suggest that energy concentrates in a small angular region, which is not the case.

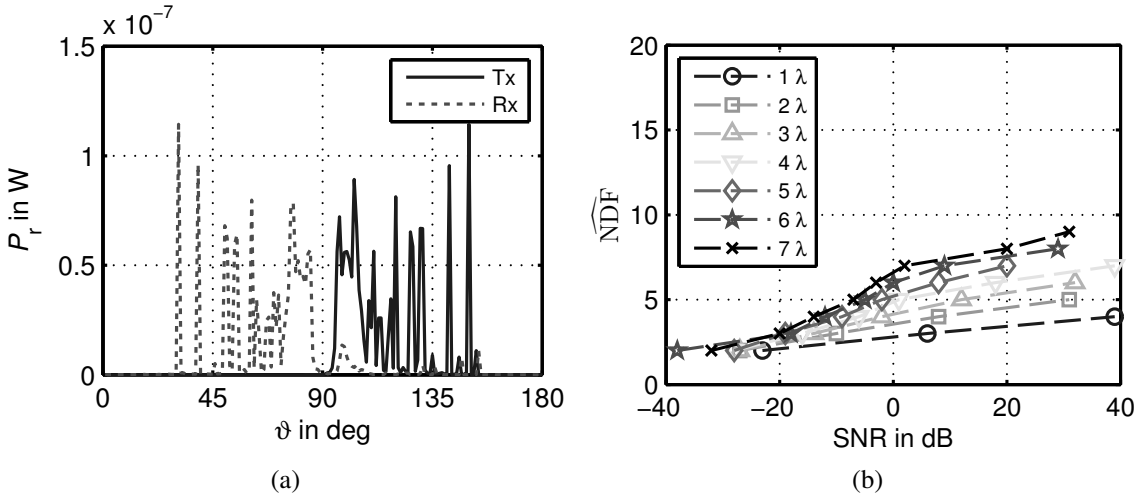


Figure 7.15: (a) Received power vs angular distribution in elevation and (b) S_C vs SNR for an array of varying length oriented in the z -direction and $N_S = 22$ averaged over all receiver positions.

From the previous results follows that for practical purposes and without previous simulation it is not possible to predict either NDF nor \widehat{NDF} , since appearance of new channels is completely random. Instead, these results should be taken as reference in order to decide, depending on the SNR regime to be used, if the communication channel, and thus the system, benefits from having larger arrays or closely spaced antennas. Moreover, it must be stressed out that in this case the effects of mutual coupling are not considered, and should be the focus of future research.

7.4 Final remarks

In this chapter the communicational limits of linear antenna arrays in three different scenarios were discussed: free space, multipath with homogeneous power distribution among all paths and multipath with uneven power distribution as in the “Karlsruhe” communication channel. As result, a method for estimating the available degrees of freedom in each case was obtained. It was seen that the number of degrees of freedom, which ultimately translates to the number of possible subchannels available, is dependent on SNR, array length and scenario. In this way, it can be concluded for real systems that depending on the SNR regime used, there will be a certain number of antennas that provides the best trade-off between cost and performance improvement. Because of this, antenna design in real settings will differ from that in free space. More importantly, in real scenarios with uneven power distributions (contrary to free space) there does not seem to be a specific number of antennas after which capacity abruptly decreases. Yet, a point can be determined after which the inclusion of additional subchannels results in only small capacity increases. Because of this, it seems likely that for systems work-

ing at high SNR regimes an optimum trade-off between number of antennas and capacity can be found depending on the array length used. For low SNR regimes, however, the use of additional subchannels seems to be less sensitive to changes in array length than to SNR. In the following the antenna synthesis problem for the urban channel from a multiple element antenna perspective will be approached.

8 Antenna design for wireless communication channels

To conclude this work, in this chapter the design of capacity maximizing MEA arrays will be handled. Contrary to chapter 5 selection of an optimum antenna array will not be done by comparison of a vast number of MEA configurations. Instead the background of chapter 7 will be used to exploit the spatial resources of the channel as shown possible from chapter 4. The approach taken here is thus novel, since it synthesizes an antenna in a capacity maximizing sense, rather than just achieving a desired radiation pattern as done in more traditional synthesis methods. The difference lies in the fact that in the case of power or pattern synthesis [Mai05, Bha07] a certain radiation property is desired, since it is assumed that in this way a better system performance concerning any parameter of interest can be attained. In this way it is customary to define a specific issue, such as pattern interference, and based on it define an optimum radiation pattern for which a certain synthesis method is then applied, as done in [PW07, PLW07]. Given that capacity is a complex measure resulting from all system component and channel interactions it is not possible to define a priori a capacity maximizing radiation pattern. Therefore, in this chapter an in-system synthesis (-optimization) method is proposed. As result, a set of suggestions toward better antenna designs for the future will be made.

This chapter is structured as follows. First, a synthesis method for fully exploiting the channel spatial resources in a capacity maximizing sense will be discussed. Then, the synthesis of capacity maximizing antenna arrays for the urban communication channel will be undertaken. And, finally, based on the results obtained antenna design concepts for the future will be proposed.

8.1 Multiple element antenna synthesis method

In chapter 7 an heuristic approach based on resolvability, similar to that in [TV05, PBT05], was taken for finding the degrees of freedom of linear MEA systems in different communication channels. This intuitive approach, however, has its background on a more involved theoretical framework focusing on the link between electromagnetism and information theory. In this section a capacity maximizing synthesis method will be derived based on this theoretical framework.

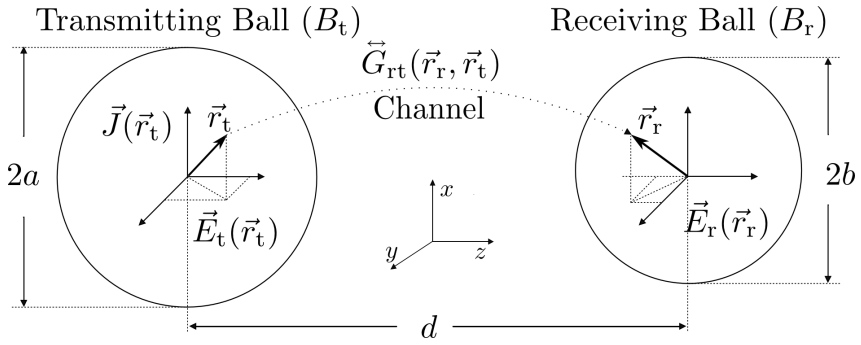


Figure 8.1: Basic model for communicating volumes.

The first works related to the informational content of electromagnetic waves date back to the seminal works of Gabor and di Francia from the 1950s in the field of optics, who studied the available channels of communication among diffraction-limited surfaces. With this background, [Mil00, PM00] investigated the available number of communication modes for arbitrary volumes in optical systems based on an eigenfunction approach. Here it was shown that for the case of communicating volumes (three dimensional balls in Figure 8.1) it is possible to express the sources and waves in terms of basis functions with coefficients β_k and α_k . In this way, the wave propagation problem can be rewritten into matrix form

$$\boldsymbol{\alpha} = \mathbf{H}\boldsymbol{\beta}. \quad (8.1)$$

As result, the problem of maximizing the information throughput is recasted as the maximization of the so-called communication operator \mathbf{H} between the three dimensional transmitting and receiving balls (volumes) B_t and B_r . Where, the non-zero elements of the otherwise infinite-dimensional \mathbf{H} matrix, i.e. the rank of \mathbf{H} , represent the available independent communication channels referred to as subchannels in the context of MIMO systems (NDF in information theory). This fundamental link between field theory and information theory poses, however, the difficulty of finding the rank of the \mathbf{H} matrix with the largest coefficients. Yet, this is only under proper definition of the basis functions ρ and τ in single polarized 3D fields (or $\vec{\rho}$ and $\vec{\tau}$ for vectorial fields as stated in [PM00])

$$E(\vec{r}) = \sum_k^{\infty} \alpha_k \rho_k, \quad (8.2)$$

$$J(\vec{r}) = \sum_k^{\infty} \beta_k \tau_k. \quad (8.3)$$

Finding a proper set of basis functions is, in consequence, the key problem in determining \mathbf{H} with maximum communication coefficients. Moreover, the dimensioning of the communication

system will depend on the number of basis functions needed to accurately represent $E(\vec{r})$ and $J(\vec{r})$ while truncating the series (8.2) and (8.3).

In [Mil00], an analytical solution for the basis functions of the scalar source in integral-equation form with aid of the prolate spheroidal wave functions for the case of three-dimensional hyper-rectangles is derived. In [PM00], on the other hand, multi-polarized fields and currents $\vec{E}(\vec{r})$ and $\vec{J}(\vec{r})$ are considered and the vectorial eigenvalue problem, found when maximizing the interconnection strengths of \mathbf{H} , is solved for vectorial basis functions of the source current with the use of a numerical technique called the Galerkin method. Later on, in [HF06] the approach in [Mil00] is extended for the case of arbitrary volumes and the effects of multiple scatterers is considered, yet similar to [PBT05, CF06, XJ06, Mig06b, Mig06a, GM08] focus is shifted from computation of the basis functions to obtention of NDF. And it was not until recently that [JW08] showed that the basis functions of the current J could themselves be approximated by a set of sub-basis functions. These sub-basis functions then sample the channel in the spatial domain so that the optimal current distributions and radiation patterns for a certain antenna size in a specific scenario can be found.

However, in [JW08] only results for a two-dimensional channel model are presented. Therefore, in this work, results for a realistic urban propagation scenario based on a three dimensional ray-tracing simulator are presented and, in addition, an extension to the synthesis method of [JW08] is also proposed.

In [JW08] it was shown that the basis functions $\vec{\rho}$ and $\vec{\tau}$ (vectorial form) could be numerically approximated as a linear combination of an additional set of sub-basis functions $\tilde{\vec{\rho}}$ and $\tilde{\vec{\tau}}$. In this way the source current, could be rewritten solely in terms of the sub-basis functions [JW08, Eq. (20)]. As result, computation of the channel matrix $\tilde{\mathbf{H}}$ between the sub-basis functions and its singular value decomposition (SVD) $\tilde{\mathbf{H}} = \tilde{\mathbf{U}}\tilde{\mathbf{S}}\tilde{\mathbf{V}}^\dagger$ suffices to determine \mathbf{H} and the optimal basis functions as

$$\begin{aligned}\rho_k &= \sum_v \tilde{V}_{vk} \tilde{\rho}_v \\ \tau_k &= \sum_u \tilde{U}_{uk} \tilde{\tau}_u,\end{aligned}\tag{8.4}$$

in the scalar case. This formal approach in determining \mathbf{H} was heuristically used in the previous chapter. The main idea was to sample the communicating space and determine its limitations. Therefore, in [JW08] the sub-basis functions act as sampling functions which then with use of a water-filling solution allow for reconstruction of the optimal current distributions and electric fields.

Computation of the optimal current distribution, requires that $\tilde{\rho}$ and $\tilde{\tau}$ are orthonormal. In [JW08] this was done by subdividing the transmit and receive apertures into N_S subapertures in each dimension (see Figure 8.2b). This resulted in an elaborate expression for $\tilde{\mathbf{H}}$ [JW08, Eq. (23)] (for the single polarized case). In this work, the use of point sources is proposed instead (see Figure 8.2c). With point sources orthonormality is maintained and a much simpler expression for $\tilde{\mathbf{H}}$ is found by substituting for the scalar case $\tilde{\rho}$ and $\tilde{\tau}$ with dirac delta functions in the expression for \tilde{H}_{vu} implicit in [JW08, Eq. (19)]

$$\begin{aligned}\tilde{H}_{vu} &= \int_{B_r} dB_r \int_{B_t} dB'_t \tilde{\rho}_v^\dagger(\vec{r}_r) G(\vec{r}_r, \vec{r}'_t) \tilde{\tau}_u(\vec{r}'_t) \\ &= G(\vec{r}_{r,v}, \vec{r}_{t,u}),\end{aligned}\quad (8.5)$$

where G is the scalar Green function of the channel (in the general case the dyadic Green function \hat{G} results). Then, under adoption of the commonly used plane wave model, (8.5) is found to be

$$G(\mathbf{r}_{r,v}, \mathbf{r}_{t,u}) = \tilde{H}_{vu} = \sum_{p=1}^P T_p e^{j\varphi(\vec{r}_{r,v}, \Omega_{r,p})} e^{j\varphi(\vec{r}_{t,u}, \Omega_{t,p})}, \quad (8.6)$$

with

$$\varphi(\vec{r}, \Omega) = \frac{2\pi}{\lambda}(x \cos \psi \sin \vartheta + y \sin \psi \sin \vartheta + z \cos \vartheta), \quad (8.7)$$

where ϑ and ψ are the elevation and azimuth angles of the receive and transmit vectors $\vec{r}_{r,v}$ and $\vec{r}_{t,u}$, of the v and u sub-basis function for the p -path and T_p is the transmission factor of the polarization component of interest.

Now, in order to synthesize the antenna radiation pattern out of the given sub-basis functions the τ basis functions are used to obtain the optimal current distribution, and out of it the radiated pattern of the ideal antennas. It should be noted though that from a communication system perspective τ_k represents the k -th subchannel. Therefore, here the fact must be stressed that even though the total current is written as in (8.3) [JW08, Eq. (6)], interest lies in the current distribution of each subchannel. It follows that $J_k = \tau_k$ and the transmitted electric field $E_{t,k}$ of the k -th subchannel can be found from

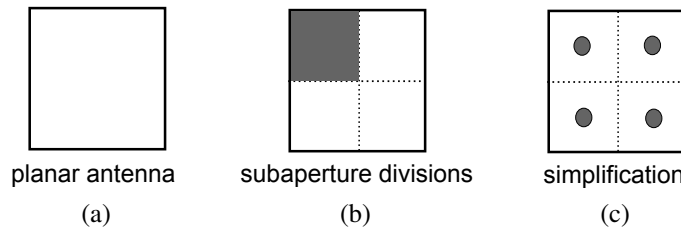


Figure 8.2: Array aperture showing the sub-basis regions with $N_S = 2$.

$$E_{t,k}(\vec{r}_t) = \frac{e^{-jkr_t}}{r_t} \int_{\Delta V_t} e^{j\varphi(\vec{r}'_t, \Omega_t)} J_k(\vec{r}'_t) d\vec{r}'_t. \quad (8.8)$$

For computing the electric field of the receiving antenna the channel matrix is transposed (inverse communication direction) and an analogous expression to (8.8) is used, but integrating over the receiving volume. In this case the optimal k -th current distribution at the receiver results from

$$J_k(\vec{r}_r) = \tau'_k(\vec{r}_r) = \sum_v \tilde{V}_{vk}^* \tilde{\rho}_v(\vec{r}_r). \quad (8.9)$$

A drawback of point sources, though, is that they are only capable of sampling the channel at discrete points, contrary to the continuous aperture approach in [JW08]. As trade-off, however, antenna synthesis can be easily integrated to existing channel simulators. In this way $\tilde{\mathbf{H}}$ can be easily computed and, in addition to point sources, regular antennas can be chosen as sub-basis functions so that an antenna type based synthesis becomes feasible. It follows, that a multi-polarized or multi-antenna synthesis is straightforward and is done by expressing each sub-basis function as a linear combination of the different polarization components or different antennas. This could be seen as a modal expansion and yields in return a tensor $\tilde{\mathbf{H}}$ matrix, i.e. a four dimensional matrix, with tensor elements \tilde{H}_{uv} , i.e. two dimensional elements. For practical purposes this is equivalent to simply computing one $\tilde{\mathbf{H}}$ for each antenna or polarization needed and arranging them in a two dimensional matrix to obtain the desired water-filling solution. The potential of this for optimizing the communication channel capacity will be shown later on.

8.2 Antenna array synthesis for the urban communication channel

In order to visually clarify the functioning and potential of the synthesis method previously described, in Figure 8.3 the synthesized antennas obtained when the receiver is located at (1637 m, 637 m) are shown, for a free space channel (Figure 8.3a) and for the channel described in section 3.3 (Figure 8.3b). The synthesized antennas are generated using a planar array with $N_s = 5$ in y and z -direction at both base station and mobile stations. $\tilde{\mathbf{H}}$ is obtained with help of the network model of chapter 3 under the assumptions of perfect impedance matching. It is seen that for free space the resulting antennas look at each other. For the multi-path propagation scenario, on the other hand, a minimum at the line of sight direction is observed. This was purportedly chosen this way to show that, even in cases where most of the incoming energy at the receiver originates from scattering objects, the method presented is capable of synthesizing an optimal current distribution, and from it an optimum antenna radiated field.

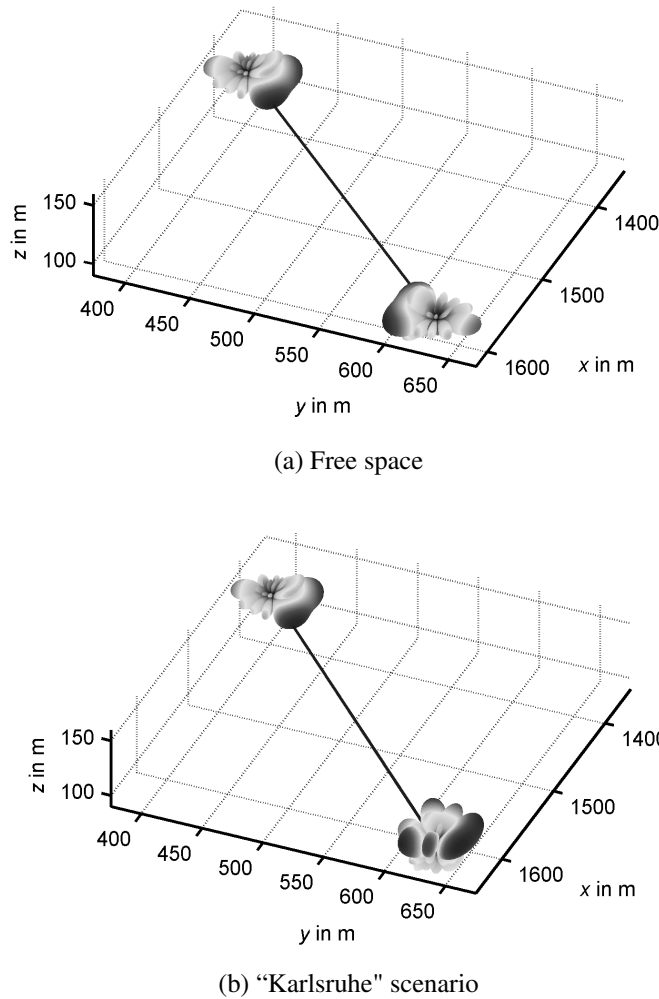


Figure 8.3: Synthesized antennas.

In the following, in order to obtain a more realistic description of the actual site, influenced to a lesser extent by the base station look direction, a three-sectorized cell is used. This means that for each sector only those mobile station positions lying within the defined angular limits are considered and the base station orientation is rotated accordingly. Orientation of mobile stations, on the other hand, is kept constant and parallel to the x -axis for all sectors. Effectively, this results in three different propagation environments and thus three different syntheses for both mobile and base station. However, since in each sector multiple antenna links exist, in order to obtain the antenna that maximizes capacity in most cases, an averaging over all links, i.e. channel realizations, is performed.

These average J_k currents are then used in (8.8) to obtain the radiated pattern. Alternatively, instead of an antenna synthesis this can be interpreted as a synthesis of the optimal current distributions for the array of point sources. In the case where specific antenna types (i.e. non-

isotropic antennas) are considered as the point sources, i.e. sub-basis functions, their radiation patterns are multiplied with J_k resulting in a weighted current J'_k . And for the more general case of multiple fully polarized (θ and ψ polarized) antennas a vectorial weighted current results \vec{J}'_k . The synthesized radiation patterns from \vec{J}'_k are then used to compute the waterfilling capacity. However, since there might be interest to use only a certain number of antennas instead of all possible, the number S_C of most significant subchannels used for synthesis is varied. The synthesized antennas are assumed to have the same location, SNR is fixed to 10 dB, and all channel matrices are normalized with the ones resulting from an equivalent (same antenna number and location) omni-directional antenna system. The antenna synthesis is done using an array of point sources of length $L = 5\lambda$ aligned in z -direction (perpendicular to ground) at both base station and mobile stations.

In Figure 8.4 capacity vs. number of synthesized subchannels S_C is shown for omni-directional antennas. The antenna elements used for each sub-basis function were omni-directional antennas either θ polarized, ψ polarized or both. Hereby, two array orientations were considered: y -direction (Figure 8.4a) and z -direction (Figure 8.4b).

It is known from the previous chapter that a larger number of subchannels in the y -direction than in the z -direction can be obtained. In Figure 8.4 this is confirmed. It is seen that when only one polarization is used, the capacity of the in y -direction synthesized antennas reaches its maximum value at $S_C = 10$. For the in z -direction synthesized antennas the capacity limit is already reached with $S_C = 5$. Remarkably though, with equal number of synthesized subchannels the in z -direction synthesized antennas achieve larger capacities. This means that narrower beams (larger gain) in elevation, compensate for the reduced angular spread inherent to arrays oriented in z -direction. This, therefore suggests that for MEA systems in urban settings with few antennas (less than 7¹), the use of the available subchannels in the elevation, rather than in azimuth, will yield the best performance. Finally, it was also seen that in bot cases when dual polarized omni-directional antennas are used for synthesis, capacity improves significantly (almost doubles) and the number of subchannels doubles as predicted in [PBT05, Mig06b].

Figure 8.5 now shows a similar result but in this case combinations of dipoles oriented parallel to the coordinate axes are considered. Here, for brevity only the case of an array in the z -direction is considered. The result for a z -oriented dipole is similar to Figure 8.4b, with small differences due to the effect of the dipole radiation pattern in comparison with an omni-directional antenna. However, it is seen that the use of two perpendicular dipoles almost completely exploits the polarization diversity (capacity stabilizes at $S_C = 9$) and that the addition of a third dipole does

¹This criterion is not arbitrarily chosen and might change depending on the propagation channel considered. It results from comparing the capacities of the in z and in y -direction synthesized antennas and finding the point from which the latter outperforms the former.

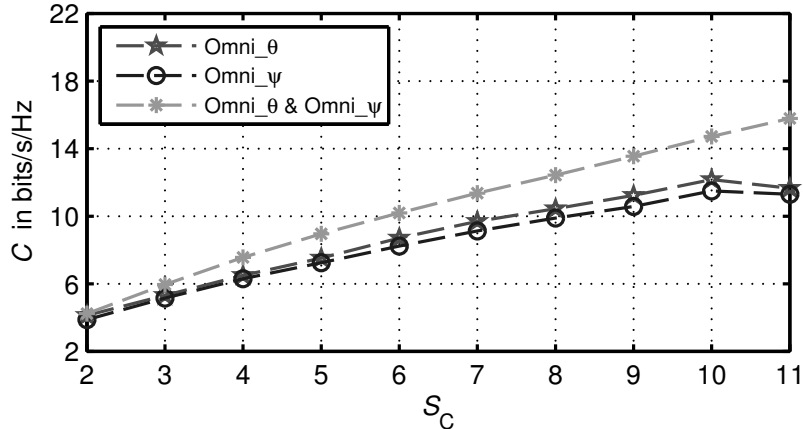
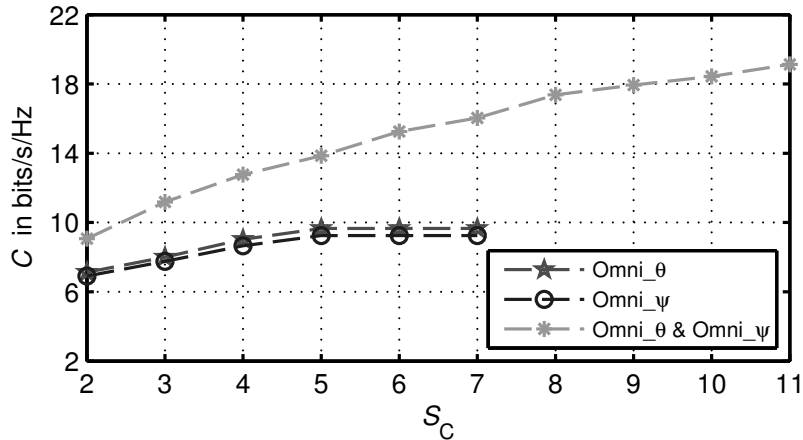
(a) Arrays of sub-basis antennas are oriented in the y -direction, $N_S = 40$ (b) Arrays of sub-basis antennas are oriented in the z -direction, $N_S = 25$

Figure 8.4: Capacity vs S_C for synthesized antenna arrays of omni-directional antennas with different polarizations. The capacity of the synthesized arrays is averaged over all channel realizations.

not improve capacity significantly (even though polarization diversity is fully exploited). This assessment is in good agreement with the results of chapter 5, where the best capacity values in 2×2 systems were obtained for the $Xk \times Xd$ setup.

Summarizing, these results are of great importance since they demonstrate that by using very simple antenna elements, capacities comparable to those of current commercial antennas in 2×2 setups can be achieved. For example, comparison of the absolute capacities of the $VV \times VV$ setup with the capacities obtained in Figure 8.4 evidences the fact that when using only two sub-channels $S_C = 2$ the synthesized antennas reach almost the same capacities as the $VV_k \times VV_d$ setup with $s_{Tx} = 5\lambda$ and $s_{Rx} = 5\lambda$. Furthermore, if it is considered that in this case the antennas are synthesized based on smaller arrays than the ones currently available in commer-

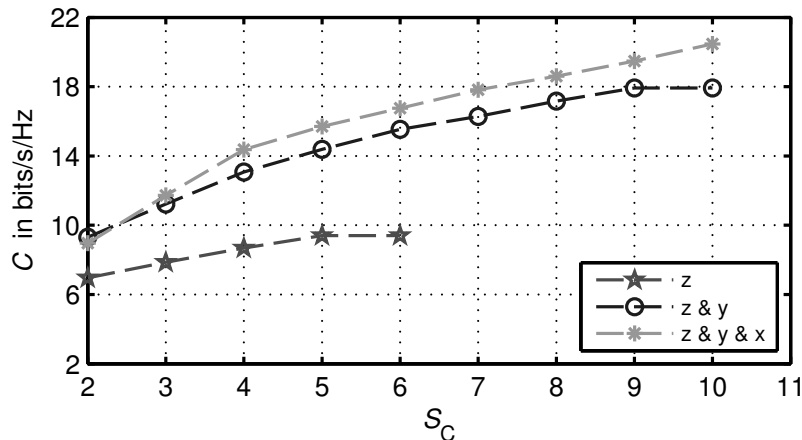


Figure 8.5: Capacity vs S_C for synthesized antenna arrays of $N_S = 25$ dipole antennas oriented parallel to the coordinate axes. The arrays of sub-basis antennas are oriented in the z -direction and their capacity is averaged over all channel realizations.

cial antennas, this could translate into significant savings for antenna providers. For example, by deploying an antenna in z -direction with two subchannels would already result in the capacity increases obtained with two base station antennas. It can be argued, though, that the $\pm 45^\circ$ polarized base station antennas considered in this work already provide these capacities, yet what these results show is that by accessing more independent subchannels (i.e. having multiple power distributions driving the same antenna elements) in a single physical antenna great capacity improvements can be achieved without the need to have additional antennas installed. As result, synthesis strategies that make better use of the available radiating elements seem more promising than adding more antennas.

8.3 Antenna design concepts for the future

The previous simulations showed that capacity of cellular systems for the urban scenario could be increased without having to use additional antennas. Instead, several array excitations could be used. This approach borrows from the diagonalization performed by the waterfilling algorithm in MIMO systems. In the waterfilling algorithm the goal is to find orthogonal subchannels to convey the largest amount of information per time. Out of it different weighting vectors for all communicating antennas for each channel realization result. In the previous section instead of having many antennas, with many radiating elements each, the antenna radiating elements of one antenna are used as single antennas. Then, out of the averaging of the subchannels for all channel realizations the optimum complex weight for each antenna element for each averaged subchannel is found. The main difference, thus, with respect to the regular waterfilling algorithm that requires dynamically driving each antenna element is that in this case fixed driving

networks suffice to provide high capacities. In this way it is found that equal or better capacity performances can be reached by exploiting the signal diversity in the elevation plane than with more antennas in the azimuth direction. In consequence, initial costs would be reduced as well as running costs, such as rent space for the antennas and transmit power. Now the problem of implementing such synthesized antennas will be addressed.

In Figure 8.6 a typical base station antenna implementation for an XX configuration, i.e. two cross polarized antennas at the base station, is depicted. It was shown in chapter 5 that this configuration results in a good compromise between capacity and number of antennas, therefore it will be used for comparison. As previously discussed this configurations yields a 4x2 MIMO system when two antennas are available at the mobile station. Thus four ports are fed into the physical layer processing unit [ITU94] after being amplified by the tower mounted amplifier (TMA). In order to make a fair comparison, resulting in the least impact to the system, in the following, two approaches with four base station antenna ports will be also discussed. It will be seen that with the solutions proposed unit costs can be reduced while still optimizing capacity.

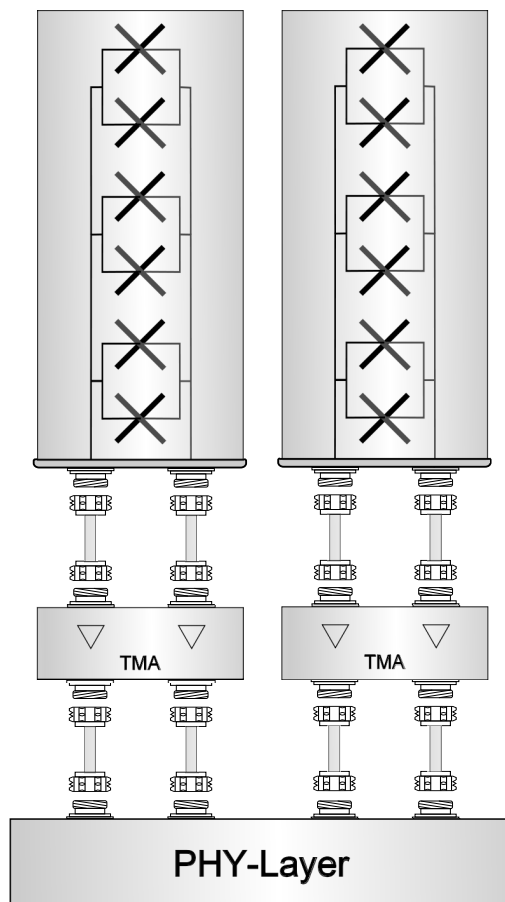


Figure 8.6: Typical base station block model [Kat09].

The main idea proposed in the previous section was to have individual array excitations for each transmitted or received signal. In this way if a MIMO system is capable of having four subchannels at any given time, then four distinct array excitations can result in a better capacity than having multiple antennas. However, current antenna systems are usually passive and consist of one driving network, i.e. one array excitation. A way in which simultaneous array excitation can be generated is if each antenna can be individually controlled by the base transceiver station. For normal antennas, this would require the processing of 8 or more parallel signals, which results in increased costs. Moreover, due to polarization diversity, as shown in this work, in order to exploit the available degrees of freedom access to a second array of orthogonal elements would also be needed to reach the capacity of cross polarized antennas. This would further increase the costs of the system and would yield such a solution unpractical. One option is therefore to avoid the use of driving networks altogether and partition the antenna radiating elements into subarrays. In this manner each subarray can be handled as an individual antenna and can make use of the signal diversity in the elevation plane.

Another alternative is to have a pre-processing unit (PU). This unit would then be responsible for mapping the received and transmitted signals to all radiating elements. An analog implementation of such a unit would require having four passive networks with additional dividers/combiners and would thus result in power losses and higher costs. The alternative is to have a digital implementation. The drawback is the cost of converting the signals at each radiating element from the analog into the digital domain. In exchange though the TMA would become unnecessary. Therefore, here, focus is given to the digital implementation of such PU. In the following two PU approaches will be proposed, with potential of efficiently driving the individual radiating elements in such a way that the most efficient array excitations result. In this case the number of array excitations is four. In real systems, on the other hand, it will depend on the allowed complexity of the system and the impact it has on the system capacity based on simulation results.

In Figure 8.7 the proposed solutions are depicted. For comparison purposes cross polarized antennas as those previously used in chapter 5 are used. This is equivalent to applying the previous synthesis method with -45° and $+45^\circ$ oriented dipoles as sub-basis functions. Such sub-basis functions would then yield very similar results as those obtained in Figure 8.5 for the z and y oriented dipoles.

In Figure 8.7a the first and relatively simple proposed implementation is shown. It consists in subdividing the antenna array into sub-arrays. In this way it is possible to access each sub-array as if it were a single antenna and thus exploit the signal diversity in the elevation plane. Even though this is not the same as controlling the excitation of each radiating element for each transmitted and received signal, it is most likely that very similar capacities as with two cross

polarized base station antennas will result due to the use of signal diversity in the elevation plane. In addition, a significant cost reduction would be achieved, since there is no longer a need for a second antenna as in 8.6.

The second approach proposed is that of Figure 8.7b. There are several differences with respect to the implementation of Figure 8.6. The first difference is the use of a so called tower mounted processing unit (TMPU). This TMPU corresponds to the physical implementation of the PU previously discussed and consists of a unit responsible for the signal processing in both the transmit and receive case and could be also placed within the physical antenna. The second difference is the use of additional ports between the antenna and the TMPU. Ideally the number of ports would be the same as that of the number of antennas, i.e. yielding an active antenna array. However, this would increase the difficulty in implementing such a scheme. One way to overcome this problem is by using subarrays, as was done in Figure 8.7a. In this case, however smaller subarrays are suggested in order to better exploit signal diversity in the elevation plane.

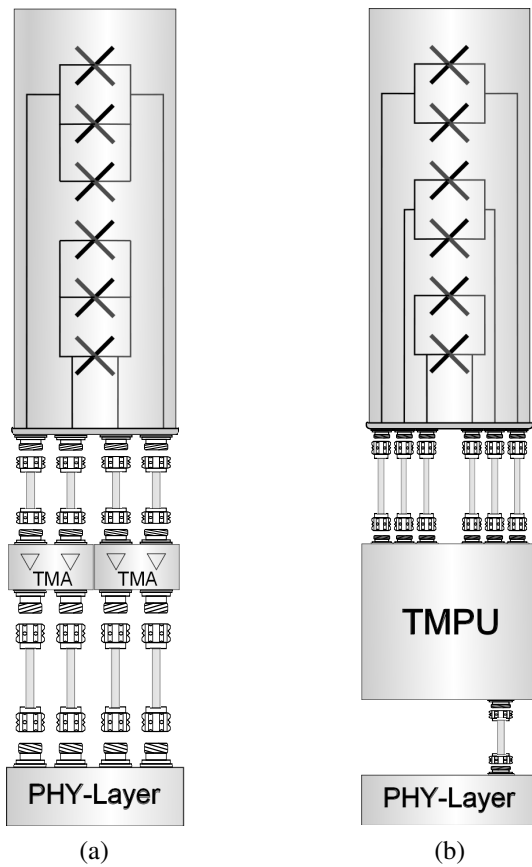


Figure 8.7: Block model of proposed base stations with (a) sub-array implementation and (b) with external tower mounted pre-processing unit (TMPU).

These two approaches exhibit advantages and disadvantages and it is not intended here to assess the viability or cost-efficiency of each approach. In the same manner no implementation details are of interest at this point. Instead, these solutions intend only to show that it is indeed possible with the available technology to try out new ways in which the spatial resources available to base station antennas can be better exploited. Furthermore, these approaches are only two out of many ways in which a more efficient use of the spatial resources can be done. As it has been shown in this work, only by knowing which are the resources available and how they can be exploited it is really possible to optimize the antennas in MEA systems. Therefore, since the results obtained show that diversity in the elevation plane suffices to reach comparable capacities as those obtained with additional antenna elements in the azimuth direction, these solutions seem as promising alternatives for the design of future base station antennas.

8.4 Final remarks

In this chapter a synthesis method for achieving maximum information throughput in MIMO channels is shown. Based on it, the communicational limits of the urban communication channel are explored. From the results presented the following conclusions can be stated:

- The number of degrees of freedom, which ultimately translates to the number of possible subchannels available is dependent on SNR, array length and scenario. If all these variables are fixed, though, it is possible by a SVD and waterfilling based approach to obtain a setup that maximizes capacity in each case for a certain set of sub-basis functions, i.e. radiating elements.
- Under the assumption of a perfect power control (PPC) scheme, as implicitly done by the normalization used throughout this work, a maximum capacity exists after which the subsequent addition of subchannels does not improve the system performance (in case of power distributions other than waterfilling -optimum- it worsens it). This maximum capacity constitutes the communicational limit of the channel. Nonetheless, it should be noted, that the addition of receiving antennas will always have a positive impact on the system in terms of power.
- It is found that a higher number of degrees of freedom is available in azimuth rather than elevation. However, these aren't enough to compensate for the achievable antenna gain and small beamwidth when several radiating elements are placed in the elevation plane. As result, the addition of subchannels in vertical oriented base station antenna is shown to yield higher capacities than the same number of subchannels in an horizontal oriented one.
- The capacity maximum reached for a certain configuration doubles if orthogonal polarizations are used for synthesis. And the use of two orthogonal dipoles yields very similar

results to two isotropic orthogonal polarizations, whereas three orthogonal dipoles provide little additional improvement.

With the results presented in this chapter it is proven for the urban communication channel that better capacities to those of commercial antenna setups could be achieved, not with more antennas, but by driving more subchannels. In consequence, contrary to larger antenna deployments, antenna driving networks capable of producing several array excitations are suggested as the next step toward better capacities in urban communication channels. Here, three possible implementations are proposed for further investigation.

9 Conclusions

The use of MEA systems for the planning of upcoming services and technologies has become the norm in the context of wireless communications. The strategies for meeting the constantly increasing data rate demand for an important number of standards for the wireless transmission of information are based on the efficient and coordinated use of the frequency, time and space resources. In this manner, space has become a significant factor for the analysis and design of antenna systems, in general. However, this is done mostly from a passive perspective, in which space is usually given as the byproduct of a certain scenario and antenna configuration. The motivation of this thesis was therefore to extend the understanding of the spatial resources when it comes to MEA systems. This was achieved for the urban "Karlsruhe" communication channel, based on the multipath modeling scheme of [Füg09]. And even though this does not result by any means in a complete statistical description depicting the behavior of all urban sites, it suggests the way urban scenarios in general might behave and provides a methodology for evaluating urban communication scenarios in general.

The goals of this work are to extend and improve the analysis of MEA systems and to gain insight into the antennas design and their most convenient implementation in terms of maximum channel capacity. Contrary to most published works in the context of MIMO and MEA systems, attention was given in this thesis to the channel-antenna interaction and how it can be better described and optimized. Therefore, the interest of this research lies in the study of the antenna contributions to the performance of MEA systems. As result, the following achievements were made:

- An improved network model based on the modal description of the antennas was implemented and proved to yield significant reductions in simulation time for the case of modal modeled dipoles.
- An exhaustive study of different antenna configurations with varying inter-element spacing at both transmitter and receiver was done for three different types of power allocation schemes.
- A comprehensive and simple pre-evaluation metric for the study of MEA systems was proposed, which separates the beamforming and multiplexing effects of the channel. This novel metric facilitates the computation of capacity for any given type of channel normalization in either the ergodic or outage sense.

- The communicational limits, in regard to the maximum number of parallel data streams supported by the channel-antenna interaction, were assessed for the first time in the context of urban channels for linear antenna arrays.
- An array synthesis method for capacity maximization was proposed which is capable of outperforming current commercial base station antennas in terms of capacity and implementation cost trade-off.

In this way, a thorough study of the antenna effects on the capacity performance of MEA systems has been given. Also, the simulation, evaluation and design frameworks for the investigation of antennas in MEA systems have been extended. The significance for the future study of antennas within MEA systems has been three-fold: 1) faster simulation, 2) comprehensive and easier evaluation and comparison and 3) optimum use of the spatial resources.

In chapter 2 the theoretical background necessary for understanding the wireless propagation of signals and the role played by the antennas within the wireless communication channel was given. With this knowledge, in chapter 3 a modeling framework for the whole communication channel of MEA systems was provided. Here, previous modeling efforts were extended with the purpose of facilitating the simulation and investigation of a large number of antenna types. By means of a modal antenna description simulation times were reduced. It was shown that when dealing with dipoles three modes suffice for describing any possible dipole orientations. In this way the computational gain of this approach increases with increasing the number of antenna orientations to be investigated. In addition, the road has been paved for a further extension of this simulation method, possibly by means of spherical modes translation and rotation in which, out of the simulation of a fixed number of modes, not only different antenna types but also different antenna locations can be computed.

Completing this theoretical background, the evaluation framework used was provided in chapter 4 based on the concept of maximum information throughput, i.e. capacity. Diversity and multiplexing effects on capacity were discussed and the duality between temporal and spatial domains in the computation of capacity was restored. On this basis, in chapter 5 a benchmark of different antenna configurations for the urban macrocell case of the "Karlsruhe" scenario showed that the significance of antenna spacing depends on the configuration studied, i.e. on whether diversity or multiplexing effects predominate for the setup being considered. It was concluded, based on the cross comparison of the capacities of three different power allocation schemes, that for real antenna configurations in urban settings 1) antenna inter-element spacing has a larger impact on multiplexing gain than on beamforming gain, 2) this impact is most noticeable for single polarized configurations and 3) for dual polarized configurations beamforming gain decreases with larger antenna spacings. Regarding the capacity dependence on

antenna rotation, robustness of cross polarized configurations toward antenna rotation was verified for all antenna spacings. Furthermore, it was seen that the optimum antenna orientation is determined by the propagation channel in the case that single polarized antennas at the mobile station are used in conjunction with dual polarized ones at the base station.

In performing the very exhaustive study of chapter 5 it became clear that it was not in all cases possible to determine the individual contribution in terms of diversity and multiplexing of a certain antenna setup or spacing. The proposed metric from chapter 6 for addressing this issue, showed that it was possible to approximate the system capacity as the contribution of three factors: SNR, a diversity measure, transferred signal power, and a multiplexing measure, eigenvalue dispersion. This novel metric was also extended for the case of arbitrarily sized systems. Its implementation for the analysis of 2x2 and 4x4 setups in the "Karlsruhe" communication channel allowed the study of multiplexing and diversity effects and the capacity reconstruction regardless of channel normalization.

In order to complete the study of the antennas impact on MEA systems their communicational limits were derived in chapter 7. In particular, a method for estimating the maximum number of parallel data streams possible was given for the cases of: free space, multipath with uniform power distribution per path and multipath with uneven power distribution as embodied by the "Karlsruhe" communication channel. This evidenced a linear dependence on array length for all cases. However, for the "Karlsruhe" communication channel it was seen that due to its uneven power distribution no clear limit to the maximum number of subchannels existed. Instead, a maximum number of antennas was found after which capacity increased at a much slower rate with each additional subchannel. From the analysis made, it was concluded that a larger number of subchannels exists along the azimuth direction than along the elevation direction.

In chapter 8 the results from chapter 7 were then used as basis for the synthesis of capacity maximizing arrays. Here, a novel in-system synthesis method was developed, which allowed the computation of optimum radiation patterns in a capacity maximizing sense, contrary to traditional approaches where the radiation characteristics are *a priori* specified. In this way, synthesized antennas were found which were capable of better exploiting the spatial resources of the communication channel. It was confirmed that the number of available subchannels for synthesized arrays along the azimuth direction is greater than along the elevation. Yet, addition of subchannels for a vertically oriented array yielded larger capacity improvements. Therefore, this chapter and this work was concluded with a discussion of future antenna implementations which, based on the guidelines derived in this work, would yield improved system performance without increasing antenna size and no significant added costs.

Bibliography

- [ABB⁺07] P. Almers, E. Bonek, A. Burr, N. Czink, M. Debbah, V. Degli-Esposti, H. Hofstetter, P. Kyösti, D. Laurenson, G. Matz, A.F. Molisch, C. Oestges, and H. Özcelik. Survey of channel and radio propagation models for wireless MIMO systems. *EURASIP Journal on Wireless Communications and Networking*, 2007(Article ID 19070), 2007.
- [AGW⁺02] Y. Adane, A. Gati, Man-Fa Wong, C. Dale, J. Wiart, and V.F. Hanna. Optimal modeling of real radio base station antennas for human exposure assessment using spherical-mode decomposition. *Antennas and Wireless Propagation Letters, IEEE*, 1:215–218, 2002.
- [Ala98] S. Alamouti. A simple transmit diversity technique for wireless communications. *IEEE Journal on Selected Areas in Communications*, 16(8):1451–1458, October 1998.
- [And00] J. B. Andersen. Array gain and capacity for known random channels with multiple element arrays at both ends. *IEEE Journal on Selected Areas in Communications*, 18(11):2172–2178, November 2000.
- [And03] Theodore W. Anderson. *An introduction to multivariate statistical analysis*. Wiley series in probability and statistics. Wiley, Hoboken, NJ, 3. ed. edition, 2003. Previous ed.: 1984; : c74.50 : CIP entry (May).
- [Bal97] C.A. Balanis. *Antenna Theory*. John Wiley & Sons, New York, NY, 1997.
- [Bha07] A. K. Bhattacharyya. Projection matrix method for shaped beam synthesis in phased arrays and reflectors. *IEEE Transactions on Antennas and Propagation*, 55:675–683, March 2007.
- [Bre59] D. G. Brennan. Linear diversity combining techniques. In *Proceedings of the IRE*, volume 47, pages 1075–1102, June 1959.
- [CF06] K. Chakraborty and M. Franceschetti. Maxwell meets shannon: Space-time duality in multiple antenna channels. *Allerton Conference on Communication, Control, and Computing*, 2006.
- [CP07] J.-M Conrat and P. Pajusco. Typical MIMO propagation channel in urban macrocells at 2 ghz. In *Proceedings of the 13th European Wireless Conference*, pages CD-ROM, Paris, France, April 2007.

- [CPGZ09] J. Corcoles, J. Pontes, M. A. Gonzalez, and T. Zwick. Modelling line-of-sight coupled MIMO systems with generalised scattering matrices and spherical wave translations. *Electronics Letters*, 45(12):598–599, June 4, 2009.
- [CS91] Y. Chen and T. Simpson. Radiation pattern analysis of arbitrary wire antennas using spherical mode expansions with vector coefficients. *Antennas and Propagation, IEEE Transactions on*, 39(12):1716–1721, Dec 1991.
- [CT91] T. M. Cover and J. A. Thomas. *Elements of Information theory*. John Wiley & Sons, Inc., 1991.
- [DC08] A. Dunand and J.-M Conrat. Polarization behaviour in urban macrocell environments at 2.2ghz. In *COST 2100, TD(08)406*, Wroklaw, Poland, February 2008.
- [ESBP02] V. Erceg, P. Soma, D. S. Baum, and A. J. Paulraj. Capacity obtained from multiple-input multiple-output channelmeasurements in fixed wireless environments at 2.5 ghz. In *Communications, 2002. ICC 2002. IEEE International Conference on*, volume 1, pages 396–400, New York, NY, USA, 2002.
- [FFLV01] F. R. Farrokhi, G. J. Foschini, A. Lozano, and R. A. Valenzuela. Link-optimal space-time processing with multiple transmit and receive antennas. *IEEE Communications Letters*, 5(3):85–87, March 2001.
- [FG98] G.J. Foschini and M.J. Gans. On limits of wireless communications in a fading environment when using multiple antennas. *Wireless Personal Communications*, 6:311–335, 1998.
- [FMKW06] T. Fügen, J. Maurer, T. Kayser, and W. Wiesbeck. Capability of 3-d ray tracing for defining parameter sets for the specification of future mobile communications systems. *IEEE Transactions on Antennas and Propagation*, 54:3125–3137, November 2006.
- [Fos96] G.J. Foschini. Layered space-time architecture for wireless communication in a facing environment. *Bell Labs Technical Journal*, pages 41–49, October 1996.
- [FSM⁺02] T. Fügen, G. Sommerkorn, J. Maurer, D. Hampicke, W. Wiesbeck, and R.S. Thomä. MIMO capacities for different antenna arrangements based on double directional wide-band channel measurements. In *Proceedings of the 13th IEEE International Symposium on Personal, Indoor and Mobile Radio Communications, PIMRC 2002*, volume 3, pages 1777–1781, Lisbon, Portugal, September 2002.
- [Füg09] Thomas Fügen. *Richtungsaufgelöste Kanalmodellierung und Systemstudien für Mehrantennensysteme in urbanen Gebieten*. PhD thesis, Universität Karlsruhe, 2009.
- [GL96] Gene Howard Golub and Charles F. Van Loan. *Matrix computations*. Johns Hopkins University Press, 1996.

- [GM08] F. K. Gruber and E. A. Marengo. New aspects of electromagnetic information theory for wireless and antenna systems. *IEEE Transactions on Antennas and Propagation*, 56(11):3470–3484, November 2008.
- [GN06] M. Gustafsson and S. Nordebo. Characterization of MIMO antennas using spherical vector waves. *IEEE Transactions on Antennas and Propagation*, 54(9):2679–2682, September 2006.
- [GW98] N. Geng and W. Wiesbeck. *Planungsmethoden für die Mobilkommunikation*. Springer, Berlin, 1998.
- [Han81] R. C. Hansen. Fundamental limitations in antennas. *Proceedings of the IEEE*, 69(2):170–182, February 1981.
- [Han88] J. E. Hansen. *Spherical Near-field Antenna Measurements: Theory and Practice*. IET, 1988.
- [HF06] L. Hanlen and M. Fu. Wireless communication systems with-spatial diversity: a volumetric model. *IEEE Transactions on Wireless Communications*, 5:133–142, January 2006.
- [IN02] M. T. Ivrlac and J. A. Nossek. Mimo eigenbeamforming in correlated fading. In *Circuits and Systems for Communications, 2002. Proceedings. ICCSC '02. 1st IEEE International Conference on*, pages 212–215, June 26–28, 2002.
- [IN03] M.T. Ivrlac and J.A. Nossek. Quantifying diversity and correlation in rayleigh fading MIMO communication systems. In *IEEE International Symposium on Signal Processing and Information Technology, ISSPIT 2003*, pages 158–161, Darmstadt, Germany, December 2003.
- [ITU94] ITU. X.200 information technology - open system interconnection - basic reference model: The basic model. Technical report, ITU-T Telecommunication Standardization Sector of International Telecommunication Unit (ITU), 1994.
- [IY02] M. F. Iskander and Zhengqing Yun. Propagation prediction models for wireless communication systems. *IEEE Transactions on Microwave Theory and Techniques*, 50(3):662–673, March 2002.
- [Jak74] W. Jakes. *Microwave Mobile Communications*. Wiley, New York, NY, 1974.
- [Jan02] R. Janaswamy. Effect of element mutual coupling on the capacity of fixed length linear arrays. *Antennas and Wireless Propagation Letters*, 1:157–160, 2002.
- [JW08] M. A. Jensen and J. W. Wallace. Capacity of the continuous-space electromagnetic channel. *IEEE Transactions on Antennas and Propagation*, 56(2):524–531, February 2008.
- [KA06] M. Kang and M. S. Alouini. Capacity of MIMO rician channels. *IEEE Transactions on Wireless Communications*, 5(1):112–122, January 2006.

- [KAE06] O. Klemp, G. Armbrecht, and H. Eul. Computation of antenna pattern correlation and MIMO performance by means of surface current distribution and spherical wave theory. *Advances in Radio Science*, 4:33–39, 2006.
- [Kat02] R. Kattenbach. Statistical modeling of small-scale fading in directional radio channels. *IEEE Journal on Selected Areas in Communications*, 20(3):584 – 592, April 2002.
- [Kat09] Kathrein-Werke KG. *DTMA-UMTS-12-AISG-CWA Datasheet*, 2009. <http://www.kathrein.de/de/mcs/produkte/download/9363122a.pdf>.
- [KBJR01] M.A. Khalighi, J. Brossier, G. Jourdain, and K. Raoof. Water filling capacity of rayleigh MIMO channels. In *Proceedings of the IEEE 12th International Symposium on Personal, Indoor and Mobile Radio Communications*, volume 1, pages 155–158, San Diego, CA , USA, September 2001.
- [KCVW03] P. Kyritsi, D.C. Cox, R.A. Valenzuela, and P.W. Wolniansky. Correlation analysis based on MIMO channel measurements in an indoor environment. *IEEE Journal on Selected Areas in Communications*, 21(5):713–720, June 2003.
- [KG06] KATHREIN-Werke KG. 790-2500 mhz base station antennas for mobile communications, 2006.
- [KHE05] O. Klemp, S. K. Hampel, and H. Eul. Study of MIMO capacity for linear dipole arrangements using spherical mode expansions. In *Proceedings of the 14. IST Mobile&Wireless Comm. Summit*, 2005.
- [Kil00] Per-Simon Kildal. *Foundations of Antennas*. Studentlitteratur, 2000.
- [KJUN02] T.P. Kurpjuhn, M. Joham, W. Utschick, and J.A. Nossek. Experimental studies about eigenbeamforming in standardization mimo channels. In *Proceedings of the 56th IEEE Vehicular Technology Conference, VTC 2002-Fall*, volume 1, pages 185–189, Vancouver, Canada, September 2002.
- [Kra88] John Daniel Kraus. *Antennas*. McGraw-Hill Companies, 1988.
- [Lee82] W.C.Y. Lee. *Mobile Communications Engineering*. McGraw-Hill, New York, 1982.
- [LOKM05] B.K. Lau, S.M.S. Ow, G. Kristensson, and A.F. Molisch. Capacity analysis for compact MIMO systems. In *Vehicular Technology Conference, 2005. VTC 2005-Spring. 2005 IEEE 61st*, volume 1, pages 165–170 Vol. 1, May-1 June 2005.
- [LS03] E.G. Larsson and P. Stoica. *Space-Time Block Coding for Wireless Communications*. Cambridge University Press, Cambridge, UK, 2003.
- [LST⁺07] M. Landmann, K. Sivasondhivat, J. Takada, I. Ida, and R.S. Thomä. Polarization behavior of discrete multipath and diffuse scattering in urban environments at 4.5 ghz. *EURASIP Journal on Wireless Communications and Networking*, 2007:Article ID 57980, 16 pages, 2007.

- [Mai05] Robert J. Mailloux. *Phased Array Antenna Handbook*. Artech House, Second Edition, 2005.
- [Mat97] Arakaparamil M. Mathai. *Jacobians of matrix transformations and functions of matrix argument*. World Scientific, Singapore [u.a.], 1997. Includes bibliographical references and indexes.
- [Mig06a] M. D. Migliore. An intuitive electromagnetic approach to MIMO communication systems. *IEEE Antennas and Propagation Magazine*, 48(3):128–137, June 2006.
- [Mig06b] M. D. Migliore. On the role of the number of degrees of freedom of the field in MIMO channels. *IEEE Transactions on Antennas and Propagation*, 54:620–628, February 2006.
- [Mig06c] M. D. Migliore. Restoring the symmetry between space domain and time domain in the channel capacity of MIMO communication systems. In *Antennas and Propagation Society International Symposium 2006, IEEE*, pages 333–336, Albuquerque, NM, July 9–14, 2006.
- [Mig08] M. D. Migliore. On electromagnetics and information theory. *IEEE Transactions on Antennas and Propagation*, 56(10):3188–3200, October 2008.
- [Mil00] David A. B. Miller. Communicating with waves between volumes: Evaluating orthogonal spatial channels and limits on coupling strengths. *Applied Optics*, 39:1681–1699, 2000.
- [MSV04] F. Mikas, J. Salo, and P. Vainikainen. A tight upper bound on the average mutual information in correlated rayleigh fading MIMO channels. In *Wireless Technology, 2004. 7th European Conference on*, pages 141–144, 2004.
- [OEP03] C. Oestges, V. Erceg, and A. J. Paulraj. A physical scattering model for MIMO macrocellular broadband wireless channels. *IEEE Journal on Selected Areas in Communications*, 21(5):721–729, June 2003.
- [OPF09] L. G. Ordóñez, D. P. Palomar, and J. R. Fonollosa. Ordered eigenvalues of a general class of hermitian random matrices with application to the performance analysis of MIMO systems. *IEEE Transactions on Signal Processing*, 57(2):672–689, February 2009.
- [OT02] Y. Oda and T. Taga. Clustering of local scattered multipath components in urban mobile environments. In *Proceedings of the 55th IEEE Vehicular Technology Conference, VTC 2002-Spring*, Vancouver, BC, Canada, September 2002.
- [Özc04] H. Özcelik. *Indoor MIMO Channel Models*. PhD thesis, Technische Universität Wien, Fakultät für Elektrotechnik und Informationstechnik, 2004.
- [PBT05] A. S. Poon, R. W. Brodersen, and D. N. Tse. Degrees of freedom in multiple-antenna channels: a signal space approach. *IEEE Transactions on Information Theory*, 51(2):523–536, February 2005.

- [PLW07] J. Pontes, A. Lambrecht, and W. Wiesbeck. Synthesized antenna arrays for future mobile networks. In *Proceedings for ACES2007*, Mar. 2007. 2007.03.20.
- [PM00] Rafael Piestun and David A. B. Miller. Electromagnetic degrees of freedom of an optical system. *J. Opt. Soc. Am. A*, 17(5):892–902, 2000.
- [PNG03] A.J. Paulraj, R. Nabar, and D. Gore. *Introduction to Space-Time Wireless Communications*. Cambridge University Press, Cambridge, UK, 2003.
- [Pro01] J. G. Proakis. *Digital Communications*. McGraw-Hill, 2001.
- [PW07] Juan Pontes and Werner Wiesbeck. Sidelobe shaping synthesis algorithm for antenna arrays. In *Proceedings for IEEE AP-S International Symposium 2007*, Jun. 2007. 2007.06.14.
- [RC98] G. G. Raleigh and J. M. Cioffi. Spatio-temporal coding for wireless communication. *IEEE Transactions on Communications*, 46(3):357–366, March 1998.
- [RGZ05] J. Rubio, M. A. Gonzalez, and J. Zapata. Generalized-scattering-matrix analysis of a class of finite arrays of coupled antennas by using 3-d fem and spherical mode expansion. *IEEE Transactions on Antennas and Propagation*, 53(3):1133–1144, March 2005.
- [Sch07] Stephan Schulteis. *Integration von Mehrantennensystemen in kleine mobile Geräte für multimediale Anwendungen*. PhD thesis, Universität Karlsruhe, Fak. f. Elektrotechnik und Informationstechnik, 2007.
- [SFGK00] Da-Shan Shiu, G. J. Foschini, M. J. Gans, and J. M. Kahn. Fading correlation and its effect on the capacity of multielement antenna systems. *IEEE Transactions on Communications*, 48(3):502–513, March 2000.
- [Sha48] C. E. Shannon. A mathematical theroy of communication. *Bell Systems Technical Journal*, 27:379–423, 1948.
- [SMM06] S. H. Simon, A. L. Moustakas, and L. Marinelli. Capacity and character expansions: Moment-generating function and other exact results for MIMO correlated channels. *IEEE Transactions on Information Theory*, 52(12):5336–5351, December 2006.
- [SMV04] J. Salo, F. Mikas, and P. Vainikainen. An upper bound on the ergodic mutual information of ricean fading MIMO channels. In *Signal Processing Symposium, 2004. NORSIG 2004. Proceedings of the 6th Nordic*, pages 288–291, 2004.
- [SSESV04] J. Salo, P. Suvikunnas, H. M. El-Sallabi, and P. Vainikainen. Some results on MIMO mutual information: the high snr case. In *Global Telecommunications Conference, 2004. GLOBECOM '04. IEEE*, volume 2, pages 943–947, November 29–December 3, 2004.

- [SSESV06a] J. Salo, P. Suvikunnas, H. M. El-Sallabi, and P. Vainikainen. Ellipticity statistic as measure of MIMO multipath richness. *Electronics Letters*, 42(3):160–162, February 2, 2006.
- [SSESV06b] J. Salo, P. Suvikunnas, H. M. El-Sallabi, and P. Vainikainen. Some insights into MIMO mutual information: The high snr case. *IEEE Transactions on Wireless Communications*, 5(11):2997–3001, November 2006.
- [SSKV05] P. Suvikunnas, J. Salo, J. Kivinen, and P. Vainikainen. Empirical comparison of MIMO antenna configurations. In *Vehicular Technology Conference, 2005. VTC 2005-Spring. 2005 IEEE 61st*, volume 1, pages 53–57, May 30–June 1, 2005.
- [SSV07] P. Suvikunnas, J. Salo, and P. Vainikainen. Impact of power normalization in experimental MIMO antenna performance studies. *IEEE Antennas and Wireless Propagation Letters*, 6:43–46, 2007.
- [SSV⁺08] P. Suvikunnas, J. Salo, L. Vuokko, J. Kivinen, K. Sulonen, and P. Vainikainen. Comparison of MIMO antenna configurations: Methods and experimental results. *IEEE Transactions on Vehicular Technology*, 57(2):1021–1031, March 2008.
- [SW08] Hyundong Shin and M. Z. Win. MIMO diversity in the presence of double scattering. *IEEE Transactions on Information Theory*, 54(7):2976–2996, July 2008.
- [Tel99] Emre Telatar. Capacity of multi-antenna gaussian channels. *Euro. Trans. Telecomm. ETT*, 1999.
- [TFS99] T. Taga, T. Furuno, and K. Suwa. Channel modeling for 2-ghz-band urban line-of-sight street microcells. *IEEE Transactions on Vehicular Technology*, 48:262–272, January 1999.
- [THL⁺03] R.S. Thomä, D. Hampicke, M. Landmann, A. Richter, and G. Sommerkorn. Measurement-based parametric channel modelling (mbpcm). In *International Conference on Electromagnetics in Advanced Applications, ICEAA 2003*, Torino, Italy, September 2003.
- [TV05] David Tse and Pramod Viswanath. *Fundamentals of Wireless Communication*. Cambridge University Press, 2005.
- [VA87] R. G. Vaughan and J. B. Andersen. Antenna diversity in mobile communications. *IEEE Transactions on Vehicular Technology*, 36(4):149–172, November 1987.
- [Wal04] Christian Waldschmidt. *Systemtheoretische und experimentelle Charakterisierung integrierbarer Antennenarrays*. PhD thesis, Universität Karlsruhe, Fak. f. Elektrotechnik und Informationstechnik, 2004.
- [WFW02] C. Waldschmidt, T. Fügen, and W. Wiesbeck. Spiral and dipole antennas for indoor MIMO-systems. *Antennas and Wireless Propagation Letters*, 1(1):176–178, 2002.

- [WG04] Zhengdao Wang and G. B. Giannakis. Outage mutual information of space-time MIMO channels. *IEEE Transactions on Information Theory*, 50(4):657–662, April 2004.
- [WHÖB06] W. Weichselberger, M. Herdin, H. Özcelik, and E. Bonek. A stochastic MIMO channel model with joint correlation of both link ends. *IEEE Transactions on Wireless Communications*, 5(1):90–100, January 2006.
- [WJ04] J. W. Wallace and M. A. Jensen. Mutual coupling in MIMO wireless systems: a rigorous network theory analysis. *IEEE Transactions on Wireless Communications*, 3(4):1317–1325, July 2004.
- [WSW04] C. Waldschmidt, S. Schulteis, and W. Wiesbeck. Complete RF system model for analysis of compact MIMO arrays. *IEEE Transactions on Vehicular Technology*, 53(3):579–586, May 2004.
- [XJ06] J. Xu and R. Janaswamy. Electromagnetic degrees of freedom in 2-d scattering environments. *IEEE Transactions on Antennas and Propagation*, 54(12):3882–3894, December 2006.
- [Zwi99] T. Zwick. *Die Modellierung von richtungsaufgelösten Mehrwegegebäudefunkkanälen durch markierte Poisson-Prozesse*. PhD thesis, Universität Karlsruhe, Fak. f. Elektrotechnik und Informationstechnik, 1999.



**Karlsruher Forschungsberichte aus dem
Institut für Hochfrequenztechnik und Elektronik**
Herausgeber: Prof. Dr.-Ing. Thomas Zwick

This work focuses on the analysis and design of multiple element antennas and their interaction with the propagation channel. In particular, attention is given to urban channels and how its information throughput, i.e. capacity, can be improved. With this in mind, an existing network model of the communication system is extended to include a modal description of both mobile and base station antennas with the aim of reducing computation time. On the basis of this model, an extensive capacity study of typical antenna setups with varying inter element spacing is performed. From this study the need of adopting a more general evaluation metric to assess multiplexing and diversity effects independently is seen and addressed. To conclude, the communicational limits of linear arrays in different propagation scenarios are explored and a scenario independent synthesis method for achieving maximum information throughput is derived.

Juan Pontes, born in 1981 in Caracas, started his studies in electronic engineering in the "Universidad Simón Bolívar" in Venezuela and obtained the title of Dipl.-Ing. in the "Universität Karlsruhe (TH)" in June 2005. Since then he worked towards his doctoral degree in the field of multiple element antenna systems and antenna theory, which he successfully obtained in February 2010.

ISSN 1868-4696

ISBN 978-3-86644-513-0

